ROYAL SOCIETY
OF CHEMISTRY

REVIEW

Recent progress in organic solar cells based on non-fullerene acceptors: materials to devices

Dou Luo,[†a] Woongsik Jang, [†b] Dickson D. Babu,[†a] Min Soo Kim, [†b] Dong Hwan Wang [*b] and Aung Ko Ko Kyaw [*ac]

Organic solar cells (OSCs) were dominated by donor–acceptor blends based on polymer donors and fullerene acceptors for nearly two decades. In the past, apprehensions about the limited efficiency of OSCs compared to other modern PV technologies had rendered them redundant. However, in the past few years, a new class of non-fullerene acceptors (NFAs) has gained prominence for OSCs owing to the significant increase in power conversion efficiency (∼2.5–18% higher than that of OSCs based on fullerene acceptors). NFAs have several advantages over their fullerene counterparts; they can be produced using facile synthesis methods and chemically manipulated to tune the morphology and electronic properties. In addition, the optical bandgap can be modified to broaden the absorption range. Herein, we review the recent advances in NFA-based OSCs and discuss the key factors enabling their fabrication, including rational design rules for donor, acceptor, and interface materials, control of the blend morphology, and engineering of the light-harvesting process and device architecture. We also provide a brief review of recent studies for increasing the stability of OSCs under various external conditions. Finally, the major challenges facing the upscaling and commercialisation of OSCs are discussed, along with the future directions for the development of OSCs.

1. Introduction

An effective approach to alleviate the current energy crisis and the challenges associated with our continued dependence on fossil fuels is to exploit renewable and green energy sources. Hence, harnessing energy from the sun continues to attract attention as photovoltaics (PV) is an established technology and the most promising method for directly converting solar energy

aDepartment of Electrical and Electronic Engineering, Southern University of Science and Technology, 1088 Xueyuan Blvd, Xili, Nanshan Shenzhen, 518088, Guangdong, China. E-mail: aung@sustech.edu.cn

bSchool of Integrative Engineering, Chung-Ang University, 84 Heukseok-ro, Dongjak-gu, Seoul, 06974, Republic of Korea. E-mail: king0401@cau.ac.kr

cShenzhen Planck Innovation Technology Co., Ltd, No. 8, Liuhe Road, Longgang District, Shenzhen, Guangdong, China

† These authors contributed equally to this manuscript.

Dou Luo is currently a post-doctoral fellow with Prof. Aung Ko Ko Kyaw's group at Southern University of Science and Technology (SUSTech), China. He received his B.S. (2014) in polymer materials science and engineering from Wuhan Institute of Technology (WIT) and his PhD (2020) in materials science from the South China University of Technology (SCUT), China. His current research focuses on organic optoelectronic materials for highly efficient organic solar cells. He is also interested in the synthesis of organic functional material for organic/perovskite solar cell and organic field effect transistors.

Woongsik Jang is currently a PhD. Candidate at the department of Integrative Engineering in Chung-Ang University. He received his M.S. degree in 2017 under supervision of Prof. Wang in the same University. His research interests include organic/perovskite solar cells and organic photodetectors. He is an excellent student in CAU with currently published 47 important SCI papers.

This journal is © The Royal Society of Chemistry 2022

J. Mater. Chem. A, 2022, **10**, 3255–3295 | **3255**

into electricity. Among the various PV technologies, organic solar cells (OSCs) based on π-conjugated systems have attracted extensive attention owing to their potential advantages such as low cost, mechanical flexibility, light weight, and suitability for roll-to-roll printing methods.[1–4]

Th first OSC was invented by Tang in 1986, who using a bilayer heterojunction structure.[5] However, due to the spatially limited exciton diffusion length (∼10–20 nm), only the excitons generated at the donor–acceptor interface can be separated into charge carriers. To address this, bulk hetero-junction (BHJ) architecture was first proposed in 1995.[6,7] Even today, the most extensively investigated solution-processed OSC devices are based on a BHJ structure. The BHJ architecture generally comprises an electron donor and electron acceptor, which are blended to form an interpenetrating network for efficient exciton dissociation and rapid charge transfer to the

respective electrodes. In the early time, $PC_{61}BM$ and $PC_{71}BM$ fullerene derivatives are the most dominant and common electron-acceptor materials for OSCs as they have high electron mobility (10^{-3} cm^2 V^{-1} s^{-1}), isotropic charge-transport behaviour, and high electron affinity. Though the fast development of OSCs based on fullerene acceptors, their performance are still limited by its inherent weak absorption, untenability of energy levels, large voltage losses (V_{loss}), morphological instabilities and so on.[8] Consequently, it is imperative to explore novel materials to further improve the PV performance of OSCs, particularly non-fullerene acceptors (NFAs), which possess stronger light absorption with a readily tuneable energy levels and can be produced using facile synthesis methods.[9,10] NFAs are typically categorised into two broad classes: small-molecule acceptors (SMAs) and polymeric acceptors. Fused-ring electron acceptors (FREAs), represented by SMAs, have been shown great

Dickson D. Babu received his master's degree from Christ University (2010–2012). He went on to pursue his PhD from the National Institute of Technology, Karnataka (NITK). Most of his PhD work was carried out in collaboration with Prof. El-Shafei's group at North Carolina State University, USA. He is currently a postdoctoral researcher with Prof. Aung Ko Ko Kyaw group at the Department of Electrical and Electronic Engineering at Southern University of Science and Technology. His research interests include the solar cells, photo/electrocatalytic systems for water splitting, NRR, CO$_2$ reduction and metal–air batteries.

Dong Hwan Wang obtained his PhD degree in Chemical and Biomolecular Engineering from KAIST in 2012 and joined the group of Professor Heeger at the University of California, Santa Barbara in 2012–2014 as a postdoctoral research fellow. He is currently a professor at the School of Integrative Engineering in Chung-Ang University since 2014. He is full professor from 2020 with over 120 published SCI papers. His research interests include solution processed organic electronics such as organic and perovskite solar cells, and organic photodetectors fabricated by newly designed nanomaterials, and nanostructure with specific optoelectronic properties.

Min Soo Kim is currently a PhD. Candidate at the department of Integrative Engineering in Chung-Ang University with GRS scholarship. He received his M.S. degree in 2021 under supervision of Prof. Wang in the same University. His research interests include polymer film synthesis/fabrication, transfer nanotechnology, and organic solar cells/photodetectors.

Aung Ko Ko Kyaw is an Associate Professor of the Department of Electrical and Electronic Engineering at Southern University of Science and Technology, China. He received both B.Eng. and PhD from Nanyang Technological University, Singapore in 2007 and 2012, respectively. From 2012 to 2014, he joined Prof Alan Heeger's lab at University of California, Santa Barbara as a post-doctoral researcher under A*STAR International Fellowship. Then, he worked as a Scientist at Institute of Materials Research and Engineering of A*STAR, Singapore from 2014 to 2017. He is listed in the World's Top 2% Scientists of 2019 released by Stanford University. His research focuses on organic and hybrid materials for energy harvesting, sensing and wearable electronics.

potential for the development of OSCs and the power conversion efficiency (PCE) has been over 18%.[11–13] FREAs often contain an electron-donating fused-ring core along with two strong electron-withdrawing terminal groups coupled by a planar π-conjugated bridge, resulting in a planar molecular structure and strong intermolecular interaction. FREAs are now the most important acceptors in the development of OSCs.

To exploit the full potential of NFAs, rational molecular optimisation of the polymer donor materials is essential. For instance, polymer donors with wide-bandgap are essential to complement the absorption with corresponding narrow-bandgap NFA. Additionally, lowering the highest-occupied molecular orbital (HOMO) level of the polymer donor is necessary to offer sufficient driving force for effective charge separation in OSCs with NFAs.[14] Moreover, the crystallinity of polymer donor is crucial for the phase separation in the active layers. All these requirements are crucial for the rational molecular design of the polymer donor. The morphology of BHJ layer is another key parameter as it has a significant effect on the overall performance of OSC. Usually, the morphology of active layers can be modified by solvent engineering, annealing treatments, and the use of various types of additives, to further increase the device efficiency.[15,16] Interface engineering is another key aspect to obtain highly efficient OSCs. As OSCs often contain multiple layers, interface engineering is required to ensure efficient charge collection at the electrodes of the devices. In addition to obtaining devices with high PCEs, achieving long-term stability is another major challenge that needs to be overcome to successfully commercialise OSCs. There are numerous factors influencing OSC stability, such as light, heat, temperature, oxygen, and humidity on device degradation.

In this review, we first discuss and highlight the recent accomplishments in the molecular design of efficient donor and acceptor materials. The second section discusses the importance of various processing factors and their influence on the OSC. The third section extends this discussion to the interfacial layers, which can significantly influence device performance and stability. Subsequently, we present the various device architectures and discuss the factors influencing OSC stability. Finally, the fundamental challenges and possible approaches for further increasing the efficiency are discussed, and strategies for achieving the commercialisation of OSCs are proposed.

2. The development of new donor and acceptor materials in the OSCs

Despite the initial success of OSCs, the inherently weak light-harvesting ability of fullerenes and other challenges have limited the applications of this technology. However, interest in OSCs was reinvigorated by the demonstration of higher PCEs, which was achieved by the design and synthesis of novel donor and acceptor materials (especially NFAs) in either binary BHJ systems or tandem-device architectures. Plentiful new materials, including small molecules and polymers, have been designed and synthesised with suitable bandgaps to proficiently harvest solar irradiation as well as the appropriate energy levels help to minimise the energy loss (E_{loss}) of OSCs. Specifically, numerous molecular design strategies, such as backbone modification, engineering of the side chains and functional groups, have been developed to efficiently modulate the optoelectronic properties of active layer.[17–19] Such design strategies allow the optimisation of the molecular frontier orbits, the more delocalization of π-electrons and suitable energy levels. In the following section, we present the recent advances in the molecular structural design of donor and acceptor materials and discuss the relationship between structure and various OSC performance.

2.1 Donor materials in the OSCs

2.1.1 Polymer donors in the OSCs.
Based on the early literature survey, polymer donors such as P3HT, PTB7, PTB7-Th *et al.* were synthesized to match with fullerenes and their derivatives, which facilitated the development of OSCs. P3HT was among the most valuable donor materials due to the large-scale preparation and easy to tune the optoelectronic properties. Despite much research effort, OSCs based on P3HT:PC$_{61}$BM achieved a PCE of only ∼5%.[20] This was because the super miscibility between P3HT and fullerenes and their derivatives, which lead to a poor phase separation in the active layer and restrict its further development. OSCs based on P3HT:O-IDTBR with a complementary absorption increased the PCE to 6.4% (due to a higher J_{sc}) as well as increasing the stability.[21] Peng *et al.* reported a NFA TrBTIC with good energy level matching with P3HT. They controlled the phase separation degree of P3HT:TrBTIC by varying the aging time in 1,2,4-trimethylbenzene (TMB) solution and obtained a high PCE of 8.25%.[22] Recently, Hou *et al.* synthesized a new NFA ZY-4Cl and they got a higher PCE of 9.46% based on P3HT:ZY-4Cl.[23] Later, they further pushed the PCE to 10.24% by preparing ternary devices with a third solid additive.[24] What's more, alternatives were designed, such as the P3HT derivative P4T2F-FD with electron-withdrawing fluorine atoms attached to the skeleton, which result in a lower HOMO. This donor yielded the highest PCE of 13.34% when combined with the Y6-BO acceptor in nonhalogenated solvent.[25]

PTB7 is another well-known polymer donor, which gave a PCE of ∼7.76% based on PTB7:PCBM with 1,8-diiodooctane (DIO).[26] However, PTB7 was soon superseded by its derivative PTB7-Th with 2-ethylhexyl-thienyl units introduced into the BDT group, thereby increasing both the molecular coplanarity and corresponding absorption coefficient as well as reducing the bandgap.[27] A high PCE of 10.1% was achieved based on PTB7-Th:PC$_{70}$BM.[28] In 2015, Zhan *et al.* developed a famous NFA ITIC and they blended PTB7-Th with ITIC, which obtained a PCE of 6.80% for the efficient charge transfer.[29] Later, the devices of PTB7-Th and CO*i*8DFIC blends had PCEs of 12.16% and 14.62% for binary and ternary devices, respectively.[30,31] Recently, tandem OSCs with an PTB7-Th:BTPV-4F:PC$_{71}$BM active layer as the rear cell accomplished a high efficiency of 16.4%.[32] The molecular structures of some representative polymer donors used in NFA-OSCs are shown in Fig. 1.

This journal is © The Royal Society of Chemistry 2022

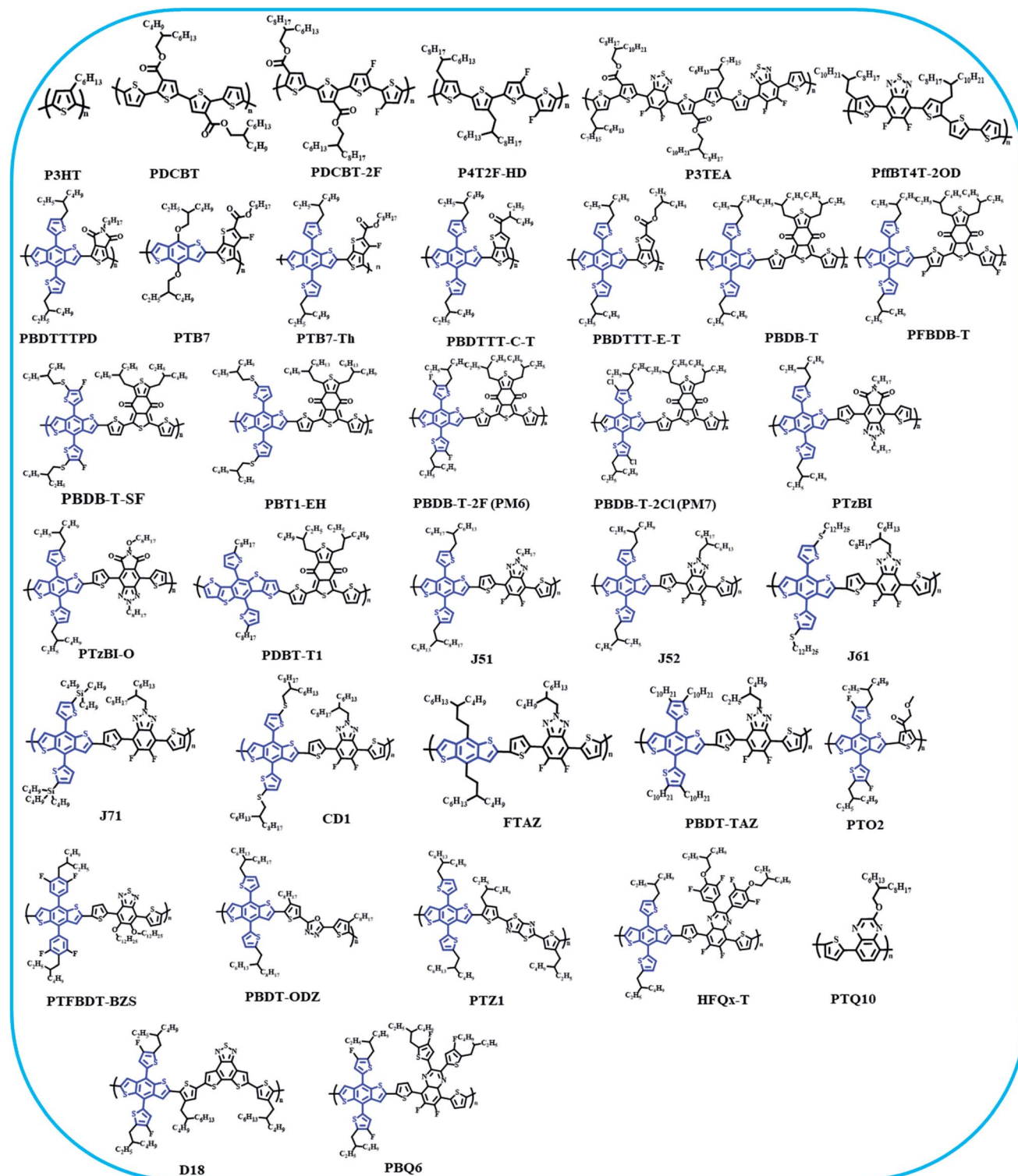*J. Mater. Chem. A*, 2022, **10**, 3255–3295 | **3257**

Fig. 1 Molecular structures of representative polymer donors used in NFA-OSCs.

To offer complementary absorption with narrow-bandgap NFAs, many wide-bandgap polymer donors are designed and synthesized, such as J-series, PBDB-series, PTQ10 and D18 and so on. Among them, PBDB-T, PBDB-T-2F (PM6) and D18 were the most frequently used polymers for their good processability, suitable energy levels and better phase separation. The PCEs have been over 18% by blending these polymers with NFAs. The details of these high-performance polymer donors will be discussed in the following acceptor materials section.

2.1.2 Small-molecule donors in the OSCs. In view of the reproducibility of polymer-based OSCs are arduous, all-small-molecule (ASM) OSCs have attracted considerable attention as

they have negligible batch-to-batch variation, along with benefits such as a well-defined chemical structure, easier purification and defined molecular weight.[33] Here we will present some high-performance small-molecule donors and give a deep review of the related OSCs device results.

In 2017, Li *et al.* reported two wide-bandgap small-molecule donors, SM1 and SM2 with weak electron-withdrawing groups.[34] The devices fabricated based on SM1:IDIC yielded a PCE of 10.11% with a high FF of 73.55%, which was much higher than that of SM2:IDIC (PCE of 5.32%). The results indicate that the cyano substitution in end group plays an important role in improving the photovoltaic performance. Later, this group synthesized another two small-molecule donors H21, H22, with alkylsily–thienyl conjugated side chain on BDT central units.[35] A high PCE of 10.29% was obtained based on H22:IDIC with V_{oc} of 0.942 V and FF of 71.15%. Wei *et al.* reported the devices based on ZR1:Y6 with a high PCE of 14.34%.[36] Though the strong crystallinity of ZR1 may increase the possibility of forming oversized phase-separated domains in the blended films, the existence of hierarchical morphologies is beneficial for the charge separation and transport. These studies showed that the crystallinity of donors was two-faced for modulating the phase separation between the donors and acceptors in OSCs. Considering this, a new donor (BTR-Cl) was developed by replacing an alkyl side chain with a Cl atom on the benzodithiophene terthiophene rhodanine (BTR) moiety.[37] Devices based on BTR-Cl:Y6 yielded an excellent PCE of 13.6% due to appropriate phase separation of the active layer. A later study enhanced the performance of BTR-Cl:Y6 system by modulating the morphology *via* changing the concentration of the precursor solution, which increased the J_{sc} while minimising recombination, resulting in a PCE of 14.7%.[38] Recently, Lu *et al.* fabricated binary OSCs based on BTR-Cl with a new NFA BTP-FCl-FCl, which gave a high PCE of 15.3% with a FF of 75.3%.[39] The improved charge generation and extraction arise from lower total dipole moment and lower distribution disorder. After that, ternary devices based on BTR-Cl:Y6:PC$_{71}$BM achieved a record PCE of 15.34% with an increased FF of 77.11%.[40] Later, the same group reported another liquid crystalline donor L2 by selenophene substitution.[45] The selenide donor L2 shows higher intramolecular interaction and presents a novel sematic liquid crystal phase, which results in more favored morphology, better light harvest and lower charge recombination with a high PCE of 15.8%. By changing the meta-position of sulphur alkyl chins of B3T-P to the para-position, a new small molecule donor named B1 was reported by Hou *et al.*[46] When prepared the ternary OSCs, a record PCE over 17% was achieved by adding BO-2Cl in the binary B1:BO-4Cl films. This is the best PCE ever reported based on all-small molecule OSCs. The molecular structures of some representative SM donors are depicted in Fig. 2 and Table 1 lists the PV performance of representative SM donors.

In summary, ASM OSCs have made substantial progress in the past few years, with the highest PCE close to 17%. However, certain key issues need to be addressed to facilitate the development of NF-ASM OSCs. For instance, morphology control remains the most problematic concern because it is difficult to form a continuous interpenetrating network owing to the strong crystallinity of small-molecule donors.[48] Additionally, novel post-processing methods or suitable additives, which are helpful in modulating the morphology, must be developed. If such limitations can be overcome, the developments of ASM OSCs will go a step further.

2.2 Non-fullerene acceptor materials in the OSCs

2.2.1 Non-fullerene small-molecule acceptors with PDI units.

It is well known that NFAs have the advantages of adjustable energy levels, NIR region absorption, and good thermal and photo-stability. Among these NFAs, perylene diimide units (PDI), with a broad and planar structure, high photochemical stability, easy synthesis and modification are widely used as n-type materials. In 2013, PDI dimers of bis-PDI-T-EG were developed, which were linked directly through thiophene.[49] This small molecule acceptor (SMA) showed significantly reduced aggregation compared to its monomeric counterpart and obtained a PCE of 4.03% based on PBDTTT-C-T:bis-PDI-T-EG. This strategy can suppress excessive aggregation between molecules and promote better charge transfer in the active layers. In 2016, Yan *et al.* reported SF(PDI)$_2$ SMA with spirofluorene as the π bridge.[50] OSCs based on P3TEA:SF(PDI)$_2$ exhibited a high PCE of 9.5% and nearly 90% internal quantum efficiency with a low voltage loss (E_{loss}) of 0.61 V.

In addition, molecules in which three or four PDIs are bound to a core, usually through their bay positions, have been extensively developed. Zhan *et al.* reported S(TPA-PDI) SMA with a triphenylamine (TPA) core.[51] This SMA has a quasi-3D nonplanar structure and isotropic optical and charge-transport properties, which weaken molecular aggregation. Later, a high PCE of 6.1% was obtained for PDBT-T1:TPA-PDI-Se, which was 38% higher than the S(TPA-PDI) reference without heteroatom annulation (PCE of 3.32%).[52] By replacing the core with 1,3,5-triazine, a new SMA with a less twisted molecular geometry as well as high crystallinity was demonstrated. Devices based on PTB7-Th:Ta-PDI exhibited a higher PCE of 8.91% for the improved π–π stacking and carrier mobility.[53]

By fusing the PDI units at the bay positions, a large nonplanar molecular geometry is formed, which can not only enhanced conjugation and molecular-packing order, but also maintain a nonplanar structure. Alex *et al.* synthesized several novel fused-derivative SMAs, FPDI-X (X = O, S, Se) through the oxidative cyclisation of PDI-T.[54] In this work, the five-membered ring creates a nonplanar skeleton which increases effective π-conjugation and delocalisation of the LUMO. Consequently, a PCE of 6.72% was obtained based on PTB7-Th:FPDI-T, which was almost double of the PCE of PDI-T-based OSCs (PCE = 3.68%). Similarly, three PDI monomers were fused with phenyl to synthesize NFA TPH and selenium-annulated TPH-Se.[55] Single-crystal structures showed a 3D networks of propeller-like THP and TPH-Se, which facilitate electron transport, resulting in high PCEs of 8.28% and 9.28%, respectively. The chemical structures of some of the PDI SMAs are shown in Fig. 3 and Table 2 lists the PV performance of representative PDI SMAs.

This journal is © The Royal Society of Chemistry 2022

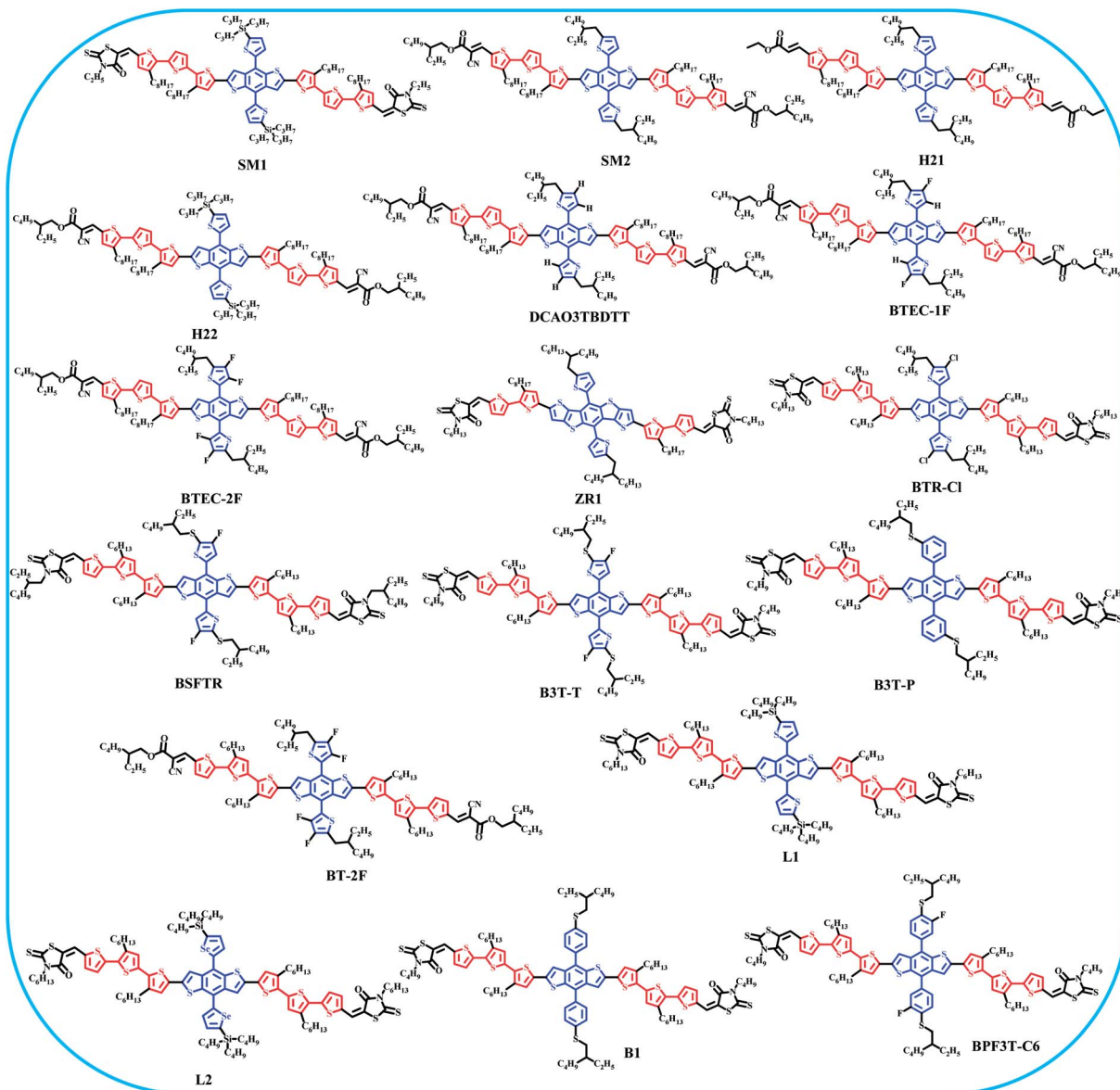*J. Mater. Chem. A*, 2022, **10**, 3255–3295 | **3259**

Fig. 2 Molecular structures of representative small-molecule donors.

2.2.2 Non-fullerene small-molecule acceptors with unfused-ring core. Unfused-ring SMAs refer to those with partially or fully unfused backbone structures,[57] where non-covalent intramolecular interactions are used to mediate the planarity of the molecular structures. Such molecules can usually be prepared by simple synthesis methods. In 2016, Chen *et al.* synthesized an unfused-ring SMA (DICTF) in three steps.[58] They achieved a high PCE of 7.93%, which provides a good example of a successful trade-off between conversion efficiency and cost. Bazan *et al.* reported two ultra-narrow bandgap unfused-ring SMAs with absorption range beyond 1000 nm (E_g of 1.1 eV), COTI-4F and SiOTI-4F, which insert alkoxythiophene as π bridge.[59] The devices based on PTB7-Th:SiOTI-4F achieved a PCE of 9%.

The synthesis process can be significantly simplified owing to the simplicity of unfused molecular structures, while enriching the diversity of molecular design. In 2017, Chen *et al.* reported

DF-PCIC with an 2,5-difluorobenzene (DFB) unfused-ring core and two 4*H*-cyclopenta[1,2-*b*:5,4-*b*]dithiophene (CPDT) moieties, which yielded a PCE of 10.14%.[60] Moreover, the corresponding devices maintained ∼70% of the original PCEs upon thermal treatment at 180 °C for 12 h, which was attributed to the F···H non-covalent bond between CPDT and DFB. Since then, several research groups focused on the development of unfused-ring SMAs based on CPDT units for easily generating non-covalent intramolecular interactions. Bo *et al.* synthesized several SMAs with 2,5-bis(alkyloxy)phenylene unit core.[61] A highest PCE of 13.24% was obtained based on PBDB-T:DOC2C6-2F with a very low non-radiative recombination voltage losses of only ∼0.2 eV, which was the best performance at that time. Very recently, Huang *et al.* reported a SMA NoCA-5 by terminal side-chain (T-SC) engineering.[62] Surprisingly, they prepared devices of J52:NoCA-5 and obtained a record PCE of 14.82% with J_{sc} of 26.02

3260 | *J. Mater. Chem. A*, 2022, **10**, 3255–3295

This journal is © The Royal Society of Chemistry 2022

Table 1 List of ASM OSCs with device characteristics

Donor	Acceptor	V_{oc} (V)	J_{sc} (mA cm^{-2})	FF	PCE (%)	Ref.
SM1	IDIC	0.905	15.18	73.55	10.11	34
SM2	IDIC	0.768	10.77	64.40	5.32	34
H21	IDIC	0.895	13.00	65.58	7.62	35
H22	IDIC	0.942	15.38	71.15	10.29	35
DCAO3TBDTT	Y6	0.804	21.71	60.95	10.64	42
BTEC-1F	Y6	0.870	21.21	61.35	11.33	42
BTEC-2F	Y6	0.854	21.55	72.35	13.34	42
ZR1	Y6	0.861	24.34	68.44	14.34	36
BTR-Cl	Y6	0.86	24.17	65.50	13.61	37
BTR-Cl	Y6	0.83	23.66	74.7	14.7	38
BTR-Cl	BTP-FCl-FCl	0.825	24.58	75.36	15.3	39
BSFTR	Y6	0.85	23.16	69.66	13.69	43
B3T-T	BO-4Cl	0.867	21.9	58.21	11.1	41
B3T-P	BO-4Cl	0.815	25.7	72.4	15.2	41
BT-2F	N3	0.845	24.28	75.02	15.39	44
L1	Y6	0.83	25.28	69.8	14.6	45
L2	Y6	0.83	26.35	72.1	15.8	45
B1	BO-4Cl	0.82	25.39	73	15.2	46
BPF3T-C6	BO-4Cl	0.857	24.7	70.2	15.2	47

mA cm^{-1}. Further study showed that introduction of T-SCs can enhance molecular rigidity, intermolecular π–π stacking, lower reorganization free energy and shorter π–π stacking distance.

Our group reported two SMAs with electron-deficient diketone core recently.[63] This design strategy can avoid the higher-lying HOMO levels of the SMAs when paired with the wide
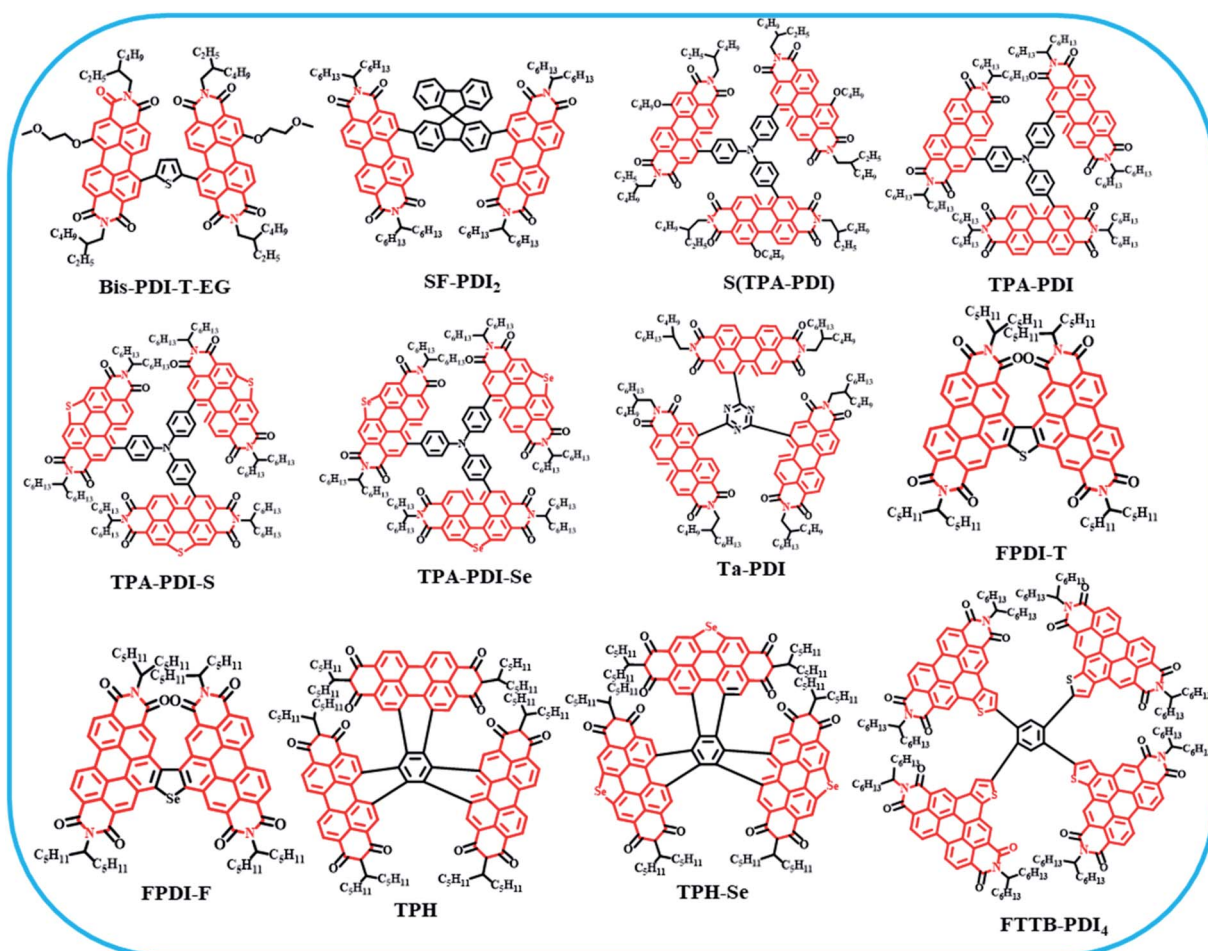

Fig. 3 Chemical structures of PDI small-molecule acceptors.

Table 2 Summary of the photovoltaic performance of OSCs with PDI small-molecule acceptors

NFA	E_g^{opt} [eV]	HOMO/LUMO [eV]	Donor	V_{oc} [V]	J_{sc} [mA cm^{-2}]	FF [%]	PCE [%]	Ref.
Bis-PDI-T-EG	1.81	−5.65/−3.84	PBDTTT-C-T	0.85	8.86	54.1	4.03	49
SF-PDI$_2$	—	−5.99/−3.62	P3TEA	1.11	13.27	64.3	9.5	50
S(TPA-PDI)	1.76	−5.40/−3.70	PBDTTT-C-T	0.88	11.92	33.6	3.32	51
TPA-PDI	1.84	−5.72/−3.88	PDBT-T1	0.94	9.91	47	4.42	52
TPA-PDI-S	1.94	−5.73/−3.79	PDBT-T1	0.99	9.53	60	5.66	52
TPA-PDI-Se	1.94	−5.74/−3.80	PDBT-T1	0.99	10.38	59	6.10	52
Ta-PDI	2.05	−6.03/−3.81	PTB7-Th	0.78	17.1	68.5	8.91	53
FPDI-T	2.22	−5.98/−3.77	PTB7-Th	0.93	12.28	59	6.72	54
FPDI-Se	2.22	−5.96/−3.76	PTB7-Th	0.92	11.36	56	5.77	54
TPH	2.19	−6.02/−3.83	PDBT-T1	0.96	12.20	70.4	8.28	55
TPH-Se	2.17	−5.97/−3.80	PDBT-T1	1.0	12.72	72.1	9.28	55
FTTB-PDI$_4$	2.14	−5.74/−3.58	P3TEA	1.13	14.05	66.4	10.58	56

bandgap polymer donors with deep HOMO levels, such as PM6 and PTQ10. As a result, devices based on PM6:TPDC-4F exhibited a high PCE of 13.35%. This research provided an effective method to elaborately design non-fused ring electron acceptor with decent performance.

In order to further reduce the synthesis steps and complete simpler SMAs, many acceptors with fully unfused backbone structures were reported. Among these, Chen *et al.* developed two fully unfused SMAs PTB4F and PTB4Cl *via* two-step synthesis from single aromatic units.[64] Their research showed that the introduction of two-dimensional chain and halogenated terminals plays synergistic roles in optimizing the solid stacking and orientation, thus promoting an elongated exciton lifetime and fast charge transfer rate in bulk heterojunction blends. Devices based on PM6:PTB4Cl enabled PCE of 12.76%. Recently, Hou *et al.* reported a totally unfused SMA named A4T-16, which contains bithiophene-based non-fused core (TT-Pi) with good planarity as well as large steric hindrance.[67] This molecule exhibited a three-dimensional interpenetrating network due to the compact π–π stacking between the adjacent end-capping groups. OSCs based on PBDB-TF:A4T-16 exhibited a high PCE of 15.2% with a FF of 79.8%. What's more, the device retains ~84% of its initial PCE after 1300 h under the simulated AM 1.5 G illumination (100 mWcm^{-2}), which shows good stability. Further, they modified the π bridges and end groups with cyano-rhodanine (RCN)-modified benzotriazole (BTA) units and synthesized another unfused SMA, namely GS-ISO.[68] This acceptor with a wide bandgap of 1.81 eV is ideal for making single junction cells for indoor photovoltaic applications and the front sub cells in the tandem OPV cells. They prepared devices with polymer PBDB-TF and yielded a PCE of 11.62% with a remarkable V_{oc} of 1.21 V. What's more, under a 500-lux light-emitting diode (LED) illumination, the GS-ISO-based cell exhibits an outstanding PCE of 28.37%, and the tandem OPV cell in which the GSISO-based cell works as front sub cell yields a PCE of 19.10%. This work demonstrates the superiorities of cyano-rhodanine (RCN)-modified benzotriazole (BTA) end groups used for synthesizing wide-bandgap NFAs and applying in indoor and tandem OPVs.

Bo *et al.* synthesized unfused SMAs 2BTh-2F, which shows a 3D network packing.[70] The devices of D18: 2BTh-2F gave a PCE

of 15.44%, which was the highest value reported for solar cells based on unfused-ring small molecule acceptors. The chemical structures of unfused-ring SMAs are shown in Fig. 4 and Table 3 lists the PV performance of representative unfused-ring SMAs.

2.2.3 Non-fullerene polymer acceptors with rylene diamide units. In addition to SMAs, polymer acceptors are promising candidates for fabricating high-performance OSCs. The polymer-based acceptors possess some outstanding characteristics, which cannot be provided by SMAs, such as good film-forming performance. Furthermore, all-polymer solar cells offer potential advantages, including long-term thermal and mechanical stability.[82] In this section, we will discuss the polymer acceptors based on PDI and naphthalene diimide (NDI) units alternated with π bridges for high-performance PSCs.[83,84]

Zhao *et al.* reported polymer acceptor of PDI-V and NDP-V, which the vinylene linkers were used to improve the backbone planarity by reducing steric hindrance around the PDI bay region, thus potentially improves π–π stacking and charge transport.[83,85] All-PSC based on the two acceptors showed PCEs of 7.57% and 8.59%, respectively. Although NDI units have electron affinities comparable to those of PDI units, conjugated NDI polymers possessed several merits such as more planar backbones, delocalization and denser π stacking for the less steric congestion. A famous NDI-bithiophene polymer acceptor N2200 was reported and directly attracted extensive attention of researchers. The PSCs with N2200 achieved very low PCE of 0.16% at the beginning, which was later increased to 9.16% when combined with donor PTzBI.[84] Chen *et al.* synthesized two novel NDI-based polymer acceptors, PNDI-2T-TR5 with rhodanine-based dye introducing into the side chain of thiophene.[86] The all-PSC based on PNDI-2T-TR5 showed a PCE of 8.13% due to its high absorption coefficient and up-shifted LUMO level. Duan *et al.* reported a new polymer acceptor by incorporating different percentages of linear ethylene oxide (OE) side chains into NDI units.[87] PSC based on polymer NOE10 attained a PCE of 8.1%. Moreover, OE engineering of the side chains can improve the blend-film morphology and long-term thermal stability with >97% of the initial PCE being maintained after 300 hours aging at 65 °C of all-PSCs. The chemical structures of polymer acceptors based on PDI and NDI acceptor units are shown in Fig. 5 and Table 4 lists the PV performance of
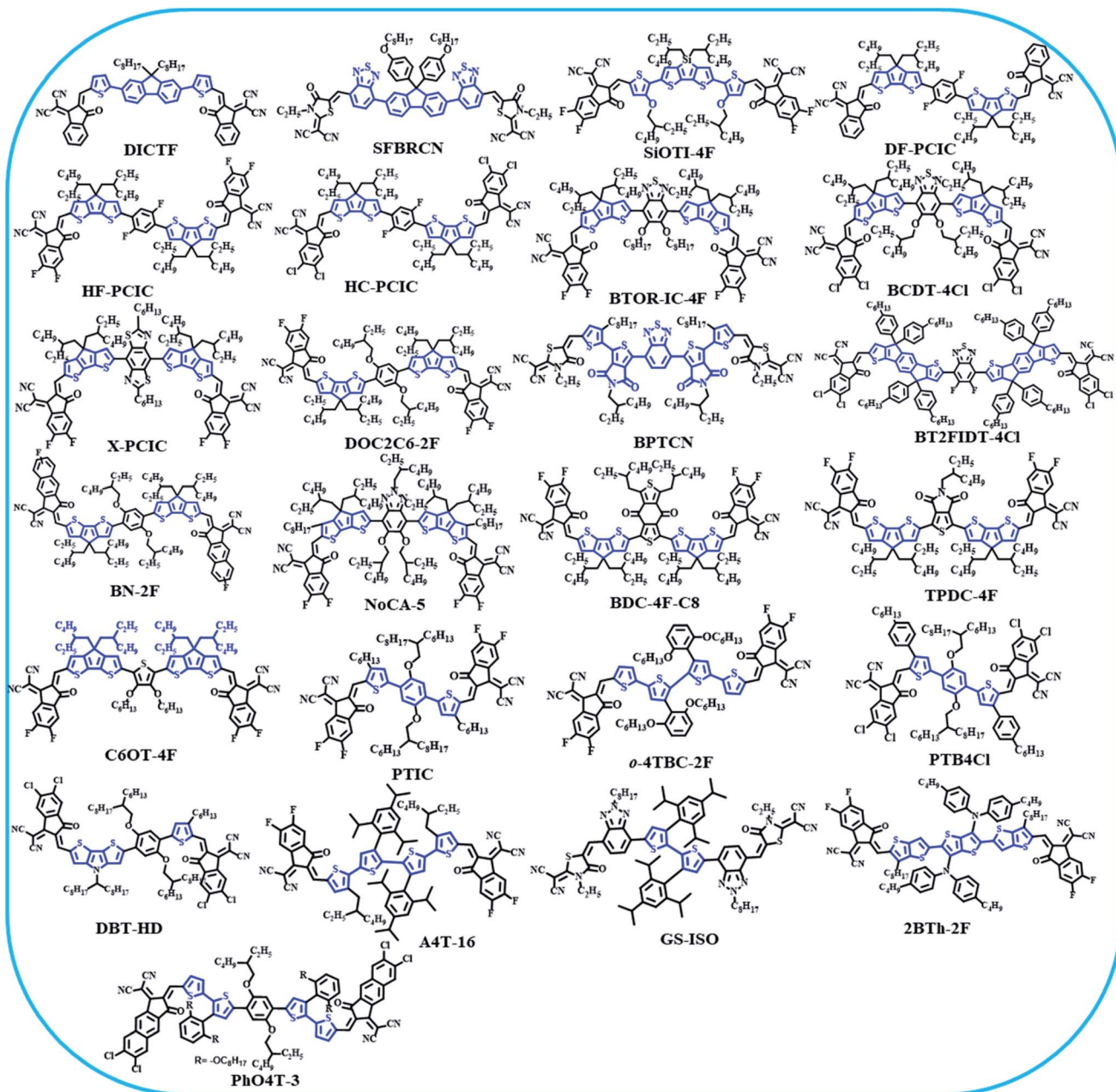
Fig. 4 Chemical structures of unfused-ring small-molecule acceptors.

some representative polymer acceptors based on PDI (NDI) units.

2.2.4 Non-fullerene polymer acceptors with other units. Though polymer acceptors based on PDI and NDI units have been researched by many groups, their inherent defects restricted the further enhancement in device performance. Therefore, it is challenging to choose suitable electron-withdrawing units and synthesize polymer acceptors with appropriate HOMO and LUMO energy levels. Liu et al. first reported polymer acceptors by replacing a C–C unit with a B←N unit. After elaborately optimising the molecular design, they synthesized several polymer acceptors and achieved decent PCEs.[93] Lately, they continuously reported a series of polymer

acceptors with B←N unit. Among them, polymer PBN-12 with B←N and BT units up-shifted the HOMO energy level with a reduced E_g. Hence, an all-PSC device based on PBN-12 showed a PCE of 10.1%, which is among the highest values reported for all-PSCs based on B←N units.[94]

Bithiophene imide (BTI) units with merits of coplanar structure, short intermolecular π–π stacking distance, and favourable solubilising substituent orientations were also used to synthesize new n-type semiconductors.[95] Guo et al. reported polymer acceptor L14 with an acceptor–acceptor strategy and gave a high PCE of 14.3%.[96] Very recently, their group reported a record PCE of 15.62% by green-solvent processing.[97]

This journal is © The Royal Society of Chemistry 2022

J. Mater. Chem. A, 2022, 10, 3255–3295 | 3263

Table 3 Summary of the photovoltaic performance of OSCs using unfused-ring small-molecule acceptors

NFA	E_g^{opt} [eV]	HOMO/LUMO [eV]	Donor	V_{oc} [V]	J_{sc} [mA cm^{-2}]	FF [%]	PCE [%]	Ref.
DICTF	1.82	−5.67/−3.79	PTB7-Th	0.86	16.61	56	7.93	58
SFBRCN	2.05	−5.93/−3.86	PTB7-Th	0.9	17.25	65.2	10.12	66
SiOTI-4F	1.7	−5.28/−4.11	PTB7-Th	0.66	22.6	65.1	9.0	59
DF-PCIC	1.59	−5.49/−3.77	PBDB-T	0.91	15.66	72.1	10.14	60
HF-PCIC	1.50	−5.53/−3.83	PBDB-TF	0.91	11.78	70.7	11.49	57
HC-PCIC	1.67	−5.54/−3.87	PBDB-TF	0.89	18.13	72.1	11.75	69
BTOR-IC4F	1.37	−5.92/−4.23	PBDB-T	0.8	20.57	69.6	11.48	71
BCDT-4Cl	1.38	−5.47/−3.88	PBDB-T	0.76	23.77	67	12.10	72
X-PCIC	1.37	−5.37/−3.79	PBDB-T	0.84	21.8	62.5	11.5	73
DOC2C6-2F	1.42	−5.49/−3.83	PBDB-T	0.85	21.35	73.1	13.24	61
BPTCN	1.72	−5.38/−3.66	PTB7-Th	0.81	14.68	54	6.42	74
BT2FIDT-4Cl	1.56	−5.70/−3.88	PM7	0.97	18.1	71.5	12.5	75
BN-2F	1.40	−5.39/−3.99	J52	0.81	25.25	70.78	14.53	76
NoCA-5	—	−5.43/−3.83	J52	0.814	26.02	69.96	14.82	62
BDC-4F-C8	1.41	−5.66/−3.73	PM6	0.89	21.32	65.6	12.53	77
TPDC-4F	1.42	−5.83/−3.99	PM6	0.852	22.19	70.6	13.35	63
C6OT-4F	1.24	−5.36/−4.03	PTB7-Th	0.76	21.5	60.1	9.83	81
o-4TBC-2F	1.34	−5.63/−4.00	PBDB-T	0.76	20.48	65.7	10.26	79
PTIC	1.53	−5.59/−3.71	PBDB-TF	0.93	16.73	66	10.27	80
PTB4Cl	1.58	−5.91/−3.93	PBDB-TF	0.93	19.01	72.17	12.76	64
DBT-HD	1.38	−5.63/−3.95	PBDB-T	0.85	21.75	73.39	13.57	65
A4T-16	1.45	−5.67/−3.96	PBDB-TF	0.876	21.8	79.8	15.2	67
GS-ISO	1.81	−5.51/−3.69	PBDB-TF	1.21	13.65	70.38	11.62	68
2BTh-2F	1.43	−5.55/−3.98	D18	0.90	23.61	72.3	15.44	70
PhO4T-3	—	−5.58/−4.09	PBDB-T	0.839	23.03	71.21	13.76	78

Li et al. first demonstrated a strategy to synthesize high-performance polymer acceptors by embedding an acceptor–donor–acceptor building block into the polymer main chain in 2017.[98] This strategy shows good potential for polymer acceptors because it overcomes the limitation of poor absorption at long wavelengths. For example, polymer acceptor PZ1 was embedded as an IDIC building block into the polymer main chain with a high absorption coefficient of 1.3×10^5 cm^{-1} and the all-PSC based on PBDB-T:PZ1 showed a PCE of 9.19%, which further increased to 11.2% when blended with PM6.[99] Very recently, Huang et al. reported a polymer acceptor named PJTVT, which contains the hienylene–vinylene–thienylene (TVT) unit.[100] The devices of JD40: PJTVT showed a PCE of 16.13% as well as superior thickness-insensitivity and long-term stability. Huang et al. synthesized a narrow-band-gap polymer acceptor PJ1 via linking the SMA building block TTPBT-IC.[101] The fabricated all-PSC based on PBDB-T:PJ1 achieved a record efficiency of 14.4%. Jen et al. reported polymer acceptor PZT-γ incorporation a benzotriazole (BTz)-core fused-ring segment.[102] By blending with PBDB-T, all-PSCs exhibited a record-high power conversion efficiency of 15.8% with a low E_{loss} of 0.51 eV. Li et al. reported polymer acceptor PN-Se and they use cryogenic transmission electron microscopy to study the aggregation behavior of the PBDB-T donor and the polymer acceptor.[104] Then they found that a bicontinuous-interpenetrating network with aggregation size of 10–20 nm and this was very favourable for the charge transfer and a high PCE of 16.16% was achieved in the OSCs. These results indicate that FREA polymerisation is a promising strategy to develop highly efficient polymers for all-PSCs. Fig. 6 depicts the chemical structures of polymer acceptors based on these units. The photovoltaic performance of the polymer acceptors based on other units is summarised in Table 5.

2.2.5 Non-fullerene small-molecule acceptors with IDT-type fused-ring core. FREAs refer to those with a large fused-ring core substituted with aryl or alkyl side chains and incorporate two strong electron-withdrawing terminal groups. Much effort has been devoted to improving FREA-based OSCs by varying the fused-ring core, side chains and end group. Through these modifications, the absorption wavelength, energy levels, and film morphology can be purposefully tuned to achieve larger V_{oc}, J_{sc}, FF, and PCE. In this part, we discuss the role of such modifications on FREAs and give a presentation to the relationship between molecular design and device performances.

2.2.5.1 Modifications on the end group. In 2015, a new FREA ITIC with a dithieno[2,3d:2′,3′d′]-sindaceno[1,2b:5,6b′]dithiophene (IDTT) core and 2-methylene-(3-(1,1-dicyanomethylene) indanone) (IC) end group was developed by Zhan et al.[29] The OSC of PTB7-Th:ITIC showed a PCE of 6.8%, which was limited by the spectral overlap of the PTB7-Th and ITIC absorption bands. Therefore, by blending with PBDB-T and J71 polymer with wide-bandgap, the devices achieved PCEs of 11.21% and 11.41%, respectively.[109,110] The IC end-group unit was elaborately modified by introducing electron-donating or electron-withdrawing units to fine tune energy levels and morphology. Hou et al. synthesized IT-M and IT-OM2 by introducing methyl and methoxyl units to the IC group and upshifted both the LUMO/HOMO levels of the related FREAs.[111,112] As results, the IT-M and IT-OM2-based OSCs achieved high PCE of 12.05% and 11.9%, respectively. Another famous acceptor IT-4F was

3264 | J. Mater. Chem. A, 2022, **10**, 3255–3295

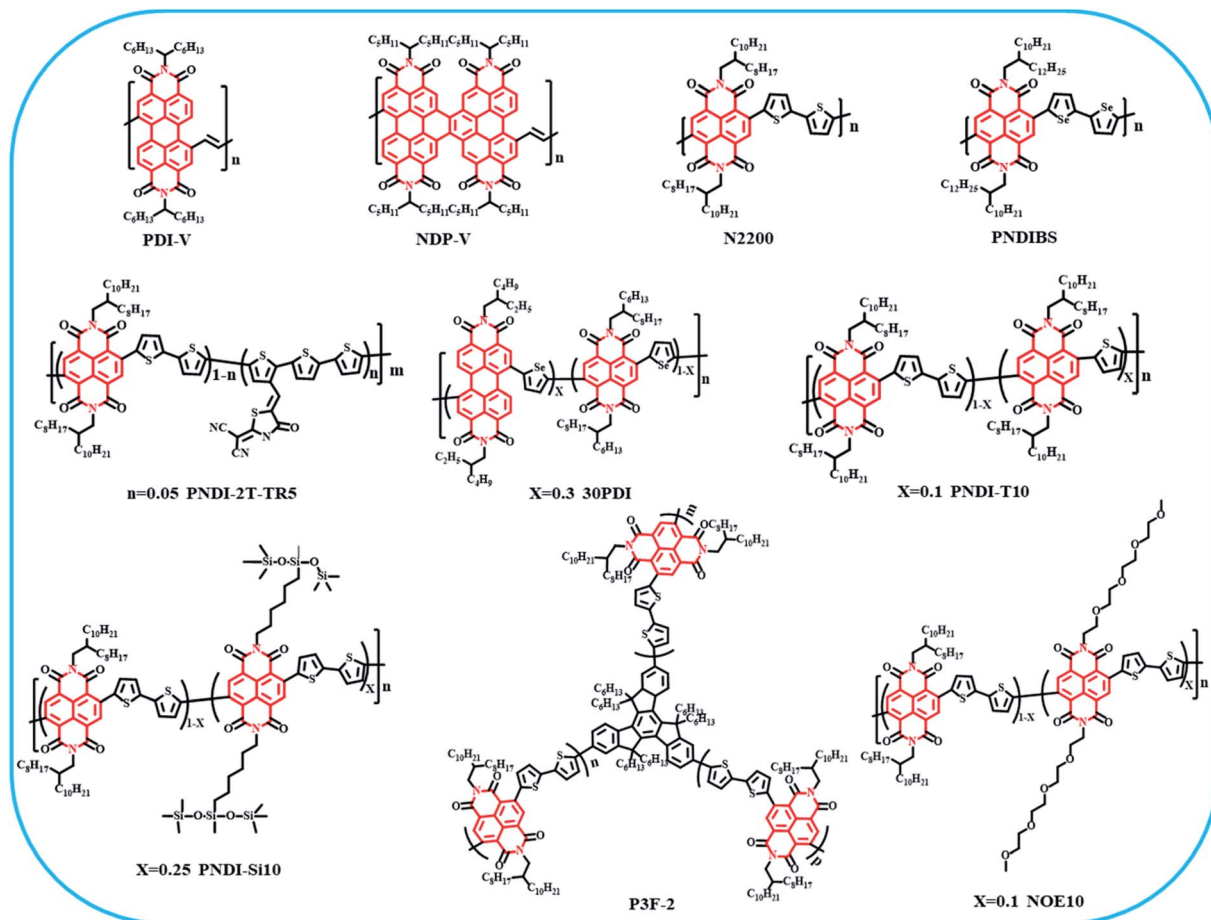This journal is © The Royal Society of Chemistry 2022

Fig. 5 Chemical structures of polymer acceptors based on PDI acceptor units.

Table 4 Summary of the photovoltaic performance of polymer acceptors based on PDI (NDI) units

NFA	E_g^{opt} [eV]	HOMO/LUMO [eV]	Donor	V_{oc} [V]	J_{sc} [mA cm^{-2}]	FF [%]	PCE [%]	Ref.
PDI-V	1.74	−5.77/−4.03	PTB7-Th	0.74	16.1	64	7.57	83
NDP-V	1.91	−5.94/−4.03	PTB7-Th	0.74	17.07	67	8.59	85
N2200	1.50	−5.45/−4.00	PTzBI	0.84	15.6	70.1	9.16	84
PNDIBS	1.4	−5.95/−3.94	PBDB-T	0.85	18.32	57	9.38	88
PNDI-2T-TR5	1.48	−5.91/−3.91	PBDB-T	0.85	14.83	64.3	8.13	86
30PDI	1.77	−5.95/−3.89	PBDTTT-C-T	0.79	18.55	45	6.29	89
PNDI-T10	1.55	−6.36/−4.05	PTB7-Th	0.83	12.9	71	7.6	90
PNDI-Si25	1.43	−6.08/−3.82	PBDB-T	0.85	12.8	68	7.4	91
NOE10	1.46	−5.81/−3.91	PBDT-TAZ	0.84	12.9	75	8.1	87
P3F-2	1.50	−5.89/−3.84	PTzBI-O	0.87	14.27	64.0	8.0	92

reported by introducing fluorine atom, which significantly enhanced intramolecular interaction and promote charge transfer. The PTO2:IT-4F devices achieved a high PCE of 14.7% and further enhanced to 15.3% based on PFBCPZ:IT-4F, which was the highest PCE for IT-4F-based OSCs so far.[113,114] As modification of IC terminals successfully produced FREAs with different optoelectronic properties, this strategy is promising for improving the performance of OSCs.

2.2.5.2 Modifications of the fused-ring core. In 2016, Zhan *et al.* reported a new high μ_e (1.1×10^{-3} cm^2 V^{-1} s^{-1}) FREA

IDIC.[117] OSCs based on IDIC showed a PCE of 8.71% when paired with PBDB-T1 donor. Different from ITIC with serious steric hindrance phenyl side chains, IDIC with alkyl side chains exhibited strong crystallinity and closer π–π stacking, thus endowed the blend films better regularity and this may result in inferior performance in turn. SMAs with a *S,N*-heteroacene backbone were reported by Alex *et al.*[118] They introduced the electron-donating pyrrole rings, thus increasing the LUMO energy levels. Devices based on SN6IC-4F showed a high PEC of 13.2%. Ding *et al.* reported a FREA CO*i*8DFIC with C–O-bridged

This journal is © The Royal Society of Chemistry 2022

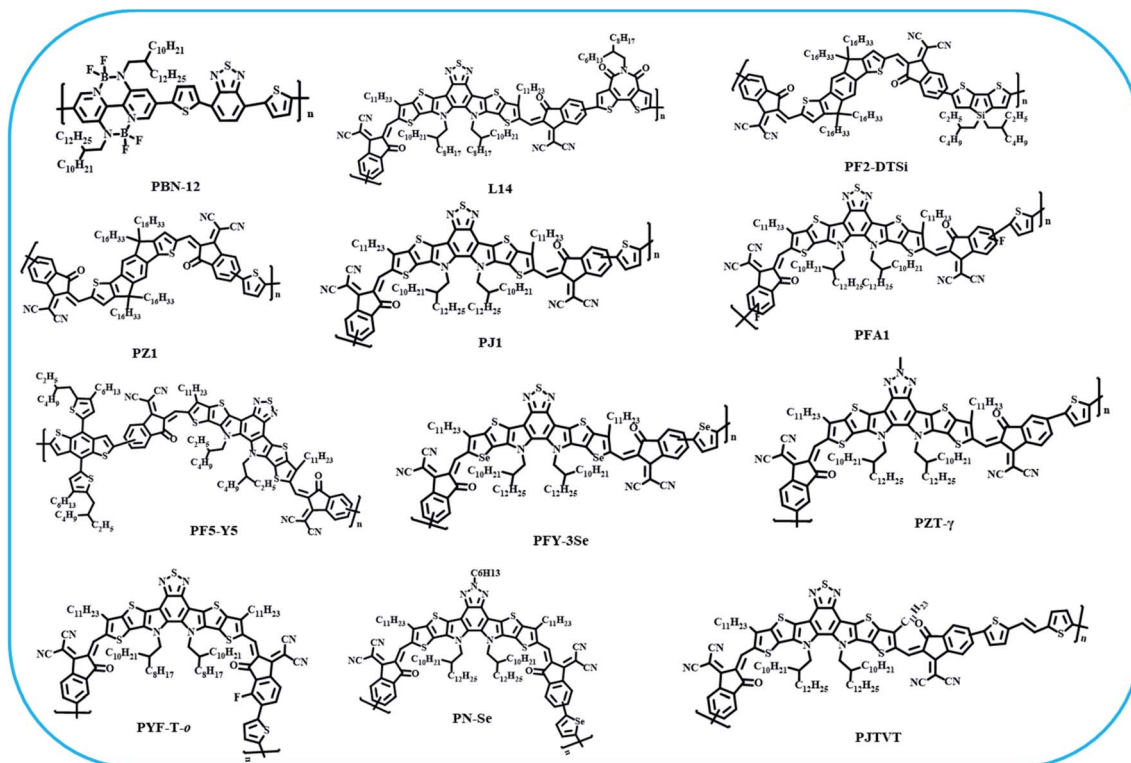*J. Mater. Chem. A*, 2022, **10**, 3255–3295 | **3265**

Fig. 6 Chemical structures of polymer acceptors based on other units.

Table 5 Photovoltaic performance of OSCs using polymer acceptors based on other units

NFA	E_g^{opt} [eV]	HOMO/LUMO [eV]	Donor	V_{oc} [V]	J_{sc} [mA cm^{-2}]	FF [%]	PCE [%]	Ref.
PBN-12	1.78	−5.52/−3.45	CD1	1.17	13.39	64	10.07	94
L14	1.39	−5.79/−4.40	PM6	0.96	20.6	72.1	14.3	96
PZ1	1.55	−5.74/−3.86	PM6	0.96	17.1	68.2	11.2	99
PF2-DTSi	1.57	−5.74/−3.87	PM6	0.99	16.48	66.1	10.77	105
PJ1	1.41	−5.64/−3.82	PBDB-T	0.90	22.3	70	14.4	101
PFA1	1.41	−5.74/−3.84	PTzBI-oF	0.87	23.96	72.6	15.11	106
PF5-Y5	1.41	−5.52/−3.84	PBDB-T	0.94	20.54	73.1	14.16	107
PFY-3Se	—	−5.65/−3.92	PBDB-T	0.871	23.6	73.7	15.1	108
PZT-γ	1.36	−5.57/−3.78	PBDB-T	0.89	24.7	71.3	15.8	102
PYF-T-o	1.38	−5.73/−3.81	PM6	0.90	23.3	72.4	15.2	103
PN-Se	1.37	−5.69/−3.88	PBDB-T	0.90	24.82	71.8	16.16	104
PJTVT	1.43	−5.57/−3.77	JD40	0.89	23.75	76.4	16.13	100

ladder-type units and gave PCEs of over 14% for single-junction and 17% for tandem OSCs.[31,119] Zheng *et al.* reported a record PCE of 16.66% based on acceptor M3 with a ladder-type heteroheptacene core.[120] Fig. 7 depicts the chemical structures of fused-ring electron acceptors modification of the end group and fused-ring core.

2.2.5.3 Side-chain engineering. Li *et al.* reported SMA *m*-ITIC, wherein the side chains exchanged *meta*-hexylphenyl groups for *para*-hexylphenyl units.[121] When paired with donor J71, *m*-ITIC showed a high PCE of 11.77% due to the higher absorption coefficient, larger crystalline coherence, and higher μ_e. The change of *para*-hexylphenyl in ITIC to *n*-octylphenyl resulted in

the C8-ITIC SMA with narrower optical band gap, higher absorptivity, and an increased crystallinity. The OSC with PFBDB-T as the donor showed a PCE of 13.2%.[122] In 2019, the MO-IDIC-2F acceptor was reported, in which alkoxy substituents were introduced into the IDIC central fused-ring unit,[115] which obtained a high PCE of 13.46% based on PTQ10:MO-IDIC-2F OSCs.

2.2.5.4 Modifications of the π bridge. In 2016, researchers reported O-IDTBR and EH-IDTBR SMAs by replacing the side chains with *n*-octyl and 2-ethylhexyl, respectively.[21] OSC of P3HT:O-IDTBR showed a high PCE of 6.3%, which pave promising prospect for P3HT-based OSCs. By replacing the

3266 | *J. Mater. Chem. A*, 2022, **10**, 3255–3295

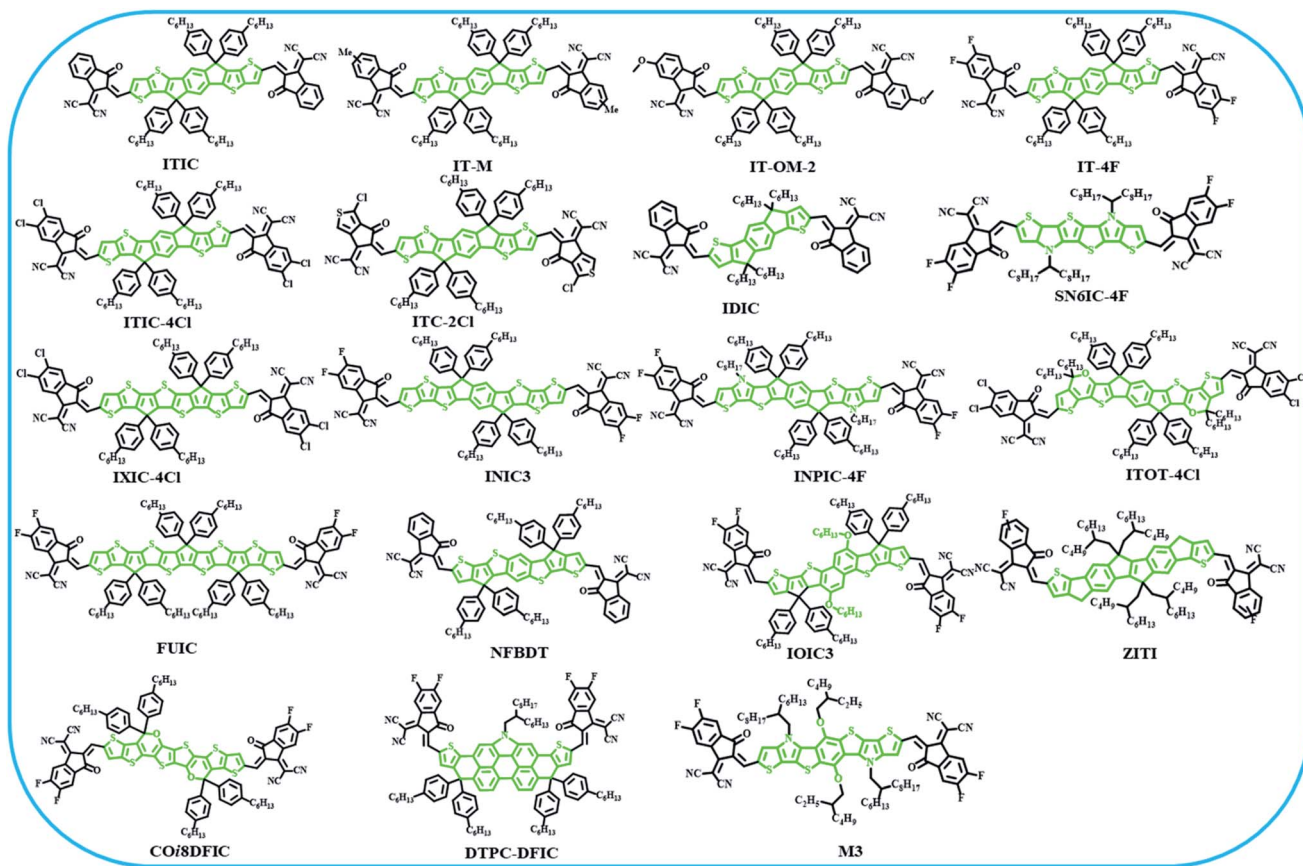This journal is © The Royal Society of Chemistry 2022

Fig. 7 Chemical structures of fused-ring small molecule acceptors modification of the end group and fused-ring core.

rhodanine-modified BT units with RCN-modified BTA groups, another well-known wide-bandgap acceptor BTA3 was synthesized by Zhou et al.[124] This acceptor possesses a large optical bandgap of 1.78 eV and uplifted LUMO and HOMO levels owing to the RCN-modified BTA end groups. By blending with a delicately designed polymer donor PBT1-C, BTA3-based OSCs showed a decent PCE of 8.6% as well as an outstanding V_{oc} of 1.21 V. What's more, a very low nonradiative recombination voltage losses ($\Delta V_{non-rad}$) of 0.16 eV was obtained by blending with another polymer PBT1-C-2Cl. This result indicates that high V_{oc} and low $\Delta V_{non-rad}$ can be achieved by the combination of an elaborate chlorinated polymer and BTA3 acceptor. Hou et al. synthesized an ultra-narrow bandgap (E_g of 1.24 eV) acceptor IEICO-4F by inserting a π bridge of 2-ethylhexyl-oxy thiophene, which showed a PCE above 10% when blended with PTB7-Th.[125] Recently, an asymmetric FREA with a unilateral alkylthio-substituted thiophene π-bridge (IDST-4F) was reported,[127] where the optimised PM6:IDST-4F-based devices had a high PCE of 14.3%. More importantly, these OSCs showed excellent thermal stability with 82% of the initial PCE remaining after thermal treatment at 150 °C for 1200 min. Fig. 8 depicts the chemical structures of fused-ring electron acceptors modification of side chain and π bridge. A summary of the PV performance of OSCs with FREAs are given in Table 6.

2.2.6 Non-fullerene small-molecule acceptors with A–DA′D–A-type fused-ring core. Since 2019, the emergence of A–DA′D–A-type FREAs, this type of acceptors has contributed to the rapid development of OSCs with PCE exceeding 18%.[11,12] Here, we will investigate the A–DA′D–A-type acceptors for high-efficiency OSCs, particularly the correlation between molecular structure and optoelectronic properties.

In 2017, an A–DA′D–A-type narrow-bandgap acceptor named BZIC with benzotriazole (BTA) core was reported for the first time.[146] Despite the low efficiency (PCE of 6.3%) of HFQx-T:BZIC devices, this was a key breakthrough for Y-series high-performance acceptors. In 2019, Zou et al. reported a novel acceptor by employing an electron-deficient core benzothiadiazole, namely Y6.[147] It has a narrow bandgap of 1.33 eV and down-shifted LUMO and HOMO levels. Devices based on PM6:Y6 yielded a record PCE of 15.7% for both conventional and inverted device architectures. Zhu et al. synthesized a new acceptor AQx-2 with quinoxaline-containing fused cores.[148] Due to the moderately electron-deficient quinoxaline block, these acceptors possessed blue-shifted absorption and up-shifted energy levels. AQx-2-based on OSCs showed PCE of 16.64% by blended with PBDB-TF. Alex et al. introduced selenophene into the backbone and reported an ultra-narrow bandgap (E_g of 1.25 eV) acceptor, mBZS-4F.[149] A high PCE of 17.02% was obtained with a supreme J_{sc} of 27.72 mA cm^{-2}.

Y-series acceptors contain two types of side chains in the molecular structure, including two branched alkyl chains on the sp^2 hybridised nitrogen atoms and two straight alkyl
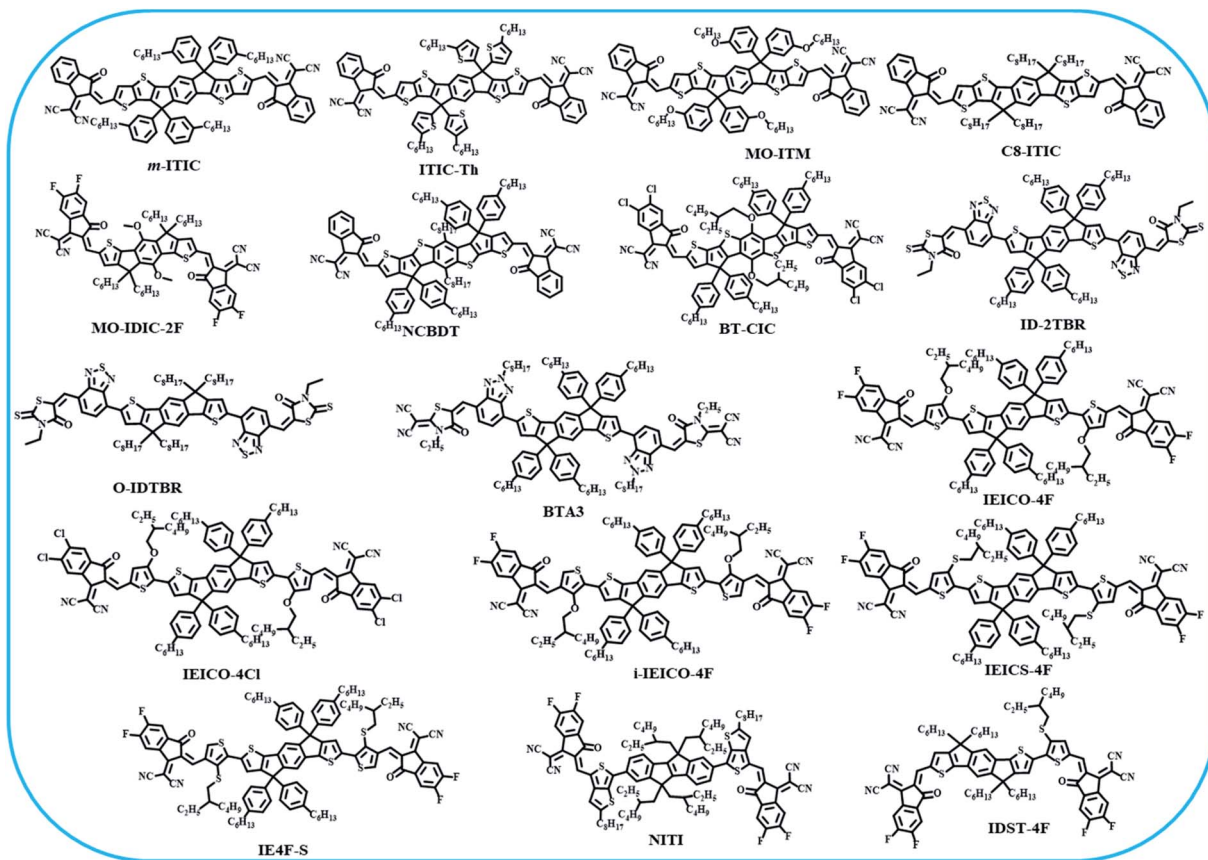
This journal is © The Royal Society of Chemistry 2022

J. Mater. Chem. A, 2022, 10, 3255–3295 | 3267

Fig. 8 Chemical structures of fused-ring small molecule acceptors modification of side chain and π bridge.

chains on the thieno[3,2-*b*]thiophene (TT) unit. Yan *et al.* first researched the alkyl chains of different sizes and branching positions of Y6.[150] They synthesized acceptors N3 and N4, of which N3 achieved better balance of good solubility and proper crystallinity and thus, a promising PCE of 15.98% was obtained for the PM6:N3 device. Recently, Hou *et al.* developed SMA, BTP-eC9, by modifying the straight alkyl chains on the TT unit; this increased the device efficiency to nearly 18%, which is the highest value for single-junction OSCs at that time.[151] Yan *et al.* focused on engineering the side-chain substitution positions (*o*-, *m*-, *p*-position) on the phenyl rings attached on the central core. Among the three acceptors, *m*-BTP-PhC6 showed a "tilted" orientation and exhibited the most ordered intermolecular packing. The PCE of the PTQ10:*m*-BTPPhC6-based devices reached 17.7%, which was the highest PCE based on PTQ10 donor so far.[152] Very recently, Sun *et al.* synthesized a series of acceptors with different branched alkyl chain to study the molecular packing.[12] L8-BO (2-butyloctyl substitution) blended with polymer donor PM6 yielded a high PCE of 18.32%, with a low E_{loss} of 0.55 eV and a high FF of 81.5%. Their work revealed the importance of the branched alkyl chain topology in tuning the molecular packing and blend morphology.

Another Y-series acceptor is Y1-4F which has the same backbone as Y1 but different end group with fluorine atom replacement.[153] PM6:Y1-4F showed a higher PCE (14.1%) than

the unmodified control. Chen *et al.* synthesized two acceptors BTP-S1 and BTP-S2 SMAs with asymmetric terminals.[154] BTP-S2 with six chlorine atoms attached at the terminals enabled the corresponding devices to achieve an outstanding electroluminescence quantum efficiency of 2.3×10^{-2}%, which significantly reduced non-radiative and energy losses of the devices. BTP-S2-based devices showed a high PCE of 16.37%. Yan *et al.* developed BTP-2F-ThCl SMA with two asymmetric terminals of IC-2F and CPTCN-Cl, which resulted in an excellent energy-level match and higher V_{oc} (0.86 V) and PCE (17.06%) values compared to those reported for the PM6:Y6 system.[155] Fig. 9 shows the chemical structures of some A–DA′D–A-type NF-SMAs with fused-ring cores. The PV performances of OSCs using A–DA′D–A-type NF-SMAs are summarised in Table 7.

3. Processing strategies for high performance OSCs

Along with the development of efficient donors and acceptors, obtaining an ideal morphology of the BHJ blends is key element for high-performance OSCs. The films morphology including molecular aggregation, phase separation, and crystallinity of the active layer is important to exciton dissociation, charge recombination and transportation of OSCs. Therefore, much

3268 | *J. Mater. Chem. A*, 2022, **10**, 3255–3295

This journal is © The Royal Society of Chemistry 2022

Table 6   Summary of the photovoltaic performance of OSCs using fused-ring electron acceptors

NFA	E_g^{opt} [eV]	HOMO/LUMO [eV]	Donor	V_{oc} [V]	J_{sc} [mA cm^{-2}]	FF [%]	PCE [%]	Ref.
ITIC	1.59	−5.48/−3.83	PTB7-Th	0.81	14.21	59.1	6.8	29
ITIC	1.59	−5.48/−3.83	PBDB-T	0.89	16.81	74.2	11.21	109
ITIC	1.59	−5.48/−3.83	J71	0.94	17.32	69.7	11.41	110
IT-M	1.60	−5.58/−3.98	PBDB-T	0.94	17.44	73.5	12.05	111
IT-OM-2	1.63	−5.49/−3.86	PBDB-T	0.93	17.53	73	11.9	112
IT-4F	1.55	−5.66/−4.11	PTO2	0.91	21.5	75	14.7	113
IT-4F	1.55	−5.66/−4.11	PFBCPZ	0.92	21.2	78.5	15.3	114
ITIC-4Cl	1.48	−5.75/−4.27	PM6	0.79	22.67	75.2	13.4	115
ITC-2Cl	1.58	−5.58/−4.01	PM7	0.91	20.27	73.9	13.72	116
IDIC	1.62	−5.69/−3.91	FTAZ	0.85	21.87	71.0	13.03	117
SN6IC-4F	1.32	−5.52/−4.11	PBDB-T	0.78	23.2	73	13.2	118
IXIC-4Cl	1.24	−5.52/−4.13	PM7	0.79	21.6	69.9	12.01	128
INIC3	1.48	−5.52/−4.02	FTAZ	0.85	19.44	67.4	11.2	129
INPIC-4F	1.39	−5.42/−3.94	PBDB-T	0.85	21.61	71.5	13.13	130
ITOT-4Cl	1.28	−5.49/−3.90	PBDB-T	0.77	22.89	70.5	12.5	131
FUIC	1.22	−5.31/−4.06	PTB7-Th	0.69	22.9	70.6	11.2	132
NFBDT	1.56	−5.40/−3.83	PBDB-T	0.86	17.85	67.2	10.42	133
IOIC3	1.45	−5.38/−3.84	PTB7-Th	0.76	22.9	74.9	13.1	134
ZITI	1.53	−5.59/−3.74	J71	0.93	20.37	69.4	13.24	135
COi8DFIC	1.26	−5.50/−3.88	PTB7-Th	0.68	26.12	68.2	12.16	30
DTPC-DFIC	1.21	−5.31/−4.10	PTB7-Th	0.76	21.92	61.3	10.21	136
M3	1.41	−5.60/−3.85	PM6	0.91	24.03	76.2	16.66	120
m-ITIC	1.58	−5.52/−3.82	J61	0.91	18.31	70.7	11.77	121
ITIC-Th	1.60	−5.66/−3.93	PBDT-ODZ	1.06	17.10	68.1	12.34	137
MO-ITM	1.60	−5.61/−3.89	PTZ1	0.96	17.5	68.8	11.6	138
C8-ITIC	1.53	−5.63/−3.91	PFBDB-T	0.94	19.6	72	13.2	122
MO-IDIC-2F	1.55	−5.80/−3.93	PTQ10	0.90	19.87	74.8	13.46	123
NCBDT	1.45	−5.36/−3.89	PBDB-T	0.83	20.33	71	12.12	139
BT-CIC	1.40	−5.49/−4.08	PTB7-Th	0.70	22.5	71.9	11.2	140
ITD-2BR	1.68	−5.52/−3.69	P3HT	0.84	8.91	68.1	5.12	141
O-IDTBR	1.63	−5.51/−3.88	P3HT	0.72	13.9	60	6.3	21
BTA3	1.78	−5.59/−3.70	PBT1-C	1.21	10.89	56.5	8.6	124
IEICO-4F	1.24	−5.44/−4.19	PTB7-Th	0.73	22.8	59.4	10.0	125
IEICO-4Cl	1.23	−5.56/−4.23	PTB7-Th	0.72	22.8	62	10.3	142
i-IEICO-4F	1.56	—	J52	0.84	22.86	67.9	13.18	143
IEICS-4F	1.35	−5.43/−4.08	PTB7-Th	0.73	20.98	67	10.3	144
IE4F-S	1.47	−5.54/−3.89	PBDB-T	0.86	22.88	69.1	13.72	145
NITI	1.49	−5.68/−3.84	PBDB-T	0.86	20.67	71	12.74	126
IDST-4F	1.40	−5.59/−4.01	PM6	0.82	24.9	70	14.3	127

effort has been made to fine tune the morphology of the active layer for efficient OSCs.

Overall, the BHJ morphology, and consequently, the device performance depends on following key parameters: total concentration of the components, type of casting solvent, presence and type of additives, and processing conditions.[163] In the following sections, some important processing strategies such as additives, ternary blend and annealing to improve the active-layer morphology and device performance are highlighted.

3.1   Additives strategy for high performance OSCs

Additives are usually used to optimise the active-layer morphology in OSCs as they could effectively modulate the molecular orientation and packing.[164] Conveniently, based on their chemical structure, solvent additives can be classified into two groups: non-conjugated and aromatic additives. Non-conjugated solvent additives, such as 1,8-diiodooctane (DIO), tend to increase the crystallinity of the

active layer. Aromatic solvent additives, such as 1-chloronaphthalene (CN), have higher affinity for the conjugated backbones of OSC materials, consequently increasing their miscibility.[165]

In 2006, Bazan et al. first reported the solvent additive of 1-octanethiol can enhance the J_{sc} of P3HT:PC$_{61}$BM blend films via inducing structural order in P3HT.[166] Later, Heeger et al. investigated several 1,8-di(R)octane compounds (where R is bromo-, chloro-, -cyano-, iodo-, or thio-) and all the additives assisted in improving phase separation of the active layer with trace volume.[176] Notably, studies revealed that DIO can influence the orientation of the alkyl side chains attached to the indacenodithiophene (IDT) backbone and thereby reduce steric hindrance between molecules to improve the miscibility. Fig. 11(a) shows a schematic of the different fabrication strategies for highly efficient OSC.[167]

Another high-boiling-point solvent additive, CN was frequently used in OSCs and yielded decent results. Baran et al. studied the effect of different amount of CN on device PCE
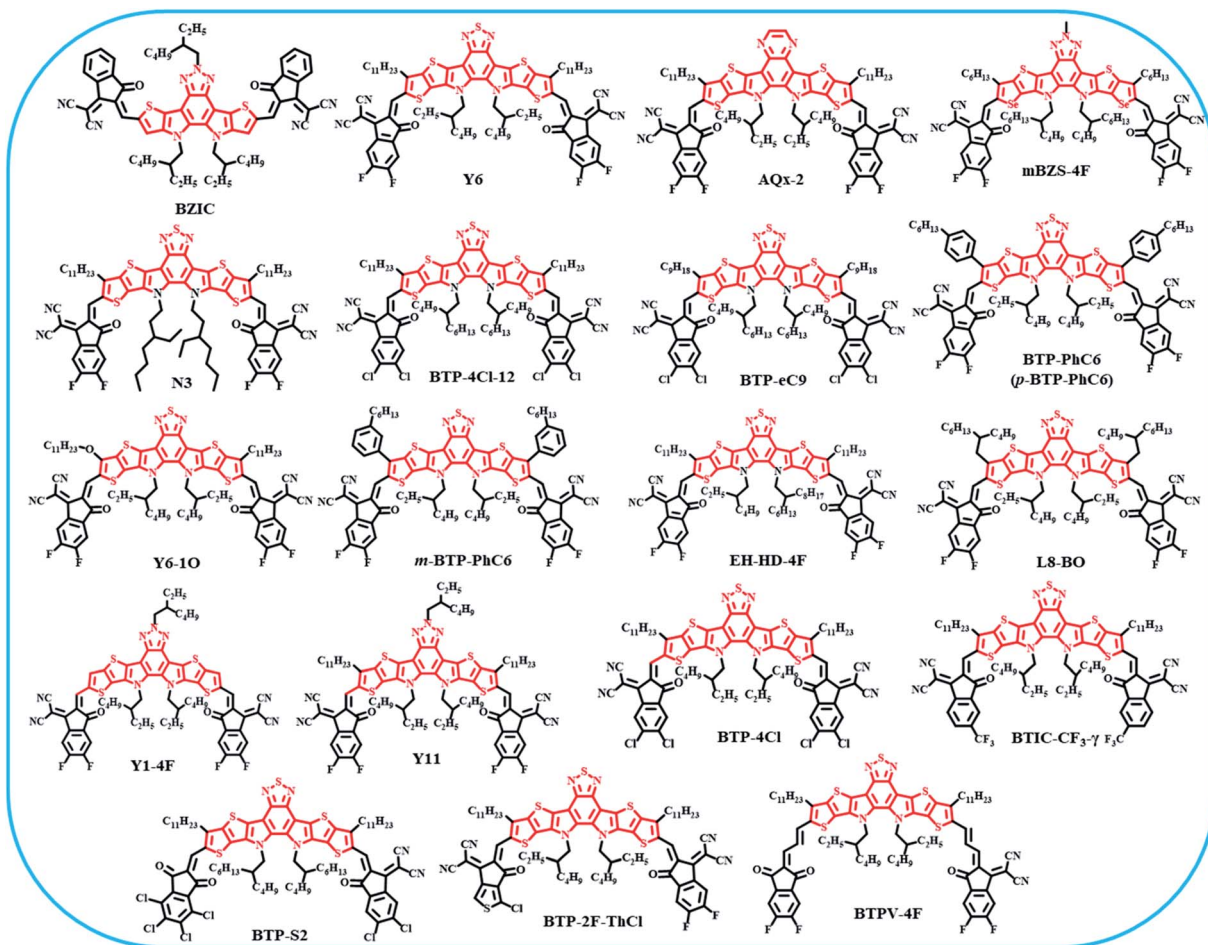
This journal is © The Royal Society of Chemistry 2022

J. Mater. Chem. A, 2022, 10, 3255–3295 | 3269

Fig. 9 Chemical structures of A–DA'D–A-type NF-SMAs with fused-ring cores.

based on PTB7-Th:IEICO-4F blend film.[168] GIWAXS studies (Fig. 10(b)) showed that 4 vol% CN can effectively optimize the π–π coherence span and obtain better domain spacing.

Recently, Kan et al. studied additive-induced miscibility and morphology control strategy to achieve the balance of exciton dissociation and charge collection, prompting the PCE of

Table 7 Summary of the photovoltaic performance of OSCs using A–DA'D–A-type NF-SMAs with fused-ring cores

NFA	E_g^{opt} [eV]	HOMO/LUMO [eV]	Donor	V_{oc} [V]	J_{sc} [mA cm^{-2}]	FF [%]	PCE [%]	Ref.
BZIC	1.54	−5.42/−3.88	HFQx-T	0.84	12.67	59	6.3	146
Y6	1.33	−5.65/−4.10	PM6	0.83	25.3	74.8	15.7	147
AQx-2	1.35	−5.62/−3.88	PBDB-TF	0.86	25.38	76.2	16.64	148
mBZS-4F	1.25	−5.60/−3.90	PM6	0.80	27.72	76.35	17.01	149
N3	—	—	PM6	0.83	25.81	73.9	15.98	150
BTP-4Cl-12	1.39	−5.66/−4.09	PBDB-TF	0.85	25.6	77.6	17.0	156
BTP-eC9	1.40	−5.64/−4.05	PBDB-TF	0.83	26.2	81.1	17.8	151
BTP-PhC6	1.36	−5.58/−3.85	PM6	0.86	25.0	77	16.7	157
Y6-1O	1.43	−5.71/−3.84	PM6	0.89	23.2	78.3	16.1	158
m-BTP-PhC6	1.35	−5.59/−3.86	PTQ10	0.88	25.3	79.3	17.7	152
p-BTP-PhC6	1.36	−5.59/−3.85	PTQ10	0.88	24.7	77.9	17.1	152
EH-HD-4F	1.39	−5.69/−4.04	PM6	0.84	27.5	79.3	18.3	11
L8-BO	1.40	−5.68/−3.90	PM6	0.87	25.72	81.5	18.32	12
Y1-4F	1.31	−5.56/−4.11	PBDB-TF	0.83	25.2	68.5	14.4	153
Y11	1.31	−5.69/−3.87	PM6	0.83	26.74	74.3	16.54	159
BTP-4Cl	1.30	−5.68/−4.12	PBDB-TF	0.86	25.4	75	16.5	160
BTIC–CF$_3$–γ	1.30	−5.45/−3.96	PM6	0.85	25.19	72.8	15.59	161
BTP-S2	—	−5.65/−4.01	PM6	0.94	24.07	72.0	16.37	154
BTP-2F-ThCl	1.34	−5.70/−3.99	PM6	0.86	25.38	77.4	17.06	155
BTPV-4F	1.21	−5.39/−4.08	PTB7-Th	0.65	28.3	65.9	12.1	162

3270 | *J. Mater. Chem. A*, 2022, **10**, 3255–3295

This journal is © The Royal Society of Chemistry 2022

PM6:Y6 devices from 15.7% to 17.5% by adding 1-fluoronaphthalene (FN), which was higher than that using additives of CN and 1-bromonaphthalene.[169] Despite the various advantages of high-boiling-point solvent additives, it is hard to absolutely remove additives from the active layers via common treatments. Residual additives in the film can generate free radicals under UV illumination and would destroy the blends over time, thereby reducing device stability.[170]

Recently, novel solid additives were developed to improve the morphology, leading to a higher PCE of the OSCs. Hou et al. synthesised a series of solid additives with similar chemical structures but different volatilities.[171] Among them, the higher volatility of SA-4 resulted in an increase in PCE from 12.1% to 13.5%, whereas using SA-7 showed a decrease in PCE. Very recently, Sun et al. prepared devices based on PM6:Y6 by using a highly volatile solid additive, ferrocene.[172] Their study showed that ferrocene can effectively increase the molecular crystallinity and improve charge transport.

In summary, the use of additives to optimise the morphology is an excellent tool for increasing the PCE. However, the adverse effects of residual additives on the device PCE need to be addressed. For example, the most common solvent additive DIO is a powerful high boiling point liquid that is usually employed in the BHJ to achieve high-efficiency OPVs. However, it is hard to remove from the BHJ due to the high boiling point of DIO. Furthermore, DIO is unstable under light exposure and photolyzes into radical species that subsequently initiate photo-oxidation of the polymers such as PTB7-Th and PTB7. In this case, it will accelerate photodegradation of BHJ films and then change the nanostructure after illumination. When more DIO amount is added, the faster destructiveness of the active layers is induced and then stability is reduced rapidly.[170] Fig. 10 shows the molecular structures of solvent additives used in NFA-OSCs and Table 8 lists the PV performance of OSCs with different representative additives.

3.2 Ternary strategy for high performance OSCs

Ternary OSCs with the incorporation of a third component, either a secondary donor or acceptor have been developed to further increase the device PCE, which the third component played a vital role to optimize the morphology, reduce the E_{loss} and contribute to charge transfer. Usually, the third component in the ternary blends exhibited several working mechanisms.

The most common mechanism is charge transfer model. In this model, for the cascade-like energy level alignment between the three components, the LUMO and HOMO levels of the third component should be between the LUMO and HOMO levels of the "host donor" and "host acceptor," which can enable the efficient charge transport in the ternary blend. Considering the purpose of achieving a higher V_{oc} in the ternary devices, the third component should be a "guest donor (acceptor)" with a lower (higher) HOMO (LUMO) than the "host donor (acceptor)". In addition, it couldn't be better to choose the third component with a complementary absorption spectrum between the "host donor" and "host acceptor," therefore maximizing the solar photons utilization. In 2010, Koppe et al. reported a ternary device of P3HT:PCPDTBT:PCBM, in which the third low bandgap polymer PCDTBT can effectively enhance photosensitivity of the ternary blend and contribute to charge transport of the devices.[177] Recently, Li et al. reported ternary
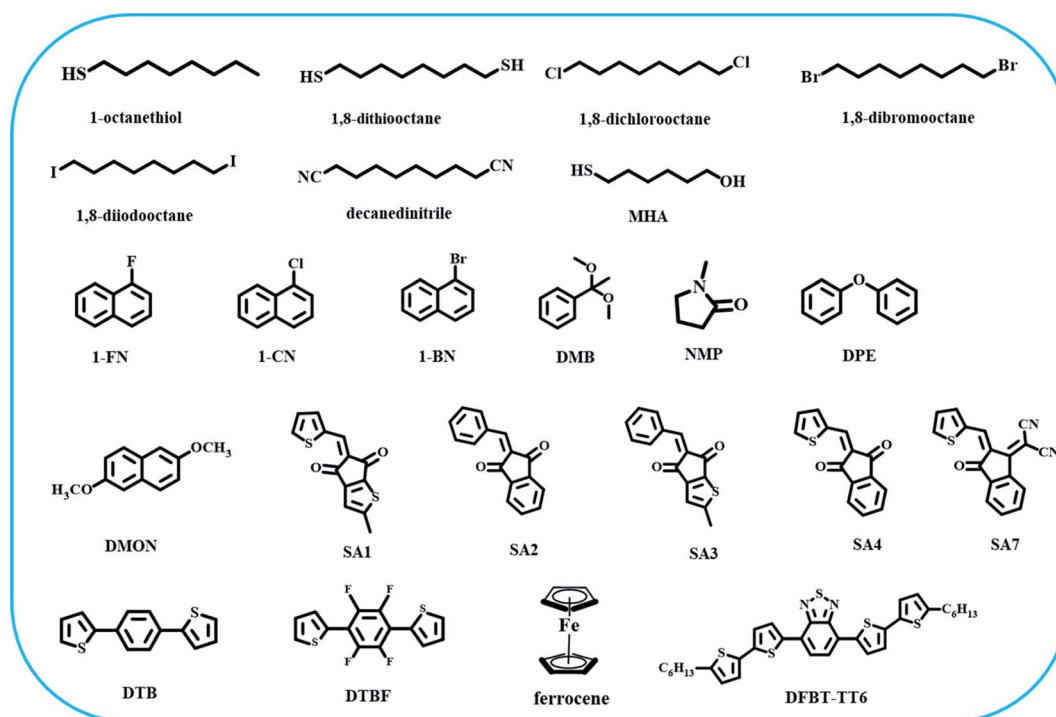

Fig. 10 Molecular structures of solvent additives used in NFA-OSCs.

This journal is © The Royal Society of Chemistry 2022

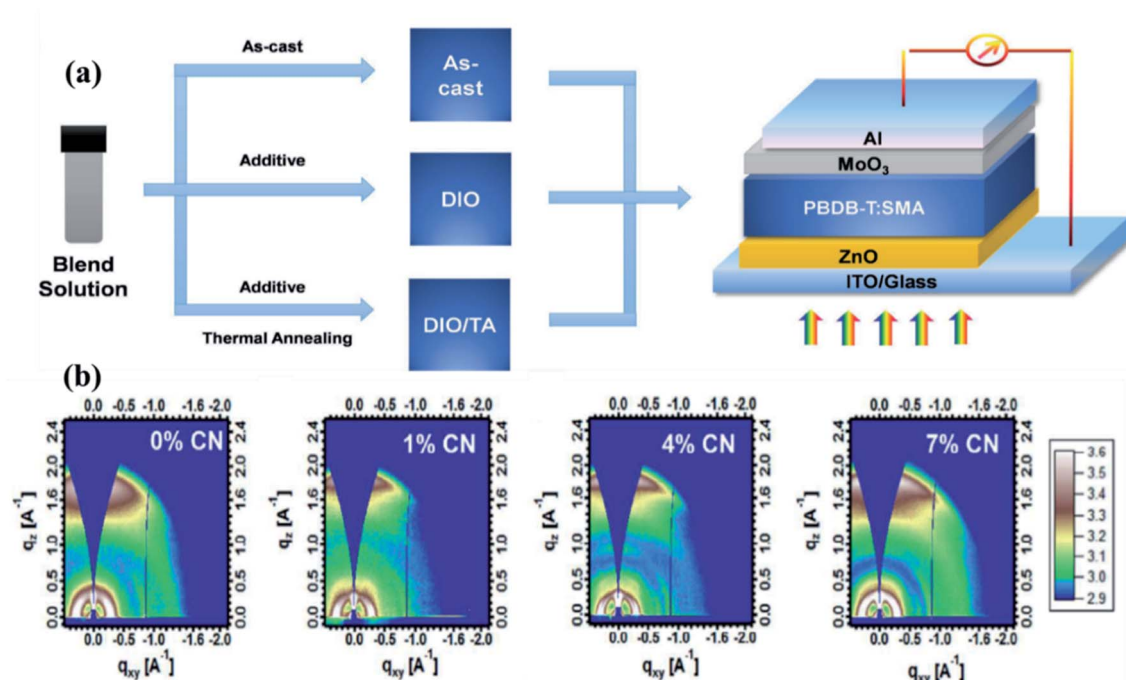J. Mater. Chem. A, 2022, 10, 3255–3295 | **3271**

Fig. 11 (a) Schematic of the fabrication process of high-efficiency NF OSCs. Reproduced with permission.[167] Copyright 2016, Wiley-VCH. (b) GIWAXS 2D patterns of PTB7-Th:IEICO-4F blend film with 0%, 1%, 4%, and 7% CN. Reproduced with permission.[168] Copyright 2020, American Chemical Society.

devices based on PM6:Y6:C8-DTC and achieved a high PCE of 17.5%.[178] Through in-depth study of the ternary OSCs, they found that the addition of C8-DTC promoted exciton dissociation, improved more balanced carrier transport and inhibited charge recombination, which led to better charge separation, lower V_{loss} and higher PCE of the ternary OSCs.

Table 8 Summary of the photovoltaic performance of OSCs with different representative additives

Active layer	Additive	V_{oc} [V]	J_{sc} [mA cm^{-2}]	FF [%]	PCE [%]	Ref.
PCPDTBC:PC$_{71}$BM	None	0.66	11.74	43	3.35	165
	HS-C$_8$H$_{16}$-SH	0.64	14.48	49	4.5	165
	Cl-C$_8$H$_{16}$-Cl	0.35	3.55	33	0.41	165
	Br-C$_8$H$_{16}$-Br	0.64	15.26	48	4.66	165
	I-C$_8$H$_{16}$-I	0.61	15.73	53	5.12	165
	CN-C$_8$H$_{16}$-CN	0.63	7.98	47	2.38	165
PM6:Y6	None	0.85	24.99	70.6	15.0	169
	1-FN	0.83	26.98	77.8	17.5	169
	1-CN	0.84	25.79	71.9	15.7	169
	1-BN	0.84	26.0	74.9	16.5	169
PTB7-Th:EH-IDTBR	None	1.02	18.0	56.8	10.41	173
	DMB	1.02	17.81	59.48	10.81	173
	MHA	1.02	18.77	59.8	11.36	173
PBDB-T:TTC8-O1-4F	None	0.84	21.93	58.2	10.75	174
	DIO/DMON	0.816	23.04	70.3	13.22	174
PBDB-TF:IT-4F	None	0.89	18.8	71	12.2	171
	SA-1	0.86	20.2	76	13.8	171
	SA-2	0.87	20.4	75	13.6	171
	SA-3	0.87	20.3	75	13.5	171
	SA-4	0.87	20.2	77	13.6	171
	SA-7	0.85	19.8	68	11.6	171
PBDB-TF:BO-4Cl	None	0.85	24.5	70.6	14.8	175
	DTB	0.85	25.0	73.5	15.6	175
	DTBF	0.84	26.2	77	17.1	175
PM6:Y6	None	0.84	25.34	73	15.16	172
	Ferrocene	0.84	26.91	77	17.01	172
PM6:Y6	None	0.84	25.2	74	15.76	176
	DFBT-TT6	0.84	26.56	76	17.05	176

The second mechanism is energy transfer, which is an effective way to improve the light harvesting ability. It is very important to choose a suitable absorption/emission spectrum of the third component in the ternary blend in the energy transfer model. Usually, the overlap integral of the energy-donor emission spectrum and the energy-acceptor absorption spectrum has significant impact on the intensity of the FRET effect. Different from charge transfer mechanism in which PL of the host components (donor or acceptor) is notably quenched by the third component, in the energy transfer mechanism, when adding the ratio of the third component, the PL intensity of the energy donor gradually decreases while the PL intensity of the "energy acceptor" gradually increases. In 2015, Heeger *et al.* demonstrated a remarkable enhancement in PCE due to ultrafast FRET in PTB7:PCDTBT:PC$_{71}$BM-based OSC.[179] A high PCE

of 8.9% was obtained for ternary devices, which was higher than the binary system. Li *et al.* reported by adding a SMA IBC-4F for preparing the ternary devices of PBDB-T:IBC-4F:IE4F-S.[180] With the optimized blend ratio of 1 : 0.2 : 1 of PBDB-T : IBC-4F : IE4F-S, the devices showed a high PCE of 15.06% (PCE of 13.7% and 0.21% for PBDB-T:IE4F-S and PBDB-T:IBC-4F, respectively). The improvement of performance was attributed to the improved charge dissociation and extraction, suppressed bimolecular and trap-assisted recombination (Fig. 12(a–c)).

The third mechanism is alloy model.[181] In this model, the ternary solar cell works like two individual sub-cells and this model requires an intimate mixing and compatibility between the "guest donor (acceptor)" and "host donor (acceptor)". The two donors (acceptors) in the ternary blends can form alloy that shares the same frontier orbital energy levels. Zhang *et al.*
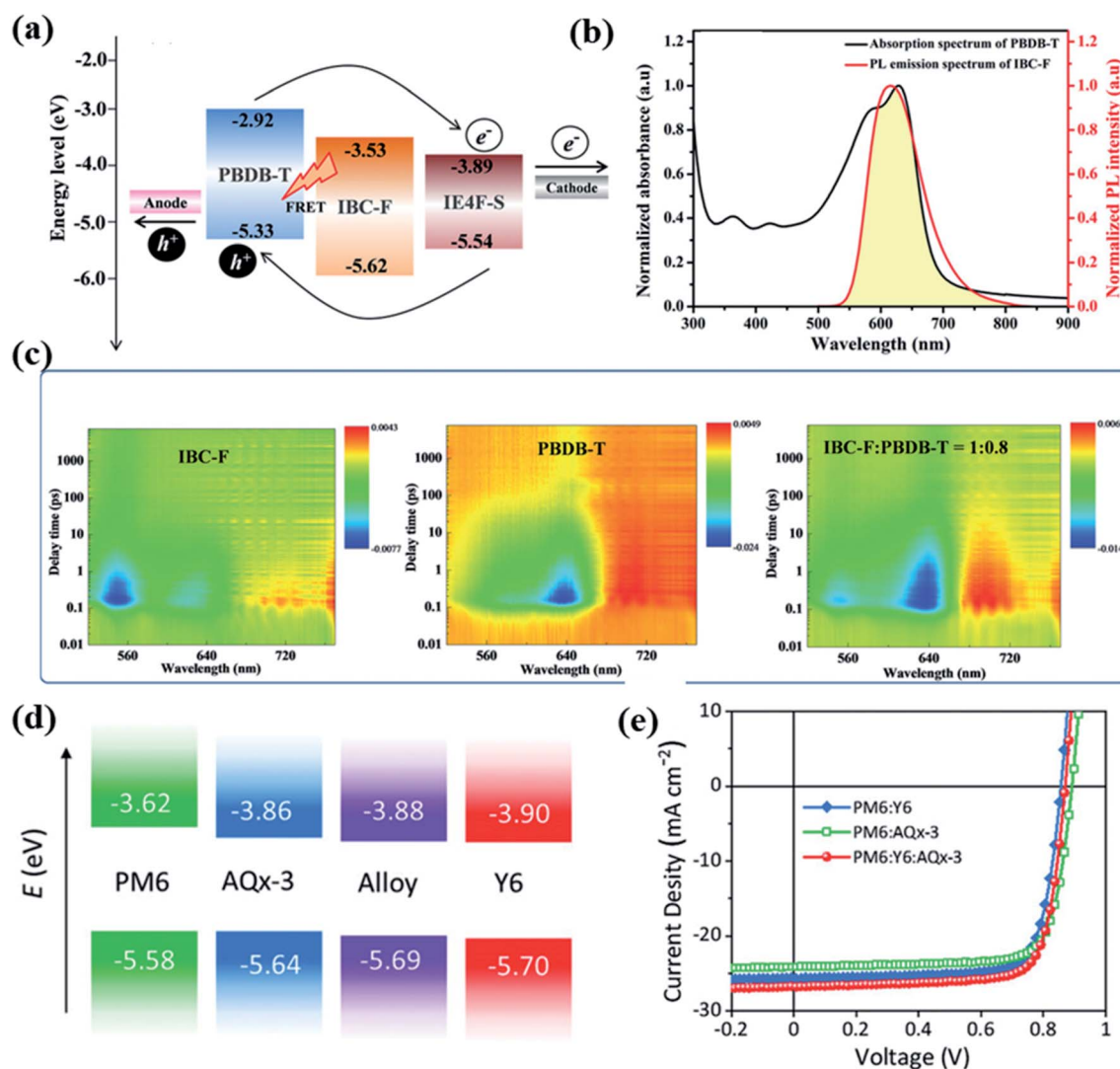

Fig. 12 (a) Energy levels of IBC-F, PBDB-T, and IE4F-S and schematic of the charge and energy transfer mechanisms involved in the PBDB-T:IBCF:IE4F-S ternary blend. (b) Absorption spectrum of PBDB-T and PL emission spectrum of IBC-F. (c) Transient absorption spectra of pristine IBC-F, pristine PBDB-T, and IBC-F : PBDB-T (1 : 0.8, w/w) blend pumped at 500 nm. Reproduced with permission.[180] Copyright 2019, Wiley-VCH. (d) Schematic energy diagrams of PM6, Y6, AQx-3, and Y6:AQx-3 alloy composite. (e) Characteristic *J*–*V* curves of binary and ternary OSCs under simulated AM 1.5G irradiation (100 mW cm^{-2}). Reproduced with permission.[187] Copyright 2021, Wiley-VCH.

reported that the alloy-like state should be the excited electrons mixture of two well-mixed materials. The energy levels of alloy-like state will be slightly adjusted by altering each component content, leading to the gradually varied V_{oc}s of ternary OSCs.[182] In this case, the third component is either donor or acceptor with complementary absorption spectra, which can utilize the photons to the maximum extent.[183–186] Very recently, Zhu *et al.* reported the alloy ternary devices of PM6:Y6:AQx-3 and achieved a remarkably PCE of 18.01%, which is higher than that of the binary devices of PM6:Y6(16.94%) and PM6:AQx-3(16.67%).[187] Their work provides a promising path for boosting the photovoltaic performance of devices (Fig. 12(d and e)).

Overall, the third component in the ternary devices can be used for multiple functionalities, such as broadening and strengthening the light absorption, increasing the charge transfer and transport, facilitating the charge collection, and reducing charge recombination at the electrodes, and improving the film morphology. Table 9 lists the PV performance of OSCs with ternary blends.

3.3 Annealing strategy for high performance OSCs

Over the years, numerous strategies have been proposed to obtain an ideal morphology, such as optimising the processing solvent, and use of solvent-vapour annealing or thermal annealing. Among them, thermal annealing and solvent-vapour annealing are effective post-treatment approaches for manipulating the morphology. Thermal annealing could help contribute to the crystallisation and better phase separation of the active-layer blends.[195] In this section, we will give a description about the annealing effect on the morphology of OSCs.

Chen *et al.* reported an effect of annealing on DR3TSBDT:DTBTF-based OSC.[196] After thermal annealing, the blend film showed clear phase separation and fibre-like crystalline structures. Laquai *et al.* studied the recombination after thermal annealing of all-PSCs.[197] They found that thermal annealing effectively reduced carrier recombination in TQ1:N2200 blends from ~35% in as-spun samples to ~7% in thermally annealed sample and doubled the EQE and increased FF, resulting in a higher PCE. Later, Hou *et al.* reported morphology optimisation *via* thermal annealing to fabricate an efficient thickness-insensitive non-fullerene PSCs.[198] Furthermore, thermal annealing of PBDB-T:IT-M films resulted in an increase in crystallinity in the out-of-phase direction (010), which increased the π–π coherence lengths of domain size (Fig. 13(a–d)).

Solvent-vapour annealing (SVA) is another effective method developed and implemented in OSCs. SVA is performed by placing the active layer film in a chamber containing vapours of the processing solvent or other solvents, which penetrate the film and modify the molecular order. For example, Vogelsang *et al.* reported a real-time observation of morphological dynamics induced by SVA in a signal chain conjugated polymer. They used single molecule fluorescence spectroscopy/ microscopy (SMS) to monitor the SVA-induced translocations to observe the dynamics. They concluded that the film absorbs the solvent and decreases its glass transition temperature and polymer chains undergo folding and unfolding events between a collapsed and extended conformation during SVA, which finally leads to a highly ordered conformation after the solvent vapor is removed.[199] Additionally, unlike thermal annealing, the extent of phase modification by the selected solvent depends on the affinity of the donor/acceptor for the solvent. Beaujuge *et al.* studied the time-dependent SVA on the phase separation of the BHJ morphology. They found that SVA treatments induce reorganization of the BHJ morphology from a highly intermixed

Table 9 Summary of the photovoltaic performance of OSCs with ternary blends

Binary blend	Third component	Weight ratio	V_{oc} [V]	J_{sc} [mA cm^{-2}]	FF [%]	PCE [%]	Ref.
PBDB-TF:HC-PCIC	PC$_{71}$BM	1 : 1.2 : 0	0.88	17.54	72.69	11.48	188
		1 : 1.02 : 0.18	0.89	19.29	70.18	12.36	
PTB7-Th:IEICO-4F	ITCC	1 : 1.4 : 0	0.71	20.7	68.2	9.8	189
		1 : 1.4 : 0.3	0.75	21.2	66	10.6	
PM6:Y6	DRTB-C4	1 : 0:1.2	0.84	24.25	79.5	16.19	190
		0.9 : 0.1 : 1.2	0.85	24.79	81.3	17.13	
PM6:Y6	C8-DTC	1 : 1.2 : 0	0.84	25.6	73.88	16.20	178
		1 : 1.08 : 0.12	0.87	26.5	75.61	17.52	
PTB7:PC$_{71}$BM	PCDTBT	1 : 0 : 1.5	0.73	14.74	63.5	6.8	179
		0.7 : 0.3 : 2	0.795	17.1	65.4	8.9	
PBDB-T:NNBDT	FDNCTF	1 : 0.8	0.88	18.63	71.7	11.7	191
		1 : 0.8 : 0.2	0.887	19.89	72.2	12.85	
PBDB-T:IE4F-S	IBC-F	1 : 0 : 1	0.86	22.85	69	13.7	180
		1 : 0.2 : 1	0.88	22.8	74.4	15.06	
PBDB-T-2F:IT-2F	FTTCN	1 : 1 : 0	0.92	17.76	73.48	12.01	192
		1 : 0.8 : 0.2	0.94	18.18	76.03	12.99	
D18-Cl:Y6	PM6	1 : 0 : 1.6	0.87	25.31	75.81	16.89	193
		0.7 : 0.3 : 1.6	0.87	26.35	76.82	17.61	
PM6:Y6	AQx-3	1 : 1.2	0.85	25.73	76.8	16.94	187
		1 : 0.8 : 0.4	0.87	26.82	77.2	18.01	
PBQx-TCl:BTP-eC9	BTA3	1 : 1.2 : 0	0.82	26	75.2	16.0	194
		1 : 1 : 0.2	0.84	26.9	79.6	18.0	

3274 | *J. Mater. Chem. A*, 2022, **10**, 3255–3295
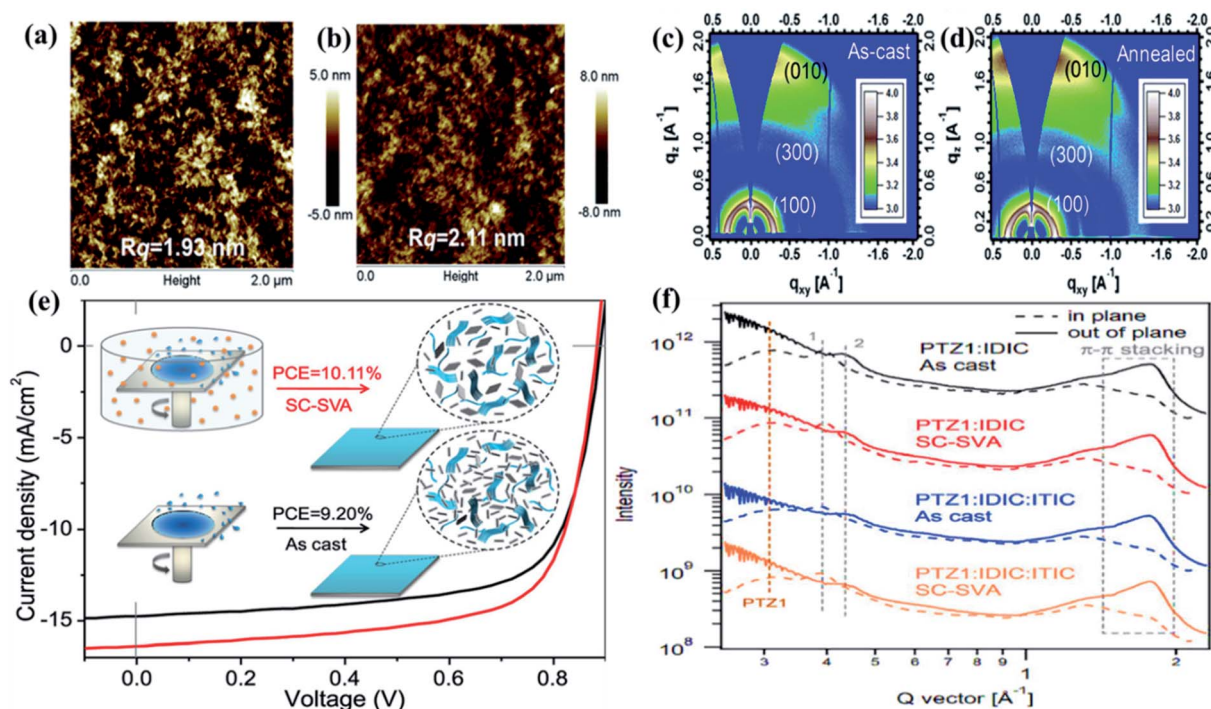
This journal is © The Royal Society of Chemistry 2022

Fig. 13 Tapping-mode AFM topography of PBDB-T/IT-M thick-film devices: (a) after annealing and (b) as-cast films; (c and d) 2D GIWAXS patterns of as-cast and annealed PBDB-T:IT-M thick-films (~250 nm). Reproduced with permission.[198] Copyright 2019, Royal Society of Chemistry. (e) J−V characteristics of PTB7-Th:ITIC devices with or without SC-SVA. (inset: diagram of PTB7-Th:ITIC blends produced with various process). (f) GIWAXS line profiles of PTZ1:IDIC and PTZ1:IDIC:ITIC blend films with or without SC-SVA. Reproduced with permission.[202] Copyright 2017, Elsevier Science Publishers.

blend with limited structural order to highly structural order and hence, dramatically improve the charge generation and collection patterns. However, extended SVA time (>60 s) induces excess crystallization and undermines device performance.[200] These works indicated that SVA protocols represent a particularly useful tool in the optimization of crystallinity and phase separation. In addition, this method prevents the need for solvent additives and enables room-temperature film processing.

In addition to this, another effective method called "up-side-down", which is operated by flipping the substrate up-side-down to apply treatment to active layer. This technology can optimize vertical phase separation according to the tension of the interstitial solvent. Zhang et al. reported binary devices by using this method and gave a higher PCE of 9.11%, which is higher than that of device without any treatment (PCE of 3.63%).[201] They found that, upside-down thermal annealing (DTA) or up-side-down solvent vapor annealing (DSVA) treatment can enhance DRCN5T crystallinity and optimize vertical phase separation, and thus was favorable to form well-ordered donor arrangement.

An in situ solvent-annealing technique was also developed, where solvent annealing was performed during spin coating (SC-SVA). Fig. 13(e) shows an illustration of the SC-SVA processes to prepare the PTB7-Th:ITIC blends. Furthermore, they fabricated binary and ternary devices of PTZ1:IDIC and PTZ1:IDIC:ITIC. As shown in GIWAXS line profiles (Fig. 13(f)), the crystallinity of IDIC was improved by SC-SVA in both

PTZ1:IDIC and PTZ1:IDIC:ITIC blends. In addition, the phase purity increased as well as the domain size decreased in the PTZ1:IDIC:ITIC blends, resulting in a better morphology.[202]

Overall, it is evident that the film crystallinity and the BHJ morphology can be controlled via various processing strategies. For example, although the adverse effect such as deteriorating the device stability, additives can indeed adjust the molecular orientation and packing and promote the performance of the OSCs. Ternary strategy can enhance the miscibility and crystallinity by adding a third component to improve the film morphology while thermal annealing and solvent-vapour annealing contribute to the crystallisation and better phase separation of the active-layer blends. All these processing methods aim to optimize the molecular aggregation, phase separation, and crystallinity of the BHJ layers and to facilitate the exciton dissociation and transportation of OSCs. Additionally, the commercialisation of OSC technology necessitates highly reproducible methods for directing the morphology of BHJ blends.

4. Interfacial layers in the OSCs

Interfacial layers in OSCs enable electrical contact between the active layer and corresponding electrode, thereby playing a crucial role for efficient charge-carrier extraction. Typically, interfacial layers are used to perform the functions of fine-tuning the energy levels of the active layer and corresponding electrodes, governing the polarity of the device, preventing

This journal is © The Royal Society of Chemistry 2022

J. Mater. Chem. A, 2022, 10, 3255–3295 | 3275

undesirable physical or chemical reactions among the OSC layers and absorbing photons.[203,204] In this section, we briefly summarise the various functions of the interfacial layers in the OSCs, including fine tuning of the energy levels, optimising charge separation and extraction, modulating light harvesting, modifying the active film morphology, and acting as a protective layer. All such interfacial materials have a direct impact on device efficiency and stability.

4.1 Organic materials interface layers

Our group and Zhou *et al.* independently reported the successful application of non-conjugated aliphatic amine-containing polymer interlayers, namely polyethylenimine (PEI) and polyethylenimine ethoxylated (PEIE).[205,206] The device fabricated using a protonated PEIE interfacial layer and PCE-10:IEICO-4F active layer showed an excellent PCE of 13.2%, which was higher than the reference devices with an ZnO interlayer (12.6%). Very recently, Huang *et al.* reported a tandem device by using an efficient interconnecting layer with the structure of ZnO NPs:PEI/PEI/PEDOT:PSS.[207] This structure of interconnecting layer increased the photon utilization in the front sub-cell without significantly increasing its thickness, which effectively suppressed the charge recombination. A highest PCE of 18.71% was obtained for the tandem OSC.

PFN and its derivatives, are among the most widely used cathode interfacial layers (CILs). Wu *et al.* used this polymer in OSCs, which resulted in simultaneous enhancement of J_{sc}, V_{oc}, and FF, dramatically improving the device performance. Deeper insight revealed that this interlayer could create a microscopic electric dipole and increase the built-in potential across the

devices, thus enhanced the device performance.[204] PFN-Br is another famous CIL that widely used to date. Zhou *et al.* reported an effective method by mixing PFN-Br with ZnO nanoparticles to modifying the surface free energy.[208] The OSC constructed using the modified CIL and an active layer of PBDB-TF:IT-4F gave a high V_{oc} of 0.87 V, J_{sc} of 20.16 mA cm^{-2}, and very high FF of 78.79%, resulting in a high PCE of 13.82% in an inverted configuration. See Fig. 14(a).

Cao *et al.* reported a narrow-bandgap NDI-based n-type water/alcohol-soluble polymer PFN-2TNDI.[209] The charge transfer between the n-type interlayer (PFN-2TNDI) and the donor provided an extra interface for charge dissociation, thus delivering an improved PCE (Fig. 14(b)). In 2014, Li *et al.* reported two CILs, which were incorporated a PDI core and amino (PDIN) or amino *N*-oxide (PDINO) as the terminal substituent.[210] Surprisingly, both interlayer materials have high conductivities of $\sim 10^{-5}$ S cm^{-1}. They fabricated devices and obtained PCEs of 8.05–8.24% for a wide range of PDI-interlayer thicknesses (10–25 nm), which were higher than that of a Ca/Al device (6.98%) and significantly higher than an Al-only device (4.43%). Very recently, Li *et al.* reported another aliphatic amine-functionalized PDI derivative, PDINN.[211] Compared with PDINO, PDINN exhibited better contact with non-fullerene active layers, stable electrode interface, higher conductivity, and stronger ability to reduce work function (WF) of the metal cathode, which make it more suitable for use as CIL in non-fullerene OSCs with air stable metal cathode, such as Ag and Cu, to improve the device stability. With PDINN/Ag as the top electrode, the OSCs based on PM6:Y6 exhibited a high PCE of 17.23%, which was much higher than that with PDINO/Ag (PCE of 15.17%).
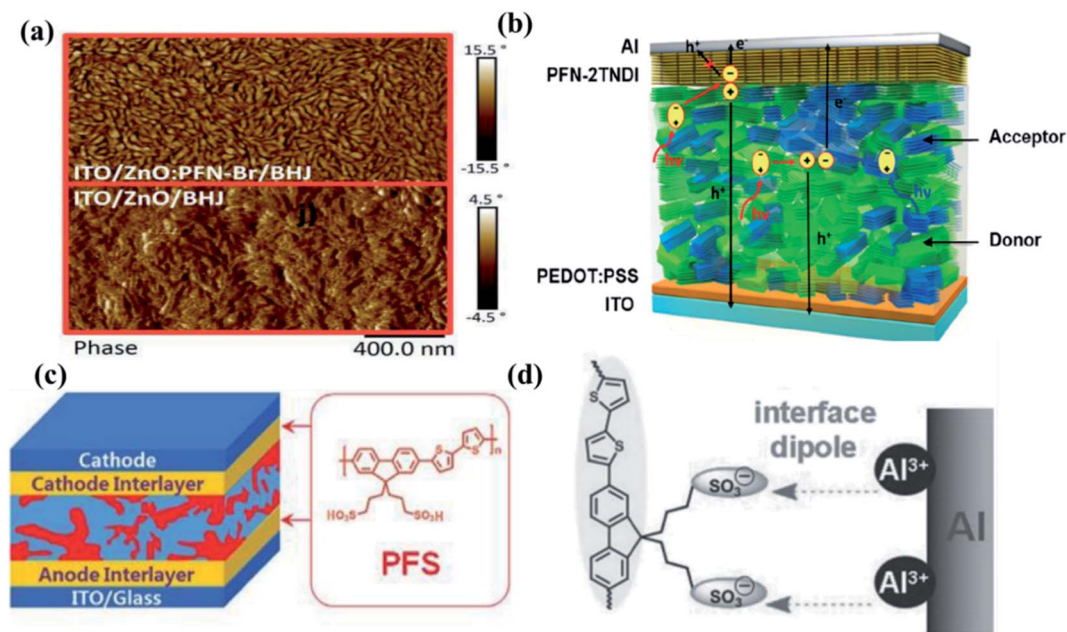

Fig. 14 (a) AFM phase images of ITO/ZnO:PFN–Br/BHJ and ITO/ZnO/BHJ. Reproduced with permission.[193] Copyright 2019, Royal Society of Chemistry (b) schematic of the exciton separation and transport in the BHJ, and the charge–transfer states at the donor/WSCP interface. Reproduced with permission.[209] Copyright 2017, Royal Society of Chemistry. (c) Structure of PFS and corresponding device. (d) Schematic diagram of the dipole at the interface of the PFS/Al electrode. Reproduced with permission.[197] Copyright 2016, Wiley-VCH.

3276 | *J. Mater. Chem. A*, 2022, **10**, 3255–3295

This journal is © The Royal Society of Chemistry 2022

Hou *et al.* reported another polyfluorene material, PFS, comprising sulfonic acid and bithiophene units, which can be used as both an anode interlayer (AIL) and CIL (Fig. 14(c)).[212] PFS is suitable as an AIL as its WF (4.92 eV) is quite close to that of PEDOT:PSS (4.97 eV), while it creates a dipole at the interface due to the reaction between the sulfonic acid groups of PFS and the Al electrode (Fig. 14(d)). These findings overturn the typical design architecture and have great potential for simplifying the fabrication of PSCs for commercial applications. Overall, the organic materials interface layers are usually possessing good charge mobility and conductivity to facilitate the electron or hole transport. What's more, the diverse molecular design of organic materials can ensure the WF match between the metal and active layers.

4.2 Inorganic metal oxides and metal salt interface layers

The n-type metal oxides, particularly titanium dioxide (TiO_2), tin oxide (SnO_2), and zinc oxide (ZnO), have been used as CIL materials in the inverted device architecture due to their low-energy levels, adequate optical transmittance, and acceptable electronic conductivity.[213–215] Our group introduced ZnO as interfacial layer in inverted organic solar cell as early as 2008.[216] ZnO nanoparticles (ZnO-NP) were another effective CIL for OSCs (Fig. 15(a)).[217] Fig. 15(b) showed the arrangements of the energy levels in the presence and absence of the ZnO-NP layer in the ITO/ZnO cathode, and the ITIC acceptor. The BHJ devices fabricated using the ZnO-NP/ZnO bilayer as a CIL and PBDB-T:ITIC as active layer yielded a PCE of 12.24%, which is significantly higher than that obtained by the control device (10.69%). SnO_2 is another material that has been widely used as a CIL in solar cells. Li *et al.* developed a simple room-temperature process to obtain a SnO_2 colloid precursor *via* a direct precipitation method and produced printable SnO_2 films by spin coating or blade coating.[218] The application of SnO_2 CILs in large-area OSCs of 25 and 100 mm^2, attained high PCEs, over 13.5% and 12.5%, respectively.

Among the transition-metal oxides, MoO_3 is the most extensively used AIL due to its neutral pH, and exceptional hole extraction and electron-blocking traits. It has been shown that the MoO_x layer deposited from a H_xMoO_3 precursor provides n-doping, attributed to the tiny amount of oxygen vacancies, which fine-tunes its properties.[219] The devices fabricated using n-doped MoOx (H:V-Mo) and P3T2:IT-M active layer yielded an excellent PCE of 10.5%, which was much higher than using H-Mo (PCE of 3.9%) ((c)). Furthermore, they fabricated devices based on PBDB-TCl:IT-4F with H:V-Mo interlayer, a comparable PCE of 14.2% was obtained (Fig. 15(d)).[219] Overall, the most impressive merits of inorganic metal oxides and metal salt interface layers are their low cost, high optical transmittance, and resistance to the H_2O and O_2 for device stability.

4.3 Hybrid and composites interface layers

The use of hybrid and composites materials as interfacial layers in OSCs is a relatively new concept that has not yet been widely applied. Recently, Vasilopoulou *et al.* reported a D/A pyrene-bodipy dye between the active layer/ZnO interface, which works as a protective layer and mitigates the degradation of NFAs triggered by the photo-catalytic activation of ZnO under UV light illumination (Fig. 16(a)).[220] The OSCs fabricated based on PM6:IT-4F using the modified ETL delivered a PCE of 11.80%, which was 13% higher than that of reference device.
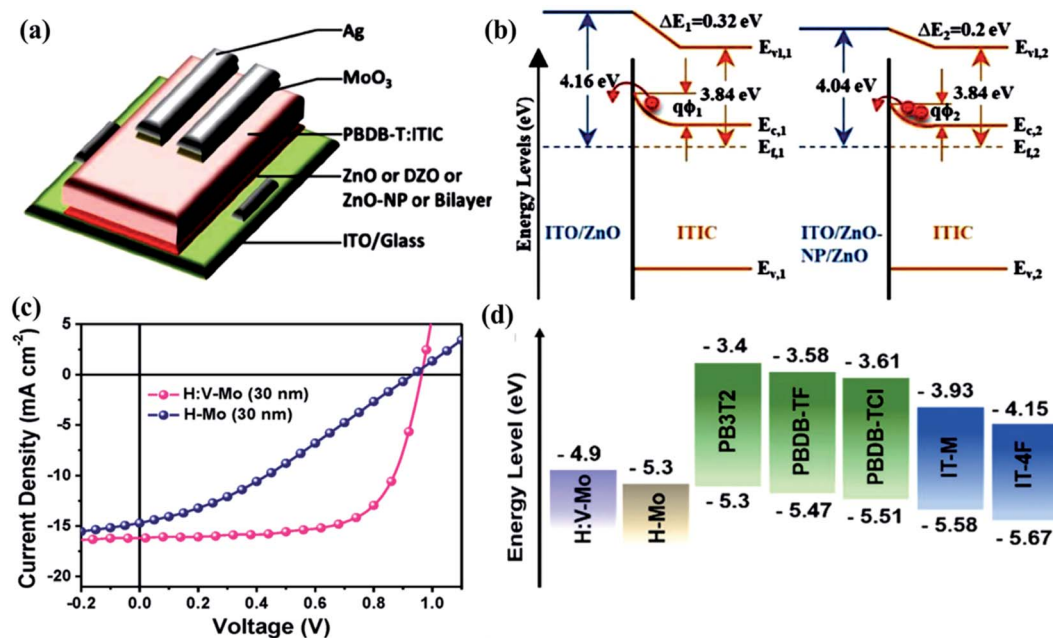

Fig. 15 (a) Schematic of the inverted BHJ device structure of the fabricated PBDB-T:ITIC OSCs with different ETLs (ZnO, DZO, ZnO-NP, and bilayer). (b) Energy-level alignments of ITO/ETL/ITIC, depicting the band-bending phenomenon. Reproduced with permission.[217] Copyright 2017, Elsevier Science Publishers. (c) *J–V* curves of PB3T2:IT-M-based OSCs with blade-coated H-Mo and H:V-Mo (NMo : VC = 100 : 5, w/w). (d) Energy-level alignments of H:V-Mo, H-Mo, donors, and acceptors. Reproduced with permission.[219] Copyright 2019, Wiley-VCH.

Zhang *et al.* used a self-assembled ultrathin APTES layer to modify ZnO and used it as CIL in OSCs (Fig. 16(b)).[221] The device of PBDB-T:IT-M with ZnO-APTES CIL yielded a PCE of 11.53%. The enhanced performance was attributed to the high charge-collection efficiency as a result of a built-in electric field and fewer oxygen defects at the ZnO surface. Yoon *et al.* recently studied composite interlayers of alcohol-soluble polyfluorene (ASP)-wrapped single-walled carbon nanotubes (SWNTs) and applied it in the OSC based on PM6:Y6 which yielded a PCE of 14.37% (Fig. 16(c and d)).[222] Hybrid and composites interface layers are rarely reported compared with organic or inorganic materials because of the difficulty to enhance the miscibility between organic molecules and metal salts. However, it is worth to trying hybrid and composites interface layers to excavate the advantages and broaden the research areas.

Although numerous composite interlayers have been synthesised and applied in OSCs, they are few compared to the number developed for NFA-based devices. Furthermore, most interfacial layers are thickness dependent, but recently many thickness-insensitive interlayers have been developed, which helps simplify the fabrication process and expedite the commercialisation of OSCs.

5. Device architecture engineering for the OSCs

The favourable aesthetics of OSCs are a result of the colourful and semi-transparent properties of organic materials.

Therefore, the introduction of a structure (such as semi-transparent devices) that accentuates the aesthetics of OSCs can broaden their commercial scope. In addition, semi-transparent organic active layers are becoming a cornerstone for the development of next-generation organic photovoltaics, such as semi-transparent OSCs (ST-OSCs) and tandem solar cells.[223] Here, the progress in the development of various OSC architectures is discussed.

5.1 Semi-transparent device structures

Based on advantages of NFAs, much research is being conducted based on ST-OSCs with NFAs.[154,156] to optimise the PCE, transmittance, and desired colour. The transmittance of a ST-OSC is an important factor, which is usually characterised by measuring the average visible transmittance (AVT) of the entire device in the visible region (370–740 nm) with a UV-vis spectrometer.[224,225] Since there is a trade-off between the PCE and AVT of ST-OSCs, the optimal photo-active layer should have strong NIR absorption but visible transmittance. Recently, to achieve this, ST-OSCs based on narrow-E_g polymer donors and NFAs had PCEs above 10%.[226,227] The detailed device performances of ST-OSCs based on such polymer donors and narrow-E_g acceptors are summarised in Table 10.

Our group reported a ST-OSC using a ternary blend of J71:Y6:PC$_{61}$BM as active layer and solution-processed silver nanoparticle and carbon nanotube composite film as top transparent electrode. This ST-OSC achieved a PCE of 7% with a high AVT of 36% and a colour rendering index of 90.[228] We
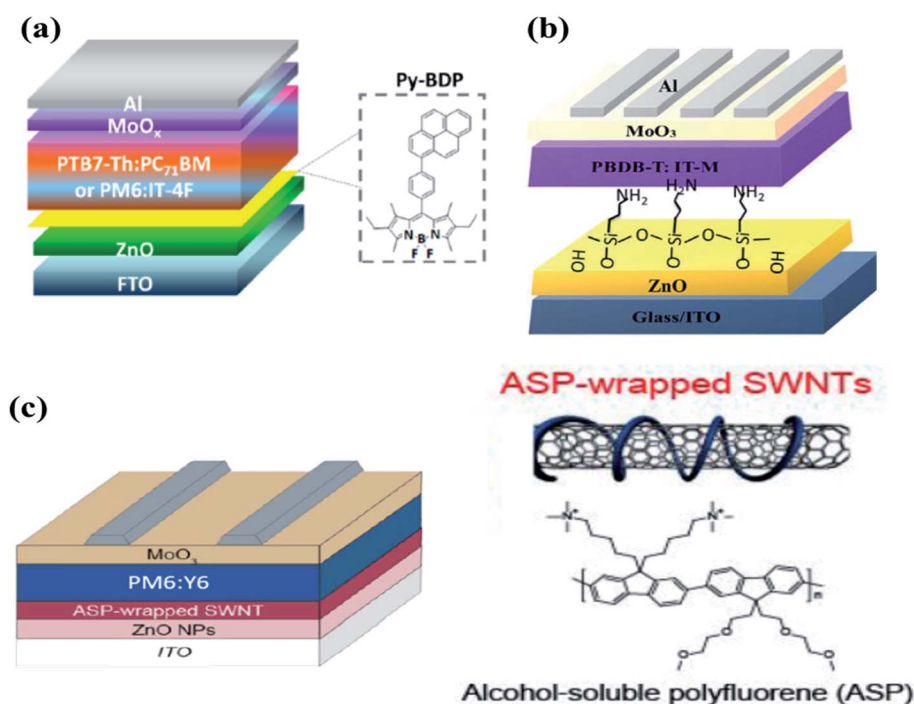

Fig. 16 (a) Device structure of fullerene and non-fullerene OSCs with pyrene–bodipy dye interlayers. Reproduced with permission.[220] Copyright 2020, American Chemical Society. (b) Schematic diagram of the structure of inverted OSCs with ZnO–APTES as CIL. Reproduced with permission.[221] Copyright 2019, Wiley-VCH. (c) Schematic of inverted organic solar cell with alcohol-soluble polyfluorene (ASP)-wrapped SWNTs as the interlayer. Reproduced with permission.[222] Copyright 2020, American Chemical Society.

3278 | *J. Mater. Chem. A*, 2022, **10**, 3255–3295

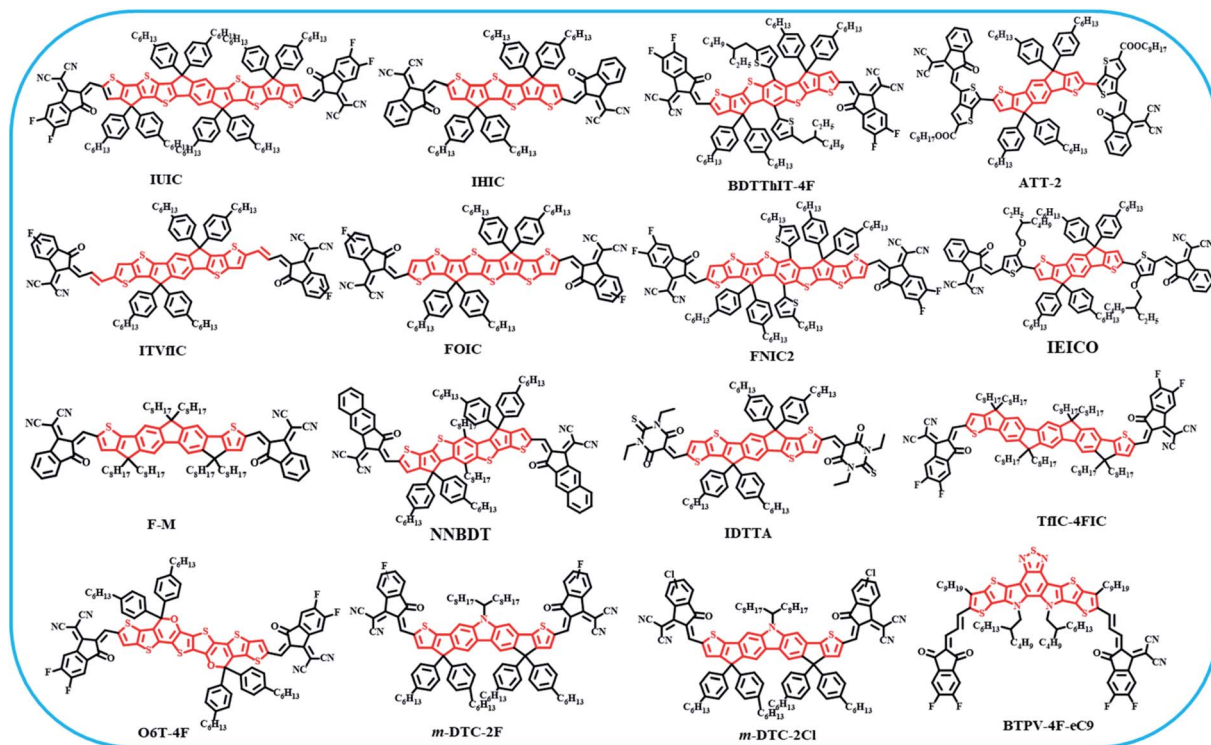This journal is © The Royal Society of Chemistry 2022

Fig. 17 Chemical structures of the acceptors used in the device architecture section except for the materials introduced in previous sections.

further improved the PCE to 13.19% with AVT of 24.56% by using a ternary blend of PBDB-TF, Y6 and our in-house designed BDC-4F-C8.[229] Hou et al. reported PBDB-T donor with IEIC-4Cl. The main absorption band of IEICO-4Cl films is at 745–945 nm, outside visible region, which is a favourable position for ST-OSCs.[142] The PBDB-T:IEICO-4Cl based ST-OSC showed 35.7% AVT and 6.24% PCE. BT-CIC has a narrow E_g of ~1.3 eV, which gives an optical absorption edge at ~1000 nm with cut-off wavelength at $\lambda = 950$ nm.[140] The device with PTB7-Th:BC-CIC

showed the best performance (PCE of 8.2% and 26% AVT) (Fig. 18(a and b)). Zhan et al. developed a fused octacylic electron acceptor (FOIC) using strong electron-withdrawing 2-(5/6-fluoro-3-oxo-2,3-dihydro-1H-inden-1-ylidene)-malonoitrile as end groups. Using the FOIC with a PTB7-Th blend for the photoactive layer of ST-OSCs gave a high PCE of 10.3% and AVT of 37%.[230] IUIC based on fused-11-ring core IU, coupled with 2-(5,6-difluoro-3-oxo-2,3-dihydro-1H-inden-1-ylidene)-malononitrile (2FIC) was developed (Fig. 17). IUIC has large π-

Table 10 Recent progress of representative NFAs based ST-OSCs

Device structure	Area (cm^2)	PCE (%)	AVT (%)	Ref.
ITO/ZnO/J71:Y6:PC$_{61}$BM/MoO$_3$/Ag-CNTs	0.11	7.00	36	228
ITO/PEDOT:PSS/PM6:Y6:BDC-4F-C8/PDINN/Ag	0.056	13.19	24.56	229
ITO/PEDOT:PSS/PBDB-T:IEICO-4Cl/PFN-Br/Au	—	6.24	35.7	142
ITO/ZnO/PTB7-Th:BT-CIC/MoO$_3$/Ag	0.02	8.2	26	140
ITO/ZnO/PTB7-Th:FOIC/MoO$_3$/Au/Ag	0.04	10.3	37.4	230
ITO/ZnO/PTB7-Th:IUIC/MoO$_x$/Au/Ag	0.04	10.2	31	226
ITO/ZnO/PTB7-Th:FNIC2/MoO$_x$/Ag	0.04	11.6	13.6	231
PES/PH1000/PEIE/P3HT:IDT-2BR/PH1000-T	0.05	3.22	53.2	141
ITO/ZnO/PBDB-T:ITIC/MoO$_3$/Ag/MoO$_3$	0.12	7.4	25.2	232
ITO/PEDOT:PSS/PTB7-Th:BDTThIT-4F/PDIN/Au/Ag	—	7.53	24.2	233
ITO/ZnO/PTB7-Th:ATT-2/MoO$_3$/Ag	0.03	7.74	37	234
ITO/PEDOT:PSS/PTB7-Th:ITVfIC/PDINO/Ag	—	8.21	26.4	235
ITO/PEDOT:PSS/PTB7-Th:IEICO-4F/PDIN/Au/Ag	0.04	9.48	23.7	236
ITO/PEDOT:PSS/J71:PTB7-Th:IHIC/PDINO/AU/Ag/3-DMs	—	9.37	21.4	36
ITO/PEDOT:PSS/D18:N3/PDIN/Au/Ag	0.04	12.91	22.5	238
ITO/PEDOT:PSS/D18-Cl:Y6-1O:Y6/PDIN/Au/Ag	0.04	13.02	20.2	239
ITO/PEDOT:PSS/PM6:Y6/PDIN/Au/Ag	0.04	12.37	18.6	240
ITO/ZnO/PBDB-T/PTAA:Y1/MoO$_3$/Au/Ag	0.1	11.7	20.1	241

This journal is © The Royal Society of Chemistry 2022

J. Mater. Chem. A, 2022, 10, 3255–3295 | 3279

conjugation and red-shifted absorption area. The PTB7-Th:IUIC based inverted ST-OSC exhibited a PCE of 10.2% and AVT of 31%.[226] In addition, FNIC2 with an isomeric fused-nine-ring core, have been developed. The ST-OSCs based on PTB7-Th:FNIC2 exhibited a maximum PCE of 11.6% and AVT of 13.6% (Fig. 18(c and d)).[231]

In another work, the flexible ST-OSC contained a blend of NFA IDT-2BR and polymer donor P3HT. IDT-2BR has strong absorption at the wavelength between 300 and 750 nm with a maximum extinction coefficient at 636 nm. The rigid device with P3HT:IDT-2BR photo-active layer had a 3.22% PCE, while the flexible device with had a 2.88% PCE and 50% AVT.[141] The
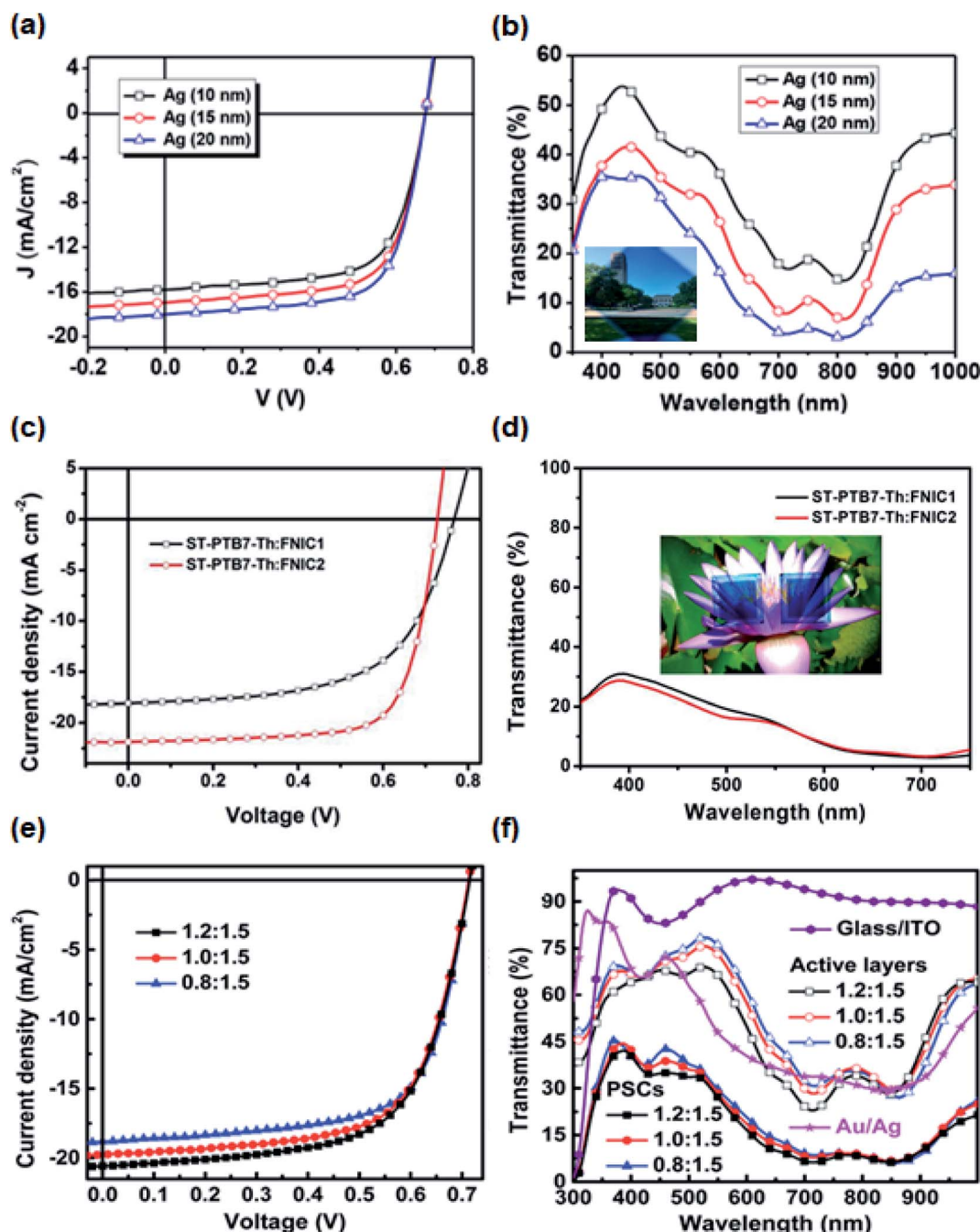
Fig. 18 (a) $J-V$ curves and (b) transmission spectra of semi-transparent OSCs (ST-OSCs) based on PTB7-Th : BT-CIC (1 : 1.5 wt%) with different Ag cathode thicknesses. Reprinted with permission.[140] Copyright (2017) American Chemical Society. (c) $J-V$ curves and (d) transmission spectra of ST-OSCs with a glass/ITO substrate, 1 nm Au/11 nm Ag ultrathin electrode, active layers with buffer layers. Reproduced from[230] with permission from The Royal Society of Chemistry. (e) $J-V$ curves, and (f) visible transmission spectrum of the optimised ST-OSCs with the structure of ITO/ZnO/PTB7-Th:acceptors/MoO$_x$/Ag (20 nm). The average visible transmittance of PTB7-Th:FNIC1 and PTB7-Th:FNIC2-based devices were 14.7% and 13.6%, respectively. Inset: photograph of the ST-OSCs based on PTB7-Th:FNIC1 (left) and PTB7-Th:FNIC2 (right). Reprinted with permission.[235] Copyright (2018) American Chemical Society.

3280 | *J. Mater. Chem. A*, 2022, **10**, 3255–3295

This journal is © The Royal Society of Chemistry 2022

$MoO_3/Ag/MoO_3$ (dielectric/metal/dielectric; D/M/D) layer functions as a transparent top electrode and the ST-OSC with PBDB-T:ITIC showed a PCE of 7.4% and AVT of 25.2%.[109,232] Zhang et al. demonstrated BDTThIT-4F narrow-E_g NFAs with PTB7-Th for ST-OSCs.[233] The ST-OSC with PTB7-Th:BDTThIT-4F layer showed PCE of 7.53% and AVT of 24.2%. Zhu et al. designed a new, deep-absorbing narrow-E_g (1.32 eV) NFA (ATT-2) by introducing 2-(3-oxo-2,3-dihydroinden-1-ylidene)malononitrile with effectively deceased LUMO level and improved ICT.[234] The device with PTB7-Th:ATT-2 gave a PCE up to 7.74% with AVT of 37%. The ITVfIC film had an absorption peak at 772 nm and an absorption edge at 900 nm corresponding to a narrow E_g of 1.37 eV. The PTB7-Th:ITVfIC blend showed strong complementary absorption (600–900 nm) and the result was a high PCE of 8.21% with an AVT of 26.4%.[235] Additionally, Zhang et al. fabricated ST-OSCs by blending PTB7-Th with IEICO-4F. The optimised blend was 0.8 : 1.5 PTB7-Th : IEICO-4F for ST-OSCs, giving a PCE of 9.06% and AVT of 27.1% (Fig. 18(e and f)).[236] Further, the authors introduced a ternary blend with two moderate-E_g donors (J71 and PTB7-Th) that showed good band alignment. The resulting ternary photo-active layer showed a complementary absorption range from 400 to 900 nm and they achieved a high PCE of 9.37%, along with a neutral colour property and acceptably high AVT values of over 20%.[237] Recently, Xu et al. reported that the wide bandgap polymer donor D18 with narrow photon harvesting in visible light range and small molecule N3 acceptor with NIR photon harvesting, are adopted to fabricate ST-OSCs. By optimizing the D18 : N3 weight ratio, the average visible transmittance (AVT) of the corresponding blend films can be achieved over 50%, demonstrating the great potential in fabricating efficient ST-OSCs. Based on the optimal blend ratio of D18 : N3 (0.7 : 1.6 wt/wt), they also controlled the thickness of the Ag electrode at 10 nm, achieving the highest light utilization efficiency of 2.90% with a PCE of 12.91% and an AVT of 22.49%.[238]

Xu et al. further reported the ST-OSCs surpassing the PCE of 13% and AVT of 20% simultaneously based on a ternary strategy which is the promising key to realizing the efficient ST-OSCs. The authors fabricated ST-OSCs with a broad bandgap polymer D18-Cl as the donor, narrow bandgap small molecule Y6-1O as the acceptor, and ultra-narrow bandgap material Y6 as the third component. They highlighted that the AVT of blend films can be notably increased from 30.3% to 47.3% with decrease in D : A from 1.1 : 1.6 to 0.7 : 1.6 (wt/wt). Keeping the D : A ratio 0.7 : 1.6 (wt/wt), the ternary blend with D18-Cl : Y6-1O : Y6 (0.7 : 0.8 : 0.8, wt/wt) as the active layers showed that the improved AVT to 50.1%. The ST-OSCs based on optimal ternary blend revealed that the PCE of 13.02%, AVT of 20.2%, and light utilization efficiency of 2.63% are obtained with Au (1 nm)/Ag (10 nm) as the electrode. They proposed that controlling the D : A weight ratio and adopting the ternary strategy have a powerful potential in simultaneously improving the PCE and AVT of ST-OSCs.[239]

They also reported the PM6:Y6 binary blend ST-OSCs by controlling the thickness of the active layer and electrode simultaneously. The authors set the active layer thickness 100 nm for best photovoltaic performance and Ag electrode 10 nm considering the trade-off between the PCE and AVT. As a result, the performance of ST-OSCs showed that PCE of 12.37% and AVT of 18.3% respectively.[240] Cheng et al. suggested transparent hole-transporting frameworks similar to the ternary system using PTAA. The device revealed PCEs of ~12% with AVTs ~20% both on rigid and flexible substrates.[241]

5.2 Tandem device structures

Tandem OSCs provide a promising device architecture that is expected to exceed the performance of single-junction cells due to the Shockely–Quiesser limit.[242] The combination with NFAs and tandem architecture shows great potential in the OSC field. Using this strategy, the photon utilisation efficiency could be considerably increased owing to the complementary absorption of the sub-cells.[243] Two-terminal tandem devices are commonly developed, where the sub-cells are connected in series by a highly transparent charger recombination layer (CRL), and photo-generated electrons from one sub-cell recombine with holes that are arriving from the sub-cell on the opposite side of the CRL.[244] Generally, the V_{oc} of the tandem structure is determined by the sum of all sub-cell voltages, while J_{sc} is limited by the smallest value of the two sub-cells, indicating that a balanced and high current between the sub-cells is crucial to achieve a high device J_{sc} and PCE in tandem architectures.[245] For optimal tandem cells, minimising the overlapping absorption wavelength between the front and rear cells is critical. Hence, the front cell absorbs the high-energy photons to provide a high V_{oc}, and rear cell absorbs low-energy photons and obtained a matched smaller J_{sc} in front or rear cells.[244]

The V_{oc} in tandem-junction devices is dependent on the changes to the incident light condition and electrical loss in the CRL. The relationship between the front and rear cells in the tandem junction affects charge generation and recombination, and hence the V_{oc} of each. The CRLs with suitable energy level can guarantee effective charge recombination rather than charge accumulation in the CRL. Additionally, although the CRLs show acceptable transmittance, they still introduce optical losses, which need to be further reduced.[246] This section presents recent progress in high-performance NFA tandem solar cells (Table 11).

In solution processes, the CRL should have proper interfacial surface energy on the active layer to obtain uniform film morphologies and sufficient chemical resistance to protect the deposited bottom active layer from being damaged by chemical solvents during processing the top active layer. PEDOT:PSS, typically used as CRL.[144,244,245,254] requires a surfactant or alcohol solvent due to its poor wettability on the hydrophobic surface of the active layers. Considering this, a hydrogen molybdenum bronze (H_xMoO_3) layer between the bottom active layer and PEDOT:PSS was developed to increase hole transport between the active layers, which has two advantages, good wettability on the hydrophobic surface and a higher WF (5.4 eV) than that of PEDOT:PSS, allowing more effective extraction of holes due to the deep HOMO energy level.[242]

Yang et al. reported a high-efficiency NFA tandem OSC based on ternary-blend sub-cells, which achieved good current

This journal is © The Royal Society of Chemistry 2022

J. Mater. Chem. A, 2022, 10, 3255–3295 | 3281

Table 11 Recent progress of representative NFAs based tandem OSCs

Front cell	Rear cell	V_{oc} (V)	J_{sc} (mA cm^{-2})	FF [%]	PCE (%)	Ref.
P3TEA:FTTB-PDI$_4$	PTB7-Th:IEICS-4F	1.72	9.83	61	10.50	144
PDBT-T1:TPH-Se:ITIC	PBDB-T:ITIC	1.84	9.60	65	11.50	247
PBDD4T-2F:PC$_{71}$BM	PBDTTT-E-T:IEICO	1.71	11.51	65	12.80	248
PBD1:PC$_{71}$BM	PTB7-Th:IEICO-4F	1.61	12.30	72	14.20	244
PBDB-T:F-M	PBDB-T:NNBDT	1.82	10.68	75	14.52	249
PBDB-T:IDTTA	PTB7-Th:IEICO-4F	1.65	13.10	68	14.70	250
PM6:TfIF-4FIC	PTB7-Th:PCDTBT:IEICO-4F	1.60	13.60	69	15.0	251
PM6:IT-4F	PTB7-Th:IEICO-4F	1.53	12.90	76	15.03	242
PM6:m-DTC-2F	PTB7-Th:BTPV-4F:PC$_{71}$BM	1.65	14.5	68	16.4	162
PTQ10: m-DTC-2Cl	PTB7-Th: BTPV-4F-eC9	1.62	14.65	70	16.67	252
PBDB-T:F-M	PTB7-Th:O6T-4F:PC$_{71}$BM	1.64	14.35	74	17.36	119
PM7:TfIF-4FIC	PTB7-Th:COi8DFIC:PC$_{71}$BM	1.64	14.59	78	18.71	207
PBDB-TF:ITIC	PBDB-TF:BCP-eC11	1.91	14.21	72	19.64	253
F:PBDB-T:ITIC-Th3	R:PBDB-T:PDPP2T-TT:Y1	1.74	11.70	72	15.10	254

matching with the absorption spectra tuned by varying its chemical composition. By introducing a wide-E_g polymer donor (PDBT-T1) which was blended with a wide-E_g NFA (TPH-Se), incident light loss is minimized. By substituting 10 wt% TPH-Se by ITIC the device enhanced, owing to its light absorption and facilitated charge separation *via* a cascade energy process, resulting in a more balanced current between the front and rear cells (Fig. 19(b and c)).[247] To achieve a PCE of 12.8% in a tandem OSC, they optimised the thickness of the active layer PBDD4T-2F:PC$_{71}$BM and PBDTTT-E-T:IEICO to ~100 nm in a single junction respectively. Since there was a trade-off between J_{sc} and FF in the tandem cell, considering these thickness issues, they fabricated tandem devices successfully.[248] Chen *et al.* reported NFA-based tandem OSCs with an outstanding PCE of 14.52% for tandem OSCs with the same polymer donor and two absorption-complementary acceptors. The two sub-cells showed high V_{oc} values of 0.99 and 0.86 V for the front cell and rear cell, respectively, along with complementary light absorption.[249]

To exceed 14% PCE, Wong *et al.* proposed a tandem OSC based on the combination of fullerene and non-fullerene materials to obtain strong complementary absorption. The enhanced performance of the tandem structure was attributed to the high EQE and FF of the wide-E_g sub-cell (Fig. 19(f)).[244] An innovative wide-E_g NFA (IDTTA) with strong absorption was developed for use in the front sub-cell in a tandem architecture. Considering these advantages of IDTTA, they produced two-terminal tandem devices based on PBDB-T:IDTTA and PTB7-Th:IEICO-4F as the front and rear sub-cells, respectively (Fig. 19(g–i)). This work revealed the high potential of new wide-E_g NFAs, which showed enhanced device performance along with appropriate electrical properties and durability.[250] A novel fluorine-substituted wide-E_g NFA (TfIF-4FIC) was introduced, which retained its optical E_g of 1.61 eV and suppressed E_{loss} by 0.63 eV.[207] For future mass-production of OSCs, Qin *et al.* introduced non-halogenated solvent system to tandem applications, because halogenated solvents classified as a hazard due to their toxicity.[252] Two small-molecule acceptor, m-DTC-2Cl and BTPV-4F-eC9, were newly designed with different bandgap energy to dissolve easily in non-halogenated solvents. Both

front and rear sub-cells were enhanced through the non-halogenated solvent processing based on tetrahydrofuran and *o*-xylene. Consequently, the tandem cell from the non-halogenated solvent exhibited the high efficiency of 16.67%.[252]

Solution-processed tandem OSCs with a PCE over 17% were reported by Chen *et al.*[119] By introducing the NFA molecule O6T-4F to ternary system with PTB7-Th and PC$_{71}$BM, they offered other optimal candidates for rear-sub-cell active materials with extensively tuneable band structure based on the A–D–A structure. By Kirchhoff's law, the highest possible current in a tandem cell should be ~15.5 mA cm^{-2} to achieve optimal performance of a 2-terminal tandem cell. As a result of these theoretical analyses, the authors combined the sub-cells to produce 2-terminal inverted tandem devices with a V_{oc} of ~1.64 V, approximately equal to the sum of those of the sub-cells.[224,225,232,237] The high and well-balanced J_{sc} of the two sub-cells was attributed to their complementary absorption ranges and high EQE.

As a result of numerous efforts to improve the performance of the tandem cell, Wang *et al.* achieved a high efficiency of 19.64% in a tandem structure, with certified value of 19.50% by the National Institute of Metrology.[253] The tandem cell revealed a high V_{oc} of 1.91 V owing to minimized voltage loss by analyzing the incident light effect for the rear sub-cell. By forming the 300 nm thick active layer of the rear sub-cell, the V_{oc} loss according to the decrease in the amount of light passing through the front sub-cell is minimized while maintaining the FF.[253] If the overlapping absorption regions and the voltage loss in the rear sub-cell is conquered, the tandem OSCs will be achieved a high PCE of over 20%.

6. Stability of the OSCs

Previous studies have emphasised significantly enhanced performance of OSCs by applying NFA materials with higher absorption coefficient and narrower E_g compared to fullerene derivatives. Despite these advancements, the long-term stability of these devices needs to be increased to enable OSCs to be competitive with other solar-cell technologies. Since organic
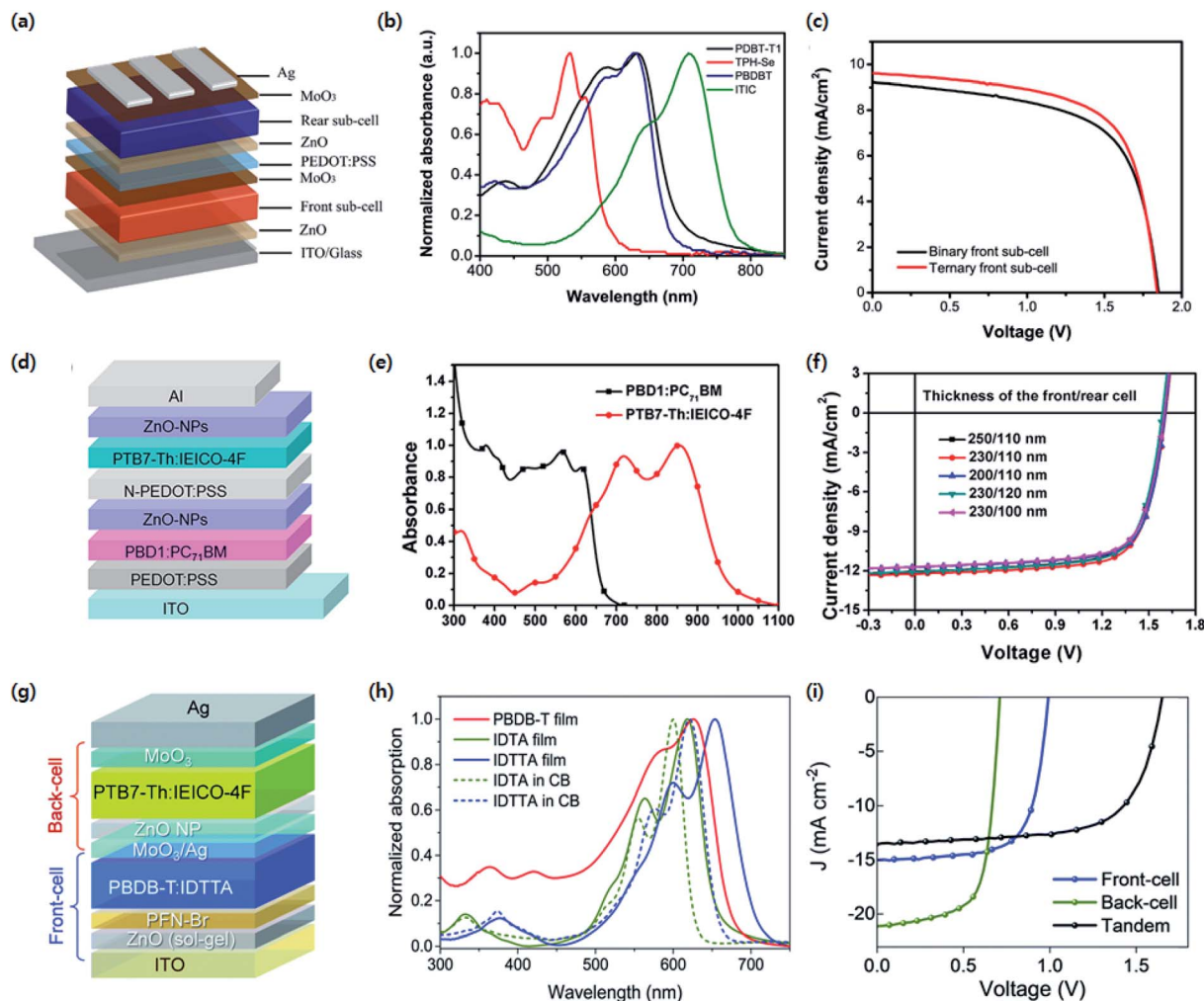
3282 | *J. Mater. Chem. A*, 2022, **10**, 3255–3295

This journal is © The Royal Society of Chemistry 2022

Fig. 19 (a) Schematic of a double-junction tandem OSC. (b) UV-Vis spectra of pure PDBT-T1, TPH-Se, PBDB-T, and ITIC films. (c) $J-V$ curves of the best-performing tandem devices based on PDBT-T1:TPH-Se binary front sub-cell and PDBT-T1 : TPH-Se : ITIC (1 : 0.9 : 0.1) ternary front sub-cell. Reprinted with permission.[247] Copyright (2018) American Chemical Society. (d) Device structure of the tandem OSC. (e) Absorption spectra of the active layers for the front (PBD1:PC$_{71}$BM) and rear cells (PTB7-Th:IEICO-4F). (f) $J-V$ characteristics of tandem OSCs with various sub-cell film thicknesses. Reprinted with permission.[244] Copyright (2018) American Chemical Society. (g) Tandem OSC device structure. (h) Absorption spectra of the donor and acceptor solutions and thin films. (i) $J-V$ curves of the optimised front cell (PBDB-T:IDTTA), rear cell (PTB7-Th:IEICO-4F), and tandem cell. Reproduced with permission[230] from The Royal Society of Chemistry.

materials are easily degraded by external factors, such as oxygen, light, and heat, various strategies for stable operation of OSCs based on NFAs have been proposed depending on the type of stress.[255]

6.1 Air stability of the OSCs

Organic materials can react with oxygen under ambient conditions, and oxidation reactions can reduce the OSC performance. In particular, since conventional photo-active layers are composed of fullerene derivatives, such as PC$_{61}$BM and PC$_{71}$BM, self-aggregation of these materials can occur when they are exposed to oxygen. Therefore, it is important to increase the intrinsic stability of photo-active materials (*i.e.*, acceptors) for industrial applications by designing acceptors with new chemical structures. Tremendous efforts have been applied to developing stable NFAs for long-term operation of

high-performance OSCs.[256] Holliday *et al.* developed the O-IDTBR NFA and compared the air stability of devices with O-IDTBR to those with fullerene acceptors in an inverted structure.[21] The PCE of the devices based on fullerene derivatives deteriorated rapidly, and after 1200 h, the devices were barely working. However, except for an initial small reduction, the device based on O-IDTBR operated stably for 1200 h, while maintaining 72% of the original PCE; this was attributed to the smooth surface of the active layer with O-IDTBR which did not aggregate under ambient conditions. Tu *et al.* achieved long-term stability (120 d) of a device with EH-IDTBR by using a newly synthesised donor material.[257] As various NFA structures were reported, the stability of highly efficient OSCs with PCEs over 10% was evaluated. OSCs based on PTB7-Th:CO*i*8DFIC or PM6:BP-4F showed only a 10% reduction in PCE after 30 d of storage in air (Fig. 20).[258,259] Cai *et al.* showed
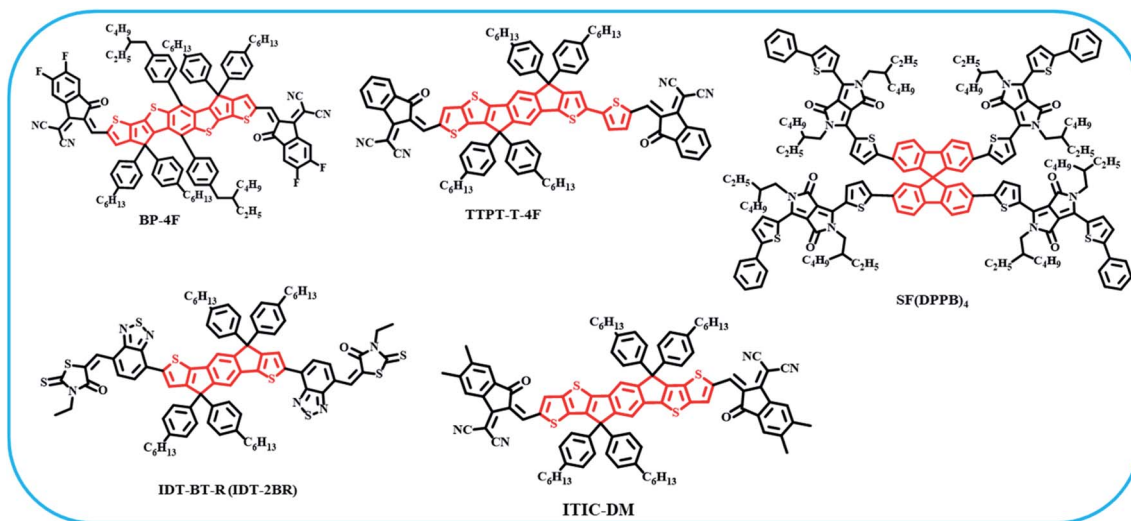
Fig. 20 Chemical structures of the acceptors used in the stability section except for the materials introduced in previous sections.

excellent storage lifetimes of 30 d for PBDB-T:BTP-4F (with INB-1F, -3F, 5F additives) with initial PCEs exceeding 15%.[260]

To further demonstrate the intrinsic stability of NFAs, durability tests of the OSCs were conducted under ambient condition without any encapsulation. By maximising the intrinsic stability of the NFA materials, stable operation F13:Y6 BHJ and L2:TTPT-T-4F BHJ systems was observed over 1000 h without encapsulation, with a high PCE above 13%.[261,262] The air stability is a big obstacle to the commercialisation of OSCs, which has been mostly overcome by modifying the intrinsic properties of the NFA materials. This is expected to open a new era of organic electronics composed of various organic semiconductors, beyond OSCs.

6.2 Thermal stability of the OSCs

Thermal stresses can cause serious deterioration of organic materials. However, since a large amount of heat is generated during the operation of the OSCs, the photo-active material is required to have excellent thermal stability. The NFAs provide a solution to the thermal stability issue owing to their structural variability. Initially, polymer NFAs were used to improve the thermal stability, but the polymer NFA-based device only maintained 70% of the initial PCE at 180 °C for 20 h.[263] Chen *et al.* designed a new NFA, SF(DPPB)$_4$ for high thermal stability. The device with SF(DPPB)$_4$ exhibited a V_{oc} of 1.14 V and PCE of 5.16% when blended with P3HT. In particular, SF(DPPB)$_4$-based devices withstood heat treatment of 150 °C for 3 h without PCE loss, while those based on fullerene derivatives showed a reduced PCE.[264] To improve the thermal stability of NFAs, ladder-type donor units (such as IDT) were introduced, which formed low-crystalline materials without aggregation. Therefore, the device with IDT-BT-R acceptor maintained a comparable PCE of 8.2% at 150 °C for 1 h.[265] Other studies introduced polymer additives to ITIC-based BHJ systems. For example, block copolymers act as compatibilisers to prevent the phases from aggregating inside the BHJ.[266] Although burn-in loss was

observed initially, the device with ITIC and a compatibiliser maintained 77% performance under thermal treatment at 100 °C for 120 h in a N$_2$ environment. Zhu *et al.* proposed a new type of all-fused-ring electron acceptor (AFRA) named ITYM. It is confirmed by single-crystal X-ray analysis, which shows a planar nonacyclic structure with strong π–π stacking. Compared with the classical carbon-bridged INCN-type acceptors, ITYM exhibits superior thermal, and chemical stability with very promising performance compared to the classical carbon-bridged NFAs.[267]

6.3 Light stability of the OSCs

Because solar cells absorb sunlight to convert the solar energy into electrical energy, continuous illumination is necessary during operation. However, sunlight induces degradation of organic materials and photoelectric effects. Therefore, in the commercialisation of OSCs, it is important to minimise the damage caused by the illumination by optimising the molecular structure. Among the various NFA units, ITIC resulted in burn-in loss and insufficient light stability after only 1 h of illumination when blended with PTB7-Th. Doumon *et al.* investigated the degradation of ITIC *via* a comparison with FAs (Fig. 21(a and b)).[268] The ITIC materials could accelerate photodegradation or aggregation of the blend film with donor materials. Park *et al.* investigated the photodegradation mechanism of ITIC, where reactions with hydroxyl radicals resulted in breakage of the double bond in ITIC.[269] Consequently, the introduction of stable functional group into the NFAs is necessary to increase their photo-stability. Du *et al.* demonstrated photo-stable devices with various ITIC derivatives (ITIC, ITIC-2F, ITIC-M, ITIC-DM, and ITIC-Th) under continuous 1 sun illumination in a N$_2$ environment.[270] (Fig. 21(c and d)). Although PBDB-T is relatively photo-stable, the ITIC-DM-based device showed fast reduction in performance due to its photo-catalytic activity. In contrast, other materials (especially ITIC-2F) operated very stably even under illumination conditions for 1600 h. It was confirmed that
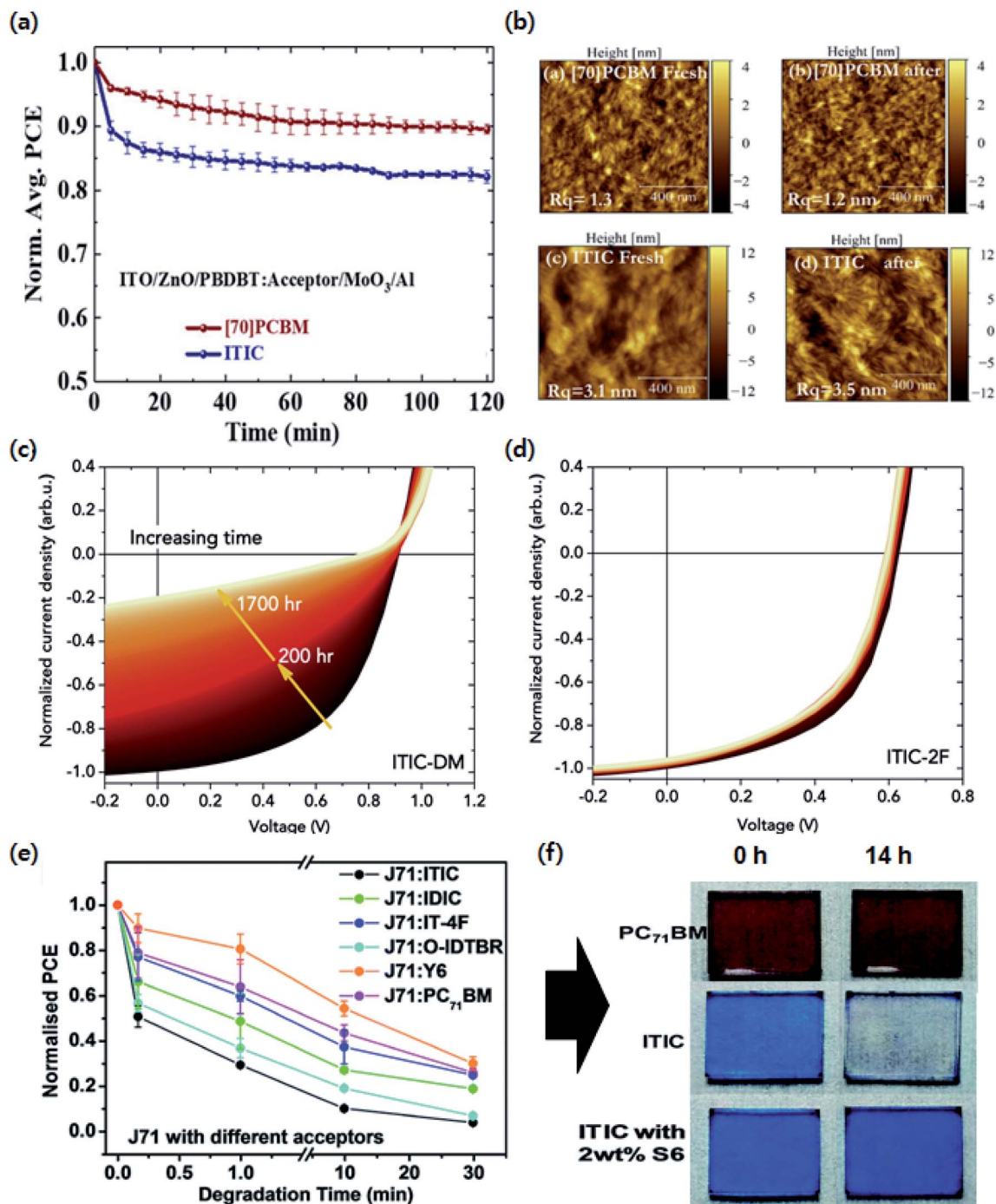
3284 | *J. Mater. Chem. A*, 2022, **10**, 3255–3295

This journal is © The Royal Society of Chemistry 2022

Fig. 21 (a) Performance of PBDB-T-based inverted OSCs under continuous illumination. (b) AFM images of fresh and exposed organic thin films (PC$_{70}$BM and ITIC). Reprinted with permission.[268] Copyright (2019) American Chemical Society. Device stability under continuous illumination in a dry nitrogen atmosphere. Normalised J–V curves of representative devices based on (c) ITIC-DM and (d) ITIC-2F under continuous LED illumination. Reproduced with permission.[270] Copyright (2019) Elsevier. (e) Normalised PCE of J71 devices based on degraded BHJ blends as a function of illumination time. (f) Photographs of photo-oxidised PC$_{71}$BM, ITIC, and ITIC with 2 wt% S6 films as a function of the exposure time. Reproduced with permission.[272] The Royal Society of Chemistry.

the photo-stability is highly dependent on the structural design of the NFAs. To enhance the photo-stability of ITIC-M, N2200 was applied to blend systems with PBDB-T and PBDB-T-2F donors.[271] While the ITIC-M increased the series resistance of the devices, N2200 acted as a stabiliser to suppress

photodegradation. Guo et al. investigated photooxidation reaction sites and mechanisms for ITIC and fullerene derivatives (Fig. 21(e and f)).[272] EH-IDTBR-based devices exhibited high illumination stability owing to three-dimensional molecular packing with donor materials (mainly PTB7-Th).[273] Liu et al.

This journal is © The Royal Society of Chemistry 2022

J. Mater. Chem. A, 2022, 10, 3255–3295 | 3285

reported a new molecular design strategy to increase the intrinsic chemical and photochemical stability of A–D–A type NFAs by introducing ring-locked C–C double bonds between D–A conjugation, attributed to increased steric hindrance of nucleophilic attack and the formation of intramolecular C–H⋯O interactions. The PTB7-Th:IDTT-CT based OSCs showed very encouraging photostability, the PCE of which could retain >80% of the initial values after 200 h one sun irradiation in air without a UV filter. Such photostability performance has greatly outperformed those from conventional NFAs like ITIC, IT-4F, and IT-M, suggesting the effectiveness of ring-locking design strategy.[274]

7. Fabrication processes for industrialization

Although OSCs have various advantageous for industrialisation as solution-based processes and a high elastic process can be applied, few groups have reported large-area or scalable fabrication due to a range of technical challenges. There are various processes that can realise large-area fabrication, but it is difficult to directly apply conventional photo-active materials to large-area processing because the film is very thin and self-aggregation of the materials occurs during the process.[275] Therefore, it is essential to develop new materials that maintain good performance and can be adapted to large-area processing. The development of NFAs made it possible to produce OSCs using large-area processes via structural evolution. Unlike the fullerene derivatives, the NFAs can be controlled the solubility enough to be soluble in relatively polar solvents, which leads to process innovations, such as organic solvent-free fabrication and sequential lamination without penetration. Since the active area is an important indicator for evaluating devices, only those with an active area over 1 cm^2 are discussed here. Moreover, since simple morphology control of the active layer is required for the industrialization of OSCs, advanced fabrication processes such as layer-by-layer (LBL) process and thick-film process are emerging.

7.1 Large-area fabrication by slot-die coating process

Brandt et al. fabricated ITO- and vacuum-free devices based on NFAs (Ph(DPP)$_3$, Ph(DPP)$_2$, and PhDMe(DPP)$_2$) with P3HT donor using a roll-coating process (Fig. 22). The structure of the devices were: PET/PEDOT:PSS(electrode)/ZnO/Active layer/PEDOT:PSS(HTL)/Ag grid. The printed devices had PCEs comparable to those of spin-coated devices after photo-annealing.[276]

Gu et al. demonstrated roll-to-roll printing of photo-active materials composed of PII2T-PS:PNDIT and PTB7-Th:PNDIE with low crystallinity.[277] The device structure was PET/ITO/ZnO NPs/active layer/MoO$_3$/Ag, where the ZnO NPs and active layer were sequentially formed using slot-die coating on PET/ITO. Although MoO$_3$ and Ag were thermally evaporated, continuously printed devices achieved a PCE of up to 5% over a large area of 1 cm^2. In addition, solar modules were successfully fabricated using this hybrid process with a PCE of 5.5%, which showed stable operation in ambient conditions after applying encapsulation.[278] Wu et al. reported highly efficient devices with IT-4F NFA and PM6 donor processed by slot-die coating. By optimising the coating process, the devices achieved 12.90% PCE with a rigid glass substrate and 12.32% PCE on a flexible PET substrate. Moreover, the large-area modules were used as a power source for an photoelectrochemical catalyst in combination with a photoelectrochemical device, resulting in a solar-to-hydrogen (STH) efficiency of 6.15% (Fig. 23(a and b)).[279]

7.2 Large-area fabrication by blade-coating process

Blade-coated OSCs with PBDT-TS1:PPDIODT were fabricated in ambient conditions using a green solvent, o-metylanisole with a low toxicity.[280] The device structure was composed of ITO/PEDOT:PSS/active layer/Ca/Al. Only the active layer was
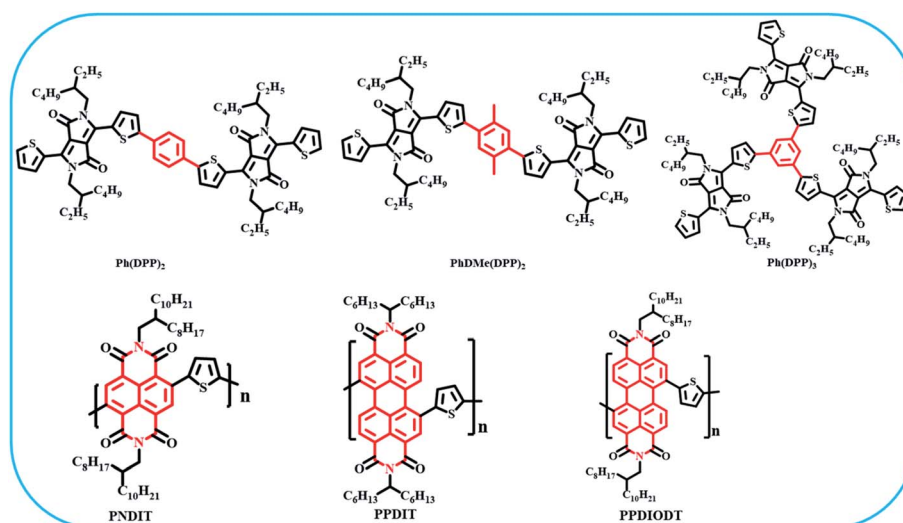

Fig. 22 Chemical structures of the acceptors used in the large-area fabrication section except for the materials introduced in previous sections.

3286 | J. Mater. Chem. A, 2022, **10**, 3255–3295

This journal is © The Royal Society of Chemistry 2022

applied by blade coating. These devices showed a high efficiency of 8.4%, in spite of the large-area process and use of a green solvent (Fig. 23(c and d)). Lin *et al.* fabricated devices with a structure of ITO/ZnO/active layer/MoOx/Al, and investigated the blade-coated active layers based on PTzBI:N2200 depending on various solvents (MeTHF, MeTHF/DIO, CF, and CB).[281] By controlling the nucleation of N2200, an impressive PCE of 8.36% was obtained from the blade-coated device processed with MeTHF and DIO. Recently, blade-coated NFA-based OSCs have also been used in indoor applications.

7.3 Layer-by-layer (LBL) process

The LBL process has advantages in morphology control, since the donor and accepter materials can be controlled independently with good crystallinity. In addition, the LBL process can induce vertical phase separation that forms the enrich donor-domains at the anode and acceptor-domains at the cathode, which improves charge transport while preventing charge recombination. Wang *et al.* proposed the LBL deposition of organic active layer as a sequential process.[282] LBL-deposited OSCs with PM6:Y6 were fabricated using additives 1,10-decanediol (DDO) and CN to form the films of PM6 and Y6 separately. The DDO not only improved the crystallinity of PM6, but also formed a morphology of PM6 that could withstand the coating of Y6 solution. Eventually, the

OSCs based on the LBL process revealed the notable PCE of 16.93% and FF of 77.45% owing to vertical phase separation, compared to the blend-coated OSCs.[282] Xu *et al.* introduced a ternary structure to the OSCs using the LBL process. The ternary structure is composed of PM6 as a wide band gap polymer and N3 as a narrow band gap NFA with a guest component, MF1.[283] The LBL process leads to the optimized phase separation and sufficient interface area between the donor and acceptor by incorporating MF1. The OSCs with the LBL-deposited ternary active layer shows the PCE of 16.75% comparable to that of the device fabricated by blend coating.[283] Ning *et al.* reported the highest PCE (17.59%) of the LBL-deposited OSCs by developing an insoluble donor, PNTB6-Cl, in CF solvent due to its stronger intermolecular interactions and shorter π–π stacking distance.[284] Although the LBL process makes the vertical phase separation, the LBL-deposited active layer is mixed by the lamination process and returned to an amorphous form. However, the insoluble PNTB6-Cl induced high enhancement while maintaining effective vertical pathways with N3.[284]

7.4 Thick-film process

Development of thick-film processed active layers for the large-area processes is required for the commercialization of the OSCs. In recent research trends, the OSCs with thick
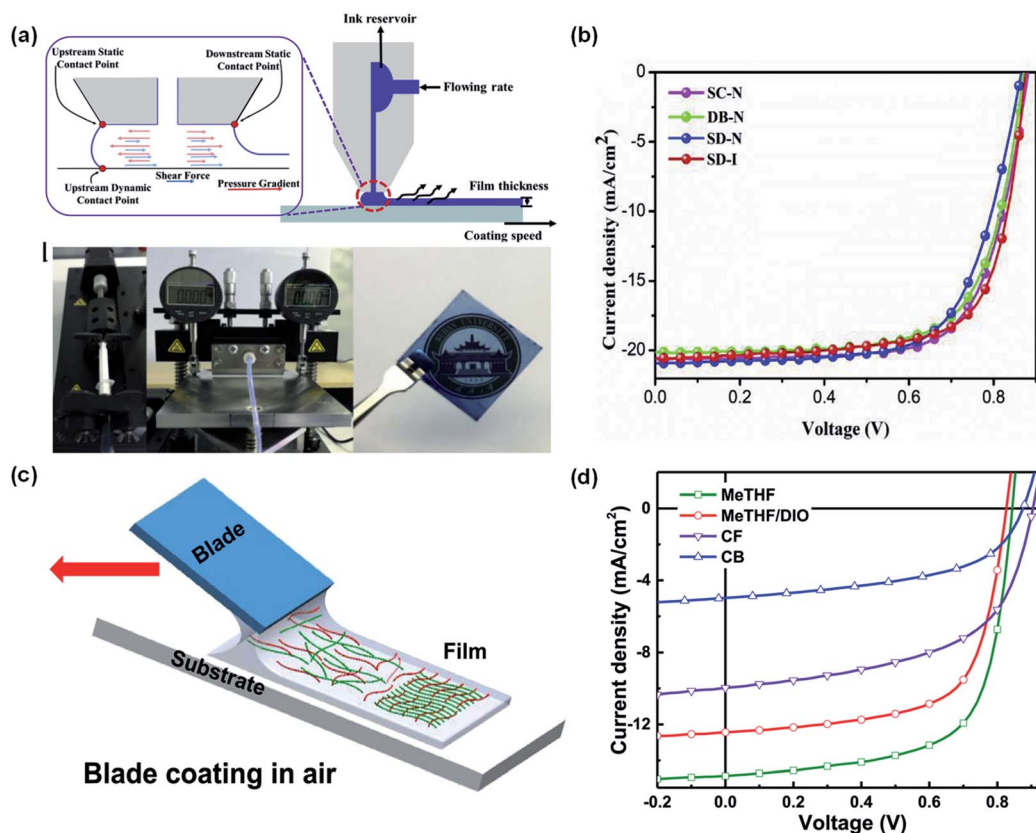

Fig. 23 (a) Slot-die coating process with independently controlled parameters. Inset: schematic of meniscus formation and the streamlines near the stagnation point in the slot-die head. Photograph of the slot-die coating setup and the achieved high-quality BHJ films with a ZnO layer. (b) *J–V* characteristics of OSCs fabricated by various printing technologies for inverted or conventional device architectures. Reproduced with permission.[279] Copyright 2019, Elsevier. (c) Schematic of the blade-coating process. (d) *J–V* curves of the short-circuit current density on light density of blade-coated films processed using different solvents. Reproduced with permission.[281] Copyright 2019, Elsevier.

This journal is © The Royal Society of Chemistry 2022

J. Mater. Chem. A, 2022, **10**, 3255–3295 | **3287**

active layer over 300 nm has exhibited lower performance than that of the OSCs with thin-film due to charge recombination in active layers. To enhance the performance of the OSCs with thick-film, charges generated before recombination should be collected by each electrode, and light loss due to thickness should be minimized. Gao *et al.* solved the thick-film issues through a ternary strategy by utilizing PBDB-T-2Cl donor and two NFAs, MF1 and BP-4F.[285] The OSCs with thick ternary active layers of 300 nm exhibit a high PCE of 14.57% and FF of 71.62%, which results from additional pathway of separated charge carriers owing to vigorous Föster energy transfer from MF1 to BP-4F. Wang *et al.* reported the OSCs with 300 nm thick-film by introducing ternary system composed of PM6 donor, BTP-4F-12 and BP-4F acceptors.[286] BP-4F plays a role as a morphology regulator that improves the molecular arrangement and phase separation of the donor and acceptor in thick films. Consequently, *via* the ternary system, even within the thick active layer, charge carriers were efficiently transferred before charge recombination. The thick-film OSCs achieved a high PCE of 15.63% and FF of 70.03%, and can be lead to large-scale fabrication process for efficient OSCs.

8. Challenges and outlook

The introduction of NFAs brought about a golden age in the development of OSCs. However, along with the enormous interest in NFAs, various challenges still exist, related to the synthesis of new materials, processing methods, device architectures, long-term durability, and fabrication processes for large-area devices.

OSCs have exhibited great potentials in improving device efficiency and long-term operational stability owing to the non-fullerene acceptors. Currently, the efficient non-fullerene acceptors are like ITIC and Y6, which are constructed by the large fused-ring with multistep synthesis. These molecules usually have the following feature: (a) electron donating units contain bulky substituents that are perpendicular to the main backbone; (b) strong electron-withdrawing units are exposed at two sides for molecular packing; (c) the main backbone of this molecules is planar. The main backbone exhibited plane characteristics, which is beneficial for efficient intramolecular charge transport and molecular packing, thus for achieving higher electron mobilities. The electron-withdrawing end groups are helpful for efficient molecular contacts, allowing efficient intermolecular charge transport. The bulky substituents are helpful to tune the molecular aggregation. Other types of non-fullerene acceptors are slightly modified on this structure and also achieve high performance OSCs. In the future, to further improve the performances of non-fullerene acceptors, the optimization can happen in the electron-donating units, the electron-withdrawing units or the bulky substituents and so on.

(1) Simple synthesis of the acceptors is urgently needed to be explored. We can focus on the following points: (a) green synthesis can be employed to reduce the use of toxic reagents, such as tin reagent, lithium reagent. (b) Appropriately decreasing the number of fused ring unit is helpful to reduce the synthesis steps. (c) Reasonable utilizing of aromatic bulky substituents and aliphatic alkyl chains to optimize molecular structure. In all, much more exploration of non-fullerene acceptors should be made so as to achieve new breakthroughs, in achieving high electron mobility, low energy loss and excellent stability.

(2) In order to utilize the photons as many as possible, hence, to obtain high current, the complementary absorption of the acceptor as well as the donor are important for achieving a high PCE performance.

(3) Suitable energy level match between donors and acceptors is also worth of consideration. HOMO and LUMO of the polymer donor and non-fullerene acceptors, which could provide the maximized V_{oc} as well as strong driving force for the charge generation and transportation should be chosen judiciously. There is no doubt that the energy loss is as low as 0.5 eV (or below) for efficient fullerene-free OSCs, but exploration of new photovoltaic materials with low energy loss is still desired.

(4) Preferred blend morphology is also quite important for the high performance OSCs. Appropriate suitable domain sizes and high domain purity with superior charge mobility is in favour of exciton separation. Furthermore, suitable film morphology with preferred face-on orientation will contribute to the vertical charge transfer.

To achieve high-performance ST-OSCs, both the performance and transmittance of the device should be optimised. Although numerous studies have been conducted to increase both the PCE and AVT of OSCs, it is still too early to commercialise ST-OSC as this still requires the development of an organic semiconductor material capable of efficiently converting light in the visible light region into electrical energy. Therefore, the role of the NFA in promoting light absorption and charge transfer is important, because the maximum power must be obtained from the organic semiconductor with the minimum thickness (to ensure transparency). In the future, the use of new NFA materials may facilitate the development of ST-OSCs with both higher PCE and AVT.

The core of tandem-device development is incorporating materials with different light-absorption regions in the front and rear cells. Through the design of NFAs with strong NIR absorption and high electron affinity, the photo-active range can be extended to long wavelengths, allowing the tandem OSC to absorb a wide range of wavelengths. In addition, to realise tandem structures, the solvent selectivity of NFA should be diversified by controlling their chemical structure to avoid the deterioration of the bottom organic materials by the solution used to deposit the upper materials.

To commercialise OSCs, their long-term stability needs to be ensured. As a result of the many efforts to improve the device stability, such as the introduction of additives and interfacial layers, and encapsulation, the performance of OSCs has now been maintained for 1000 h. Although the stability of the OSCs against atmospheric, thermal, and illumination stresses has been confirmed, the morphological and chemical stability of the NFAs against the combination of many factors, such as oxygen, moisture, heat and illumination still need to be enhanced by controlling their molecular structure.

3288 | *J. Mater. Chem. A*, 2022, **10**, 3255–3295

This journal is © The Royal Society of Chemistry 2022

With the introduction of NFAs, OSCs have achieved high PCEs of over 18%, and expectations for their commercialisation are increasing annually. However, the highest performance of NFA-based OSC was achieved at the laboratory scale, and there are few reports on large-area OSCs. In particular, for the implementation of large-area OSCs, large-scale fabrication processes that do not degrade the OSC performance need to be developed. To date, various large-area fabrication methods, such as slot-die coating and blade coating, have been proposed for OSCs. However, there are many obstacles to be overcome before the commercialisation of OSCs is viable, such as dual temperature control for solutions and substrates, the use of halogenated solvents, and the formation of discontinuous interfacial layers. To effectively overcome these issues, it is essential to develop appropriate NFA materials that are soluble in green solvents at low temperature and are stable during continuous production processes.

Conflicts of interest

There are no conflicts to declare.

Acknowledgements

References

1 S. Park, A. Roy, S. Beaupré, S. Cho, N. Coates, J. Moon, D. Moses, M. Leclerc, K. Lee and A. J. Heeger, *Nat. Photonics*, 2009, **3**, 297–302.

2 Y. Huang, E. J. Kramer, A. J. Heeger and G. C. Bazan, *Chem. Rev.*, 2014, **114**, 7006–7043.

3 D. M. Stoltzfus, J. E. Donaghey, A. Armin, P. E. Shaw, P. L. Burn and P. Meredith, *Chem. Rev.*, 2016, **116**, 12920–12955.

4 G. Li, W.-H. Chang and Y. Yang, *Nat. Rev. Mater.*, 2017, **2**, 17043.

5 C. W. Tang, *Appl. Phys. Lett.*, 1986, **48**, 183–185.

6 G. Yu, J. Gao, J. C. Hummelen, F. Wudi and A. J. Heeger, *Science*, 1995, **270**, 1789.

7 J. J. Halls, C. A. Walsh, N. C. Greenham, E. A. Marseglia, R. H. Friend, S. C. Moratti and A. B. Holmes, *Nature*, 1995, **376**, 498–500.

8 Y. He and Y. Li, *Phys. Chem. Chem. Phys.*, 2011, **13**, 1970–1983.

9 J. Hou, O. Inganäs, R. H. Friend and F. Gao, *Nat. Mater.*, 2018, **17**, 119–128.

10 C. Yan, S. Barlow, Z. Wang, H. Yan, A. K.-Y. Jen, S. R. Marder and X. Zhan, *Nat. Rev. Mater.*, 2018, **3**, 18003.

11 S. Chen, L. Feng, T. Jia, J. Jing, Z. Hu, K. Zhang and F. Huang, *Sci. China Chem.*, 2021, **64**, 1192–1199.

12 C. Li, J. Zhou, J. Song, J. Xu, H. Zhang, X. Zhang, J. Guo, L. Zhu, D. Wei, G. Han, J. Min, Y. Zhang, Z. Xie, Y. Yi, H. Yan, F. Gao, F. Liu and Y. Sun, *Nat. Energy*, 2021, **6**, 605–613.

13 P. Cheng, G. Li, X. Zhan and Y. Yang, *Nat. Photonics*, 2018, **12**, 131.

14 N. K. Elumalai and A. Uddin, *Energy Environ. Sci.*, 2016, **9**, 391.

15 L. Ye, Y. Xiong, Q. Zhang, S. Li, C. Wang, Z. Jiang, J. Hou, W. You and H. Ade, *Adv. Mater.*, 2018, **30**, 1705485.

16 Z. Zhang, L. Fenga, S. Xua, J. Yuan, Z.-G. Zhang, H. Penga, Y. Li and Y. Zou, *J. Mater. Chem. A*, 2017, **5**, 11286–11293.

17 H.-Y. Chen, J. Hou, S. Zhang, Y. Liang, G. Yang, Y. Yang, L. Yu, Y. Wu and G. Li, *Nat. Photonics*, 2009, **3**, 649–653.

18 Z.-G. Zhang and Y. Li, *Sci. China: Chem.*, 2015, **58**, 192–209.

19 S. Xiao, Q. Zhang and W. You, *Adv. Mater.*, 2017, **29**, 1601391.

20 M. Dang, L. Hirsch and G. Wantz, *Adv. Mater.*, 2011, **23**, 3597–3602.

21 S. Holliday, R. Ashraf, A. Wadsworth, D. Baran, S. Yousaf, C. B. Nielsen, C.-H. Tan, S. D. Dimitrov, Z. Shang, N. Gasparini, M. Alamoudi, F. Laquai, C. J. Brabec, A. Salleo, J. R. Durrant and I. McCulloch, *Nat. Commun.*, 2016, **7**, 11585.

22 X. Xu, G. Zhang, L. Yu, R. Li and Q. Peng, *Adv. Mater.*, 2019, **31**, 1906045.

23 C. Yang, S. Zhang, J. Ren, M. Gao, P. Bi, L. Ye and J. Hou, *Energy Environ. Sci.*, 2020, **13**, 2864–2869.

24 C. Yang, R. Yu, C. Liu, H. Li, S. Zhang and J. Hou, *ChemSusChem*, 2021, **14**, 3607.

25 J. Xiao, X. Jia, C. Duan, F. Huang, H.-L. Yip and Y. Cao, *Adv. Mater.*, 2021, **33**, 2008158.

26 W. Kim, J. Kim, E. Kim, T. Ahn, D. Wang and J. Park, *J. Phys. Chem. C*, 2015, **119**, 5954–5961.

27 S.-H. Liao, H.-J. Jhuo, Y.-S. Cheng and S.-A. Chen, *Adv. Mater.*, 2013, **25**, 4766–4771.

28 J.-D. Chen, C. Cui, Y.-Q. Li, L. Zhou, Q.-D. Ou, C. Li, Y. Li and J.-X. Tang, *Adv. Mater.*, 2015, **27**, 1035–1041.

29 Y. Lin, J. Wang, Z.-G. Zhang, H. Bai, Y. Li, D. Zhu and X. Zhan, *Adv. Mater.*, 2015, **27**, 1170–1174.

30 Z. Xiao, X. Jia, D. Li, S. Wang, X. Geng, F. Liu, J. Chen, S. Yang, T. P. Russel and L. Ding, *Sci. Bull.*, 2017, **62**, 1494–1496.

31 H. Li, Z. Xiao, L. Ding and J. Wang, *Sci. Bull.*, 2018, **63**, 340–342.

32 Z. Jia, S. Qin, L. Meng, Q. Ma, I. Angunawela, J. Zhang, X. Li, Y. He, W. Lai, N. Li, H. Ade, C. J. Brabec and Y. Li, *Nat. Commun.*, 2021, **12**, 178.

33 S. D. Collins, N. A. Ran, M. C. Heiber and T.-Q. Nguyen, *Adv. Energy Mater.*, 2017, **7**, 1602242.

This journal is © The Royal Society of Chemistry 2022

J. Mater. Chem. A, 2022, **10**, 3255–3295 | **3289**

34 B. Qiu, L. Xue, Y. Yang, H. Bin, Y. Zhang, C. Zhang, M. Xiao, K. Park, W. Morrison, Z.-G. Zhang and Y. Li, *Chem. Mater.*, 2017, **29**, 7543–7553.

35 H. Bin, J. Yao, J. Yang, I. Angunawela, C. Sun, L. Gao, L. Ye, B. Qiu, L. Xue, C. Zhu, C. Yang, Z.-G. Zhang, H. Ade and Y. Li, *Adv. Mater.*, 2018, **30**, 1706361.

36 R. Zhou, Z. Jiang, C. Yang, J. Yu, J. Feng, M. Adil, D. Deng, W. Zou, J. Zhang, K. Lu, W. Ma, F. Gao and Z. Wei, *Nat. Commun.*, 2019, **10**, 5393.

37 H. Chen, D. Hu, Q. Yang, J. Gao, J. Fu, K. Yang, H. He, S. Chen, Z. Kan, T. Duan, C. Yang, J. Ouyang, Z. Xiao, K. Sun and S. Lu, *Joule*, 2019, **3**, 3034–3047.

38 H. Tang, H. Chen, C. Yan, J. Huang, P. W. K. Fong, J. Lv, D. Hu, R. Singh, M. Kumar, Z. Xiao, Z. Kan, S. Lu and G. Li, *Adv. Energy Mater.*, 2020, **10**, 2001076.

39 D. Hu, Q. Yang, Y. Zheng, H. Tang, S. Chung, R. Singh, J. Lv, J. Fu, Z. Kan, B. Qin, Q. Chen, Z. Liao, H. Chen, Z. Xiao, K. Sun and S. Lu, *Adv. Sci.*, 2021, **8**, 2004262.

40 D. Hu, Q. Yang, H. Chen, F. Wobben, V. M. Corre, R. Singh, T. Liu, R. Ma, H. Tang, L. Koster, T. Duan, H. Yan, Z. Kan, Z. Xiao and S. Lu, *Energy Environ. Sci.*, 2020, **13**, 2134–2141.

41 C. An, Y. Qin, T. Zhang, Q. Lv, J. Qin, S. Zhang, C. He, H. Ade and J. Hou, *J. Mater. Chem. A*, 2021, **9**, 13653–13660.

42 J. Ge, L. Xie, R. Peng, B. Fanady, J. Huang, W. Song, T. Yan, W. Zhang and Z. Ge, *Angew. Chem., Int. Ed.*, 2020, **59**, 2808–2815.

43 Q. Yue, H. Wu, Z. Zhou, M. Zhang, F. Liu and X. Zhu, *Adv. Mater.*, 2019, **31**, 1904283.

44 J. Ge, L. Hong, W. Song, L. Xie, J. Zhang, Z. Chen, K. Yu, R. Peng, X. Zhang and Z. Ge, *Adv. Energy Mater.*, 2021, **11**, 2100800.

45 T. Xu, J. Lv, K. Yang, Y. He, Q. Yang, H. Chen, Q. Chen, Z. Liao, Z. Kan, T. Duan, K. Sun, J. Ouyang and S. Lu, *Energy Environ. Sci.*, 2021, **14**, 5366–5376.

46 J. Qin, Z. Chen, P. Bi, Y. Yang, J. Zhang, Z. Huang, Z. Wei, C. An, H. Yao, X. Hao, T. Zhang, Y. Cui, L. Hong, C. Liu, Y. Zu, C. He and J. Hou, *Energy Environ. Sci.*, 2021, **14**, 5903.

47 Q. Lv, C. An, T. Zhang, J. Zhang, S. Zhang, P. Zhou, C. He and J. Hou, *Sci. China: Chem.*, 2021, **64**, 1200–1207.

48 Y. Huo, H.-L. Zhang and X. Zhan, *ACS Energy Lett.*, 2019, **4**, 1241–1250.

49 X. Zhang, Z. Lu, L. Ye, C. Zhan, J. Hou, S. Zhang, B. Jiang, Y. Zhao, J. Huang, S. Zhang, Y. Liu, Q. Shi, Y. Liu and J. Yao, *Adv. Mater.*, 2013, **25**, 5791–5797.

50 J. Liu, S. Chen, D. Qian, B. Gautam, G. Yang, J. Zhao, J. Bergqvist, F. Zhang, W. Ma, H. Ade, O. Inganäs, K. Gundogdu, F. Gao and H. Yan, *Nat. Energy*, 2016, **1**, 16089.

51 Y. Lin, Y. Wang, J. Wang, J. Hou, Y. Li, D. Zhu and X. Zhan, *Adv. Mater.*, 2014, **26**, 5137–5142.

52 Z. Luo, W. Xiong, T. Liu, W. Cheng, K. Wu, Y. Sun and C. Yang, *Org. Electron.*, 2017, **41**, 166–172.

53 Y. Duan, X. Xu, H. Yan, W. Wu, Z. Li and Q. Peng, *Adv. Mater.*, 2017, **29**, 1605115.

54 H. Zhong, C. H. Wu, C.-Z. Li, J. Carpenter, C. C. Chueh, J. Y. Chen, H. Ade and A. K. Jen, *Adv. Mater.*, 2016, **28**, 951–958.

55 D. Meng, H. Fu, C. Xiao, X. Meng, T. Winands, W. Ma, W. Wei, B. Fan, L. Huo, N. L. Doltsinis, Y. Li, Y. Sun and Z. Wang, *J. Am. Chem. Soc.*, 2016, **138**, 10184–10190.

56 J. Zhang, Y. Li, J. Huang, H. Hu, G. Zhang, T. Ma, P. C. Y. Chow, H. Ade, D. Pan and H. Yan, *J. Am. Chem. Soc.*, 2017, **139**, 16092–16095.

57 S. Li, L. Zhan, W. Zhao, S. Zhang, B. Ali, Z. Fu, T.-K. Lau, X. Lu, M. Shi, C.-Z. Li, J. Hou and H. Chen, *J. Mater. Chem. A*, 2018, **6**, 12132–12141.

58 M. Li, Y. Liu, W. Ni, F. Liu, H. Feng, Y. Zhang, T. Liu, H. Zhang, X. Wan, B. Kan, Q. Zhang, T. P. Russell and Y. Chen, *J. Mater. Chem. A*, 2016, **4**, 10409–10413.

59 J. Lee, S. J. Ko, M. Seifrid, H. Lee, B. R. Luginbuhl, A. Karki, M. Ford, K. Rosenthal, K. Cho, T. Q. Nguyen and G. C. Bazan, *Adv. Energy Mater.*, 2018, **8**, 1801212.

60 S. Li, L. Zhan, F. Liu, J. Ren, M. Shi, C.-Z. Li, T. P. Russell and H. Chen, *Adv. Mater.*, 2018, **30**, 1705208.

61 H. Huang, Q. Guo, S. Feng, C. Zhang, Z. Bi, W. Xue, J. Yang, J. Song, C. Li, X. Xu, Z. Tang, W. Ma and Z. Bo, *Nat. Commun.*, 2019, **10**, 3038.

62 X. Zhang, C. Li, L. Qin, H. Chen, J. Yu, Y. Wei, X. Liu, J. Zhang, Z. Wei, F. Gao, Q. Peng and H. Huang, *Angew. Chem., Int. Ed.*, 2021, **60**, 17720.

63 D. Luo, L. Li, Y. Shi, J. Zhang, K. Wang, X. Guo and A. K. K. Kyaw, *J. Mater. Chem. A*, 2021, **9**, 14948–14957.

64 T.-J. Wen, Z.-X. Liu, Z. Chen, J. Zhou, Z. Shen, Y. Xiao, X. Lu, Z. Xie, H. Zhu, C.-Z. Li and H. Chen, *Angew. Chem., Int. Ed.*, 2021, **60**, 12964.

65 J. Cao, H. Wang, L. Yang, F. Du, J. Yu and W. Tang, *Chem. Eng. J.*, 2021, **427**, 131828.

66 G. Zhang, G. Yang, H. Yan, J. H. Kim, H. Ade, W. Wu, X. Xu, Y. Duan and Q. Peng, *Adv. Mater.*, 2017, **29**, 1606054.

67 L. Ma, S. Zhang, J. Zhu, J. Wang, J. Ren, J. Zhang and J. Hou, *Nat. Commun.*, 2021, **12**, 5093.

68 P. Bi, S. Zhang, J. Ren, Z. Chen, Z. Zheng, Y. Cui, J. Wang, S. Wang, T. Zhang, J. Li, Y. Xu, J. Qin, C. An, W. Ma, X. Hao and J. Hou, *Adv. Mater.*, 2021, 2108090.

69 S. Li, L. Zhan, C. Sun, H. Zhu, G. Zhou, W. Yang, M. Shi, C.-Z. Li, J. Hou, Y. Li and H. Chen, *J. Am. Chem. Soc.*, 2019, **141**, 3073–3082.

70 X. Wang, H. Lu, Y. Liu, A. Zhang, N. Yu, H. Wang, S. Li, Y. Zhou, X. Xu, Z. Tang and Z. Bo, *Adv. Energy Mater.*, 2021, **11**, 2102591.

71 Y. Wang, Z. Liu, X. Cui, C. Wang, H. Lu, Y. Liu, Z. Fei, Z. Ma and Z. Bo, *J. Mater. Chem. A*, 2020, **8**, 12495–12501.

72 C. He, Y. Li, S. Li, Z. P. Yu, Y. Li, X. Lu, M. Shi, C.-Z. Li and H. Chen, *ACS Appl. Mater. Interfaces*, 2020, **12**, 16700–16706.

73 S. Li, L. Zhan, T.-K. Lau, Z. P. Yu, W. Yang, T. R. Andersen, Z. Fu, C.-Z. Li, X. Lu, M. Shi and H. Chen, *Small Methods*, 2019, **3**, 1900531.

74 D. Luo, M. Zhang, J.-B. Li, Z. Xiao, F. Liu, L. Ding and X.-H. Zhu, *J. Mater. Chem. C*, 2020, **8**, 6196–6202.

75 C. Zhang, X. Song, K. K. Liu, M. Zhang, J. Qu, C. Yang, G. Z. Yuan, A. Mahmood, F. Liu, F. He, D. Baran and J. Wang, *Small*, 2020, **16**, 1907681.

76 X. Zhang, L. Qin, J. Yu, Y. Li, Y. Wei, X. Liu, X. Lu, F. Gao and H. Huang, *Angew. Chem., Int. Ed.*, 2021, **60**, 12475.

3290 | *J. Mater. Chem. A*, 2022, **10**, 3255–3295

This journal is © The Royal Society of Chemistry 2022

77 D. Luo, X. Lai, N. Zheng, C. Duan, Z. Wang, K. Wang and A. K. K. Kyaw, *Chem. Eng. J.*, 2021, **420**, 129768.

78 C. Li, X. Zhang, N. Yu, X. Gu, L. Qin, Y. Wei, X. Liu, J. Zhang, Z. Wei, Z. Tang, Q. Shi and H. Huang, *Adv. Funct. Mater.*, 2021, 2108861.

79 Y.-N. Chen, M. Li, Y. Wang, J. Wang, M. Zhang, Y. Zhou, J. Yang, Y. Liu, F. Liu, Z. Tang, Q. Bao and Z. Bo, *Angew. Chem., Int. Ed.*, 2020, **59**, 22714.

80 Z. P. Yu, Z. X. Liu, F. X. Chen, R. Qin, T.-K. Lau, J. Yin, X. Kong, X. Lu, M. Shi, C.-Z. Li and H. Chen, *Nat. Commun.*, 2019, **10**, 2152.

81 D. Luo, Y. Zhang, L. Li, C. Shan, Q. Liu, Z. Wang, W. C. H. Choy and A. K. K. Kyaw, *Mater. Today Energy*, 2022, **24**, 100938.

82 K. D. Deshmukh, T. Qin, J. K. Gallaher, A. C. Y. Liu, E. Gann, K. O'Donnell, L. Thomsen, J. M. Hodgkiss, S. E. Watkins and C. R. McNeill, *Energy Environ. Sci.*, 2015, **8**, 332–342.

83 Y. Guo, Y. Li, O. Awartani, H. Han, J. Zhao, H. Ade, H. Yan and D. Zhao, *Adv. Mater.*, 2017, **29**, 1700309.

84 B. Fan, L. Ying, Z. Wang, B. He, X.-F. Jiang, F. Huang and Y. Cao, *Energy Environ. Sci.*, 2017, **10**, 1243–1251.

85 Y. Guo, Y. Li, O. Awartani, J. Zhao, H. Han, H. Ade, D. Zhao and H. Yan, *Adv. Mater.*, 2016, **28**, 8483–8489.

86 D. Chen, J. Yao, L. Chen, J. Yin, R. Lv, B. Huang, S. Liu, Z. G. Zhang, C. Yang, Y. Chen and Y. Li, *Angew. Chem., Int. Ed.*, 2018, **57**, 4580–4584.

87 X. Liu, C. Zhang, C. Duan, M. Li, Z. Hu, J. Wang, F. Liu, N. Li, C. J. Brabec, R. A. J. Janssen, G. C. Bazan, F. Huang and Y. Cao, *J. Am. Chem. Soc.*, 2018, **140**, 8934–8943.

88 N. B. Kolhe, H. Lee, D. Kuzuhara, N. Yoshimoto, T. Koganezawa and S. A. Jenekhe, *Chem. Mater.*, 2018, **30**, 6540–6548.

89 Y. J. Hwang, T. Earmme, B. A. Courtright, F. N. Eberle and S. A. Jenekhe, *J. Am. Chem. Soc.*, 2015, **137**, 4424–4434.

90 Z. Li, X. Xu, W. Zhang, X. Meng, W. Ma, A. Yartsev, O. Inganäs, M. R. Andersson, R. A. J. Janssen and E. Wang, *J. Am. Chem. Soc.*, 2016, **138**, 10935–10944.

91 S. Feng, C. Liu, X. Xu, X. Liu, L. Zhang, Y. Nian, Y. Cao and J. Chen, *ACS Macro Lett.*, 2017, **6**, 1310–1314.

92 K. Li, R. Xie, W. Zhong, K. Lin, L. Ying, F. Huang and Y. Cao, *Sci. China: Chem.*, 2018, **61**, 576–583.

93 R. Zhao, C. Dou, Z. Xie, J. Liu and L. Wang, *Angew. Chem. Int. Ed.*, 2016, **55**, 5313–5317.

94 R. Zhao, N. Wang, Y. Yu and J. Liu, *Chem. Mater.*, 2020, **32**, 1308–1314.

95 J. A. Letizia, M. R. Salata, C. M. Tribout, A. Facchetti, M. A. Ratner and T. J. Marks, *J. Am. Chem. Soc.*, 2008, **130**, 9679–9694.

96 H. Sun, H. Yu, Y. Shi, J. Yu, Z. Peng, X. Zhang, B. Liu, J. Wang, R. Singh, J. Lee, Y. Li, Z. Wei, Q. Liao, Z. Kan, L. Ye, H. Yan, F. Gao and X. Guo, *Adv. Mater.*, 2020, **32**, 2004183.

97 B. Liu, H. Sun, J.-W. Lee, J. Yang, J. Wang, Y. Li, B. Li, M. Xu, Q. Liao, W. Zhang, D. Han, L. Niu, H. Meng, B. J. Kim and X. Guo, *Energy Environ. Sci.*, 2021, **14**, 4499–4507.

98 Z. Zhang, Y. Yang, J. Yao, L. Xue, S. Chen, X. Li, W. Morrison, C. Yang and Y. Li, *Angew. Chem. Int. Ed.*, 2017, **56**, 13503–13507.

99 Y. Meng, J. Wu, X. Guo, W. Su, L. Zhu, J. Fang, Z.-G. Zhang, F. Liu, M. Zhang, T. P. Russell and Y. Li, *Sci. China: Chem.*, 2019, **62**, 845–850.

100 J. Zhang, C.-H. Tan, K. Zhang, T. Jia, Y. Cui, W. Deng, X. Liao, H. Wu, Q. Xu, F. Huang and Y. Cao, *Adv. Energy Mater.*, 2021, 2102559.

101 T. Jia, J. Zhang, W. Zhong, Y. Liang, K. Zhang, S. Dong, L. Ying, F. Liu, X. Wang, F. Huang and Y. Cao, *Nano Energy*, 2020, **72**, 104718.

102 H. Fu, Y. Li, J. Yu, Z. Wu, Q. Fan, F. Lin, H. Woo, F. Gao, Z. Zhu and A. K.-Y. Jen, *J. Am. Chem. Soc.*, 2021, **143**, 2665–2670.

103 H. Yu, M. Pan, R. Sun, I. Agunawela, J. Zhang, Y. Li, Z. Qi, H. Han, X. Zou, W. Zhou, S. Chen, J. Lai, S. Luo, Z. Luo, D. Zhao, X. Lu, H. Ade, F. Huang, J. Min and H. Yan, *Angew. Chem., Int. Ed.*, 2021, **60**, 10137.

104 J. Du, K. Hu, J. Zhang, L. Meng, J. Yue, I. Angunawela, H. Yan, S. Qin, X. Kong, Z. Zhang, B. Guan, H. Ade and Y. Li, *Nat. Commun.*, 2021, **12**, 5264.

105 Q. Fan, W. Su, S. Chen, W. Kim, X. Chen, B. Lee, T. Liu, U. A. Méndez-Romero, R. Ma, T. Yang, W. Zhuang, Y. Li, Y. Li, T.-S. Kim, L. Hou, C. Yang, H. Yan, D. Yu and E. Wang, *Joule*, 2020, **4**, 658–672.

106 F. Peng, K. An, W. Zhong, Z. Li, L. Ying, N. Li, Z. Huang, C. Zhu, B. Fan, F. Huang and Y. Cao, *ACS Energy Lett.*, 2020, **5**, 3702–3707.

107 Q. Fan, Q. An, Y. Lin, Y. Xia, Q. Li, M. Zhang, W. Su, W. Peng, C. Zhang, F. Liu, L. Hou, W. Zhu, D. Yu, M. Xiao, E. Moons, F. Zhang, T. D. Anthopoulos, O. Inganäse and E. Wang, *Energy Environ. Sci.*, 2020, **13**, 5017–5027.

108 Q. Fan, H. Fu, Q. Wu, Z. Wu, F. Lin, Z. Zhu, J. Min, H. Woo and A. K.-Y. Jen, *Angew. Chem., Int. Ed.*, 2021, **60**, 2–11.

109 W. Zhao, D. Qian, S. Zhang, S. Li, O. Inganas, F. Gao and J. Hou, *Adv. Mater.*, 2016, **28**, 4734–4739.

110 H. Bin, L. Gao, Z. Zhang, Y. Yang, Y. Zhang, C. Zhang, S. Chen, L. Xue, C. Yang, M. Xiao and Y. Li, *Nat. Commun.*, 2016, **7**, 13651.

111 S. Li, L. Ye, W. Zhao, S. Zhang, S. Mukherjee, H. Ade and J. Hou, *Adv. Mater.*, 2016, **28**, 9423–9429.

112 S. Li, L. Ye, W. Zhao, S. Zhang, H. Ade and J. Hou, *Adv. Energy Mater.*, 2017, **7**, 1700183.

113 H. Yao, Y. Cui, D. Q.ian, C. S. Ponseca Jr, A. Honarfar, Y. Xu, J. Xin, Z. Chen, L. Hong, B. Gao, R. Yu, Y. Zu, W. Ma, P. Chabera, T. Pullerits, A. Yartsev, F. Gao and J. Hou, *J. Am. Chem. Soc.*, 2019, **141**, 7743–7750.

114 J. Wu, Q. Fan, M. Xiong, Q. Wang, K. Chen, H. Liu, M. Gao, L. Ye, X. Guo, J. Fang, Q. Guo, W. Su, Z. Ma, Z. Tang, E. Wang, H. Ade and M. Zhang, *Nano Energy*, 2021, **82**, 105679.

115 H. Zhang, H. Yao, J. Hou, J. Zhu, J. Zhang, W. Li, R. Yu, B. Gao, S. Zhang and J. Hou, *Adv. Mater.*, 2018, **30**, 1800613.

116 Z. Luo, T. Liu, Y. Wang, G. Zhang, R. Sun, Z. Chen, C. Zhong, J. Wu, Y. Chen, M. Zhang, Y. Zou, W. Ma,

This journal is © The Royal Society of Chemistry 2022

J. Mater. Chem. A, 2022, **10**, 3255–3295 | **3291**

H. Yan, J. Min, Y. Li and C. Yang, *Adv. Energy Mater.*, 2019, **9**, 1900041.

117 Y. Lin, F. Zhao, Y. Wu, K. Chen, Y. Xia, G. Li, S. K. Prasad, J. Zhu, L. Huo, H. Bin, Z. Zhang, X. Guo, M. Zhang, Y. Sun, F. Gao, Z. Wei, W. Ma, C. Wang, J. Hodgkiss, Z. Bo, O. Inganas, Y. Li and X. Zhan, *Adv. Mater.*, 2017, **29**, 1604155.

118 C. Huang, X. Liao, K. Gao, L. Zuo, F. Lin, X. Shi, C.-Z. Li, H. Liu, X. Li, F. Liu, Y. Chen, H. Chen and A. K. Y. Jen, *Chem. Mater.*, 2018, **30**, 5429–5434.

119 L. Meng, Y. Zhang, X. Wan, C. Li, X. Zhang, Y. Wang, X. Ke, Z. Xiao, L. Ding, R. Xia, H.-L. Yip, Y. Cao and Y. Chen, *Science*, 2018, **361**, 1094–1098.

120 Y. Ma, M. Zhang, S. Wan, P. Yin, P. Wang, D. Cai, F. Liu and Q. Zheng, *Joule*, 2021, **5**, 1–13.

121 Y. Yang, Z. Zhang, H. Bin, S. Chen, L. Gao, L. Xue, C. Yang and Y. Li, *J. Am. Chem. Soc.*, 2016, **138**, 15011–15018.

122 Z. Fei, F. D. Eisner, X. Jiao, M. Azzouzi, J. A. Rohr, Y. Han, M. Shahid, A. S. R. Chesman, C. D. Easton, C. R. McNeill, T. D. Anthopoulos, J. Nelson and M. Heeney, *Adv. Mater.*, 2018, **30**, 1705209.

123 X. Li, F. Pan, C. Sun, M. Zhang, Z. Wang, J. Du, J. Wang, M. Xiao, L. Xue, Z. Zhang, C. Zhang, F. Liu and Y. Li, *Nat. Commun.*, 2019, **10**, 519.

124 N. An, Y. Cai, H. Wu, A. Tang, K. Zhang, X. Hao, Z. Ma, Q. Guo, H. S. Ryu, H. Y. Woo, Y. Sun and E. Zhou, *Adv. Mater.*, 2020, **32**, 2002122.

125 H. Yao, Y. Cui, R. Yu, B. Gao, H. Zhang and J. Hou, *Angew. Chem. Int. Ed.*, 2017, **56**, 3045–3049.

126 S. Xu, Z. Zhou, W. Liu, Z. Zhang, F. Liu, H. Yan and X. Zhu, *Adv. Mater.*, 2017, **29**, 1704510.

127 Q. Guo, J. Lin, H. Liu, X. Dong, X. Guo, L. Ye, Z. Ma, Z. Tang, H. Ade, M. Zhang and Y. Li, *Nano Energy*, 2020, **74**, 104861.

128 T. Liu, Z. Luo, Y. Chen, T. Yang, Y. Xiao, G. Zhang, R. Ma, X. Lu, C. Zhan, M. Zhang, C. Yang, Y. Li, J. Yao and H. Yan, *Energy Environ. Sci.*, 2019, **12**, 2529–2536.

129 S. Dai, F. Zhao, Q. Zhang, T.-K. Lau, T. Li, K. Liu, Q. Ling, C. Wang, X. Lu, W. You and X. Zhan, *J. Am. Chem. Soc.*, 2017, **139**, 1336–1343.

130 J. Sun, X. Ma, Z. Zhang, J. Yu, J. Zhou, X. Yin, L. Yang, R. Geng, R. Zhu, F. Zhang and W. Tang, *Adv. Mater.*, 2018, **30**, 1707150.

131 X. Ke, L. Meng, X. Wan, Y. Cai, H.-H. Gao, Y.-Q.-Q. Yi, Z. Guo, H. Zhang, C. Li and Y. Chen, *Nano Energy*, 2020, **75**, 104988.

132 T. Li, L. Yang, Y. Xiao, K. Liu, J. Wang, X. Lu and X. Zhan, *J. Mater. Chem. A*, 2019, **7**, 20667–20674.

133 B. Kan, H. Feng, X. Wan, F. Liu, X. Ke, Y. Wang, Y. Wang, H. Zhang, C. Li, J. Hou and Y. Chen, *J. Am. Chem. Soc.*, 2017, **139**, 4929–4934.

134 J. Zhu, Y. Xiao, J. Wang, K. Liu, H. Jiang, Y. Lin, X. Lu and X. Zhan, *Chem. Mater.*, 2018, **30**, 4150–4156.

135 W. Liu, J. Zhang, Z. Zhou, D. Zhang, Y. Zhang, S. Xu and X. Zhu, *Adv. Mater.*, 2018, **30**, 1800403.

136 Z. Yao, X. Liao, K. Gao, F. Lin, X. Xu, X. Shi, L. Zuo, F. Liu, Y. Chen and A. K. Y. Jen, *J. Am. Chem. Soc.*, 2018, **140**, 2054–2057.

137 X. Xu, Z. Li, Z. Bi, T. Yu, W. Ma, K. Feng, Y. Li and Q. Peng, *Adv. Mater.*, 2018, **30**, 1800737.

138 W. Su, Q. Fan, X. Guo, J. Chen, Y. Wang, X. Wang, P. Dai, C. Ye, X. Bao, W. Ma, M. Zhang and Y. Li, *J. Mater. Chem. A*, 2018, **6**, 7988–7996.

139 B. Kan, J. Zhang, F. Liu, X. Wan, C. Li, X. Ke, Y. Wang, H. Feng, Y. Zhang, G. Long, R. H. Friend, A. A. Bakulin and Y. Chen, *Adv. Mater.*, 2018, **30**, 1704904.

140 Y. Li, J. Lin, X. Che, Y. Qu, F. Liu, L. S. Liao and S. R. Forrest, *J. Am. Chem. Soc.*, 2017, **139**, 17114–17119.

141 Y. Wu, H. Bai, Z. Wang, P. Cheng, S. Zhu, Y. Wang, W. Ma and X. Zhan, *Energy Environ. Sci.*, 2015, **8**, 3215–3221.

142 Y. Cui, C. Yang, H. Yao, J. Zhu, Y. Wang, G. Jia, F. Gao and J. Hou, *Adv. Mater.*, 2017, **29**, 1703080.

143 W. Wang, B. Zhao, Z. Cong, Y. Xie, H. Wu, Q. Liang, S. Liu, F. Liu, C. Gao, H. Wu and Y. Cao, *ACS Energy Lett.*, 2018, **3**, 1499–1507.

144 S. Chen, H. Yao, B. Hu, G. Zhang, L. Arunagiri, L.-K. Ma, J. Huang, J. Zhang, Z. Zhu, F. Bai, W. Ma and H. Yan, *Adv. Energy Mater.*, 2018, **8**, 1800529.

145 Y. Zou, Y. Dong, C. Sun, Y. Wu, H. Yang, C. Cui and Y. Li, *Chem. Mater.*, 2019, **31**, 4222–4227.

146 L. Feng, J. Yuan, Z. Zhang, H. Peng, Z. Zhang, S. Xu, Y. Liu, Y. Li and Y. Zou, *ACS Appl. Mater. Interfaces*, 2017, **9**, 31985–31992.

147 J. Yuan, Y. Zhang, L. Zhou, G. Zhang, H.-L. Yip, T.-K. Lau, X. Lu, C. Zhu, H. Peng, P. A. Johnson, M. Leclerc, Y. Cao, J. Ulanski, Y. Li and Y. Zou, *Joule*, 2019, **3**, 1140–1151.

148 Z. Zhou, W. Liu, G. Zhou, M. Zhang, D. Qian, J. Zhang, S. Chen, S. Xu, C. Yang, F. Gao, H. Zhu, F. Liu and X. Zhu, *Adv. Mater.*, 2020, **32**, 1906324.

149 F. Qi, K. Jiang, F. Lin, Z. Wu, H. Zhang, W. Gao, Y. Li, Z. Cai, H. Woo, Z. Zhu and A. K.-Y. Jen, *ACS Energy Lett.*, 2021, **6**, 9–15.

150 K. Jiang, Q. Wei, J. Y. L. Lai, Z. Peng, H. K. Kim, J. Yuan, L. Ye, H. Ade, Y. Zou and H. Yan, *Joule*, 2019, **3**, 3020–3033.

151 Y. Cui, H. Yao, J. Zhang, K. Xian, T. Zhang, L. Hong, Y. Wang, Y. Xu, K. Ma, C. An, C. He, Z. Wei, F. Gao and J. Hou, *Adv. Mater.*, 2020, **32**, 1908205.

152 G. Chai, Y. Chang, J. Zhang, X. Xu, L. Yu, X. Zou, X. Li, Y. Chen, S. Luo, B. Liu, F. Bai, Z. Luo, H. Yu, J. Liang, T. Liu, K. S. Wong, H. Zhou, Q. Peng and H. Yan, *Energy Environ. Sci.*, 2021, **14**, 3469–3479.

153 R. Wang, J. Yuan, R. Wang, G. Han, T. Huang, W. Huang, J. Xue, H. C. Wang, C. Zhang, C. Zhu, P. Cheng, D. Meng, Y. Yi, K. H. Wei, Y. Zou and Y. Yang, *Adv. Mater.*, 2019, **31**, 1904215.

154 S. Li, L. Zhan, Y. Jin, G. Zhou, T.-K. Lau, R. Qin, M. Shi, C.-Z. Li, H. Zhu, X. Lu, F. Zhang and H. Chen, *Adv. Mater.*, 2020, **32**, 2001160.

155 Z. Luo, R. Ma, T. Liu, J. Yu, Y. Xiao, R. Sun, G. Xie, J. Yuan, Y. Chen, K. Chen, G. Chai, H. Sun, J. Min, J. Zhang, Y. Zou, C. Yang, X. Lu, F. Gao and H. Yan, *Joule*, 2020, **4**, 1236–1247.

156 Y. Cui, H. Yao, L. Hong, T. Zhang, Y. Tang, B. Lin, K. Xian, B. Gao, C. An, P. Bi, W. Ma and J. Hou, *Natl. Sci. Rev.*, 2020, **7**, 1239–1246.

157 G. Chai, Y. Chang, Z. Peng, Y. Jia, X. Zou, D. Yu, H. Yu, Y. Chen, P. C. Y. Chow, K. S. Wong, J. Zhang, H. Ade, L. Yang and C. Zhan, *Nano Energy*, 2020, **76**, 105087.

158 Y. Chen, F. Bai, Z. Peng, L. Zhu, J. Zhang, X. Zou, Y. Qin, H. K. Kim, J. Yuan, L.-K. Ma, J. Zhang, H. Yu, P. C. Y. Chow, F. Huang, Y. Zou, H. Ade, F. Liu and H. Yan, *Adv. Energy Mater.*, 2021, **11**, 2003141.

159 S. Liu, J. Yuan, W. Deng, M. Luo, Y. Xie, Q. Liang, Y. Zou, Z. He, H. Wu and Y. Cao, *Nat. Photonics*, 2020, **14**, 300–305.

160 Y. Cui, H. Yao, J. Zhang, T. Zhang, Y. Wang, L. Hong, K. Xian, B. Xu, S. Zhang, J. Peng, Z. Wei, F. Gao and J. Hou, *Nat. Commun.*, 2019, **10**, 2515.

161 H. Lai, Q. Zhao, Z. Chen, H. Chen, P. Chao, Y. Zhu, Y. Lang, N. Zhen, D. Mo, Y. Zhang and F. He, *Joule*, 2020, **4**, 688–700.

162 Z. Jia, S. Qin, L. Meng, Q. Ma, I. Angunawela, J. Zhang, X. Li, Y. He, W. Lai, N. Li, H. Ade, C. J. Brabec and Y. Li, *Nat. Commun.*, 2021, **12**, 178.

163 C. McDowell, M. Abdelsamie, M. F. Toney and G. C. Bazan, *Adv. Mater.*, 2018, **30**, 1707114.

164 E. F. Manley, J. Strzalka, T. J. Fauvell, N. E. Jackson, M. J. Leonardi, N. D. Eastham, T. J. Marks and L. Chen, *Adv. Mater.*, 2017, **29**, 1703933.

165 J. K. Lee, W. Ma, C. J. Brabec, J. Yuen, J. S. Moon, J. Y. Kim, K. Lee, G. C. Bazan and A. J. Heeger, *J. Am. Chem. Soc.*, 2008, **130**, 3619–3623.

166 J. Peet, C. Soci, R. C. Coffin, T. Q. Nguyen, A. Mikhailovsky, D. Moses and G. C. Bazan, *Appl. Phys. Lett.*, 2006, **89**, 252105.

167 L. Ye, W. Zhao, S. Li, S. Mukherjee, J. H. Carpenter, O. Awartani, X. Jiao, J. Hou and H. Ade, *Adv. Energy Mater.*, 2017, **7**, 1602000.

168 X. Song, N. Gasparini, L. Ye, H. Yao, J. Hou, H. Ade and D. Baran, *ACS Energy Lett.*, 2018, **3**, 669–676.

169 J. Lv, H. Tang, J. Huang, C. Yan, K. Liu, Q. Yang, D. Hu, R. Singh, J. Lee, S. Lu, G. Li and Z. Kan, *Energy Environ. Sci.*, 2021, **14**, 3044–3052.

170 B. J. T. Villers, K. A. O'Hara, D. P. Ostrowski, P. H. Biddle, S. E. Shaheen, M. L. Chabinyc, D. C. Olson and N. Kopidakis, *Chem. Mater.*, 2016, **28**, 876–884.

171 R. Yu, H. Yao, L. Hong, Y. Qin, J. Zhu, Y. Cui, S. Li and J. Hou, *Nat. Commun.*, 2018, **9**, 4645.

172 L. Ye, Y. Cai, C. Li, L. Zhu, J. Xu, K. Weng, K. Zhang, M. Huang, M. Zeng, T. Li, E. Zhou, S. Tan, X. Hao, Y. Yi, F. Liu, Z. Wang, X. Zhan and Y. Sun, *Energy Environ. Sci.*, 2020, **13**, 5117–5125.

173 Z. Hu, Q. Wang, Z. Wang, F. Pan, L. Zhang, Y. Cao and J. Chen, *Org. Electron.*, 2020, **83**, 105762.

174 Y. Ding, X. Zhang, H. Feng, X. Ke, L. Meng, Y. Sun, Z. Guo, Y. Cai, C. Jiao, X. Wan, C. Li, N. Zheng, Z. Xie and Y. Chen, *ACS Appl. Mater. Interfaces*, 2020, **12**, 27425–27432.

175 R. Yu, H. Yao, Y. Xu, J. Li, L. Hong, T. Zhang, Y. Cui, Z. Peng, M. Gao, L. Ye, Z. Tan and J. Hou, *Adv. Funct. Mater.*, 2021, **31**, 2010535.

176 X. Liao, Q. He, G. Zhou, X. Xia, P. Zhu, Z. Xing, H. Zhu, Z. Yao, X. Lu and Y. Chen, *Chem. Mater.*, 2021, **33**, 430–440.

177 M. Koppe, H.-J. Egelhaaf, G. Dennler, M. C. Scharber, C. J. Brabec, P. Schilinsky and C. N. Hoth, *Adv. Funct. Mater.*, 2010, **20**, 338–346.

178 Q. Ma, Z. Ji, L. Meng, J. Zhang, H. Zhang, W. Huang, J. Yuan, F. Gao, Y. Wan, Z. Zhang and Y. Li, *Nano Energy*, 2020, **78**, 105272.

179 V. Gupta, V. Bharti, M. Kumar, S. Chand and A. J. Heeger, *Adv. Mater.*, 2015, **27**, 4398–4404.

180 Y. Dong, Y. Zou, J. Yuan, H. Yang, Y. Wu, C. Cui and Y. Li, *Adv. Mater.*, 2019, **31**, 1904601.

181 L. Yang, H. Zhou, S. C. Price and W. You, *J. Am. Chem. Soc.*, 2012, **134**, 5432–5435.

182 Q. An, J. Wang, W. Gao, X. Ma, Z. Hu, J. Gao, C. Xu, M. Hao, X. Zhang, C. Yang and F. Zhang, *Sci. Bull.*, 2020, **65**, 538–545.

183 C. Xu, H. Chen, Z. Zhao, J. Gao, X. Ma, S. Lu, X. Zhang, Z. Xiao and F. Zhang, *J. Energy Chem.*, 2021, **57**, 610–617.

184 J. Gao, J. Wang, Q. An, X. Ma, Z. Hu, C. Xu, X. Zhang and F. Zhang, *Sci. China: Chem.*, 2020, **63**, 83–91.

185 X. Ma, Y. Mi, F. Zhang, Q. An, M. Zhang, Z. Hu, X. Liu, J. Zhang and W. Tang, *Adv. Energy Mater.*, 2018, **8**, 1702854.

186 X. Ma, W. Gao, J. Yu, Q. An, M. Zhang, Z. Hu, J. Wang, W. Tang, C. Yang and F. Zhang, *Energy Environ. Sci.*, 2018, **11**, 2134.

187 F. Liu, L. Zhou, W. Liu, Z. Zhou, Q. Yue, W. Zheng, R. Sun, W. Liu, S. Xu, H. Fan, L. Feng, Y. Yi, W. Zhang and X. Zhu, *Adv. Mater.*, 2021, **33**, 2100830.

188 L. Zhan, S. Li, S. Zhang, X. Chen, T.-K. Lau, X. Lu, M. Shi, C.-Z. Li and H. Chen, *ACS Appl. Mater. Interfaces*, 2018, **10**, 42444–42452.

189 H.-W. Cheng, H. Zhang, Y.-C. Lin, N.-Z. She, R. Wang, C.-H. Chen, J. Yuan, C.-S. Tsao, A. Yabushita, Y. Zou, F. Gao, P. Cheng, K.-H. Wei and Y. Yang, *Nano Lett.*, 2019, **19**, 5053–5061.

190 D. Li, L. Zhu, X. Liu, W. Xiao, J. Yang, R. Ma, L. Ding, F. Liu, C. Duan, M. Fahlman and Q. Bao, *Adv. Mater.*, 2020, **32**, 2002344.

191 B. Kan, Y.-Q.-Q. Yi, X. Wan, H. Feng, X. Ke, Y. Wang, C. Li and Y. Chen, *Adv. Energy Mater.*, 2018, **8**, 1800424.

192 M. Zhanga, R. Ming, W. Gao, Q. An, X. Ma, Z. Hu, C. Yang and F. Zhang, *Nano Energy*, 2019, **59**, 58–65.

193 C. Xu, X. Ma, Z. Zhao, M. Jiang, Z. Hu, J. Gao, Z. Deng, Z. Zhou, Q. An, J. Zhang and F. Zhang, *Sol. RRL*, 2021, **5**, 2100175.

194 Y. Xu, Y. Cui, H. Yao, T. Zhang, J. Zhang, L. Ma, J. Wang, Z. Wei and J. Hou, *Adv. Mater.*, 2021, **33**, 2101090.

195 C. R. McNeill and N. C. Greenham, *Adv. Mater.*, 2009, **21**, 3840–3850.

196 W. Ni, M. Li, B. Kan, F. Liu, X. Wan, Q. Zhang, H. Zhang, T. P Russell and Y. Chen, *Chem. Commun.*, 2016, **52**, 465–468.

197 S. Karuthedath, A. Melianas, Z. Kan, V. Pranculis, M. Wohlfahrt, J. I. Khan, J. Gorenflot, Y. Xia, O. Inganäs, V. Gulbinas, M. Kemerink and F. Laquai, *J. Mater. Chem. A*, 2018, **6**, 7428–7438.

198 X. Liu, L. Ye, W. Zhao, S. Zhang, S. Li, G. M. Sud, C. Wang, H. Ade and J. Hou, *Mater. Chem. Front.*, 2017, **1**, 2057–2064.

199 J. Vogelsang, J. Brazard, T. Adachi, J. C. Bolinger and P. F. Barbara, *Angew. Chem., Int. Ed.*, 2011, **50**, 2257–2261.

200 M. Babics, R.-Z. Liang, K. Wang, F. Cruciani, Z. Kan, M. Wohlfahrt, M.-C. Tang, F. Laquai and P. M. Beaujuge, *Chem. Mater.*, 2018, **30**, 789–798.

201 M. Zhang, F. Zhang, Q. An, Q. Sun, W. Wang, X. Ma, J. Zhang and W. Tang, *J. Mater. Chem. A*, 2017, **5**, 3589.

202 L. Zhang, B. Lin, Z. Ke, J. Chen, W. Li, M. Zhang and W. Ma, *Nano Energy*, 2017, **41**, 609–617.

203 H. Wu, F. Huang, Y. Mo, W. Yang, D. Wang, J. Peng and Y. Cao, *Adv. Mater.*, 2004, **16**, 1826–1830.

204 Z. He, C. Zhong, X. Huang, W.-Y. Wong, H. Wu, L. Chen, S. Su and Y. Cao, *Adv. Mater.*, 2011, **23**, 4636–4643.

205 Y. Zhou, C. F. Hernandez, J. Shim, J. Meyer, A. J. Giordano, H. Li, P. Winget, T. Papadopoulos, H. Cheun, J. Kim, M. Fenoll, A. Dindar, W. Haske, E. Najafabadi, T. M. Khan, H. Sojoudi, S. Barlow, S. Graham, J.-L. Brédas, S. R. Marder, A. Kahn and B. Kippelen, *Science*, 2012, **336**, 327.

206 A. K. K. Kyaw, D. H. Wang, V. Gupta, J. Zhang, S. Chand, G. C. Bazan and A. J. Heeger, *Adv. Mater.*, 22013, **25**, 2397–2402.

207 G. Liu, R. Xia, Q. Huang, K. Zhang, Z. Hu, T. Jia, X. Liu, H.-L. Yip and F. Huang, *Adv. Funct. Mater.*, 2021, **31**, 2103283.

208 Z. Zheng, S. Zhang, J. Wang, J. Zhang, D. Zhang, Y. Zhang, Z. Wei, Z. Tang, J. Hou and H. Zhou, *J. Mater. Chem. A*, 2019, **7**, 3570–3576.

209 C. Sun, Z. Wu, Z. Hu, J. Xiao, W. Zhao, H.-W. Li, Q.-Y. Li, S. Tsang, Y.-X. Xu, K. Zhang, H.-L. Yip, J. Hou, F. Huang and Y. Cao, *Energy Environ. Sci.*, 2017, **10**, 1784–1791.

210 Z.-G. Zhang, B. Qi, Z. Jin, D. Chi, Z. Qi, Y. Li and J. Wang, *Energy Environ. Sci.*, 2014, **7**, 1966–1973.

211 J. Yao, B. Qiu, Z.-G. Zhang, L. Xue, R. Wang, C. Zhang, S. Chen, Q. Zhou, C. Sun, C. Yang, M. Xiao, L. Meng and Y. Li, *Nat. Commun.*, 2020, **11**, 2726.

212 B. Xu, Z. Zheng, K. Zhao and J. Hou, *Adv. Mater.*, 2016, **28**, 434–439.

213 M. Nam, J. Y. Huh, Y. Park, Y. Hong and D.-H. Ko, *Adv. Energy Mater.*, 2018, **8**, 1703064.

214 S. Trost, A. Behrendt, T. Becker, A. Polywka, P. Görrn and T. Riedl, *Adv. Energy Mater.*, 2015, **5**, 1500277.

215 B. J. Richardson, X. Wang, A. Almutairi and Q. Yu, *J. Mater. Chem. A*, 2015, **3**, 5563–5571.

216 A. K. K. Kyaw, X. W. Sun, C. Y. Jiang, G. Q. Lo, D. W. Zhao and D. L. Kwong, *Appl. Phys. Lett.*, 2008, **93**, 221107.

217 M. Upamaa, N. Elumalai, M. Mahmuda, C. Xua, D. Wang, M. Wrighta and A. Uddin, *Sol. Energy Mater. Sol. Cells*, 2018, **187**, 273–282.

218 Y. Bai, C. Zhao, S. Zhang, S. Zhang, R. Yu, J. Hou, Z. Tan and Y. Li, *Sci. China: Chem.*, 2020, **63**, 957–965.

219 B. Yang, Y. Chen, Y. Cui, D. Liu, B. Xu and J. Hou, *Adv. Energy Mater.*, 2018, **8**, 1800698.

220 A. Soultati, A. Verykios, S. Panagiotakis, K.-K. Armadorou, M. Haider, A. Kaltzoglou, C. Drivas, A. Fakharuddin, X. Bao, C. Yang, R. Yusoff, E. K. Evangelou, I. Petsalakis, S. Kennou, P. Falaras, K. Yannakopoulou, G. Pistolis, P. Argitis and M. Vasilopoulou, *ACS Appl. Mater. Interfaces*, 2020, **12**, 21961–21973.

221 G. Xie, Z. Zhang, J. Li, Y. Hu, X. Ge, G. Tu, X. Zhang, X. Zhang and J. Zhang, *Phys. Status Solidi RRL*, 2019, **13**, 1900372.

222 S.-H. Lee, S.-J. Ko, S. Eom, H. Kim, D. Kim, C. Lee and S. Yoon, *ACS Appl. Mater. Interfaces*, 2020, **12**, 14244–14253.

223 Q. Tai and F. Yan, *Adv. Mater.*, 2017, **29**, 1700192.

224 S. Dai and X. Zhan, *Adv. Energy Mater.*, 2018, **8**, 1800002.

225 T. Smith and J. Guild, *Trans. Opt. Soc.*, 1931, **33**, 73–134.

226 B. Jia, S. Dai, Z. Ke, C. Yan, W. Ma and X. Zhan, *Chem. Mater.*, 20018, **30**, 239–245.

227 Z. Hu, J. Wang, X. Ma, J. Gao, C. Xu, K. Yang, Z. Wang, J. Zhang and F. Zhang, *Nano Energy*, 2020, **78**, 105376.

228 Y. Zhang, X. He, D. Babu, W. Li, X. Gu, C. Shan, A. K. K. Kyaw and W. C. H. Choy, *Adv. Opt. Mater.*, 20021, **9**, 2002108.

229 Y. Zhang, D. Luo, C. Shan, Q. Liu, X. Gu, W. Li, W. C. H. Choy and A. K. K. Kyaw, *Sol. RRL*, 2021, **6**, 2100785.

230 T. Li, S. Dai, Z. Ke, L. Yang, J. Wang, C. Yan, W. Ma and X. Zhan, *Adv. Mater.*, 2018, **30**, 1705969.

231 J. Wang, J. Zhang, Y. Xiao, T. Xiao, R. Zhu, C. Yan, Y. Fu, G. Lu, X. Lu, S. R. Marder and X. Zhan, *J. Am. Chem. Soc.*, 2018, **140**, 9140–9147.

232 M. Upama, M. Wright, N. Elumalai, M. Mahmud, D. Wang, C. Xu and A. Uddin, *ACS Photonics*, 2017, **4**, 2327–2334.

233 Z. Hua, J. Wang, Z. Wang, W. Gaoc, Q. Ana, M. Zhang, X. Ma, J. Wang, J. Miao, C. Yang and F. Zhang, *Nano Energy*, 2019, **55**, 424–432.

234 F. Liu, Z. Zhou, C. Zhang, J. Zhang, Q. Hu, T. Vergote, F. Liu, T. P. Russell and X. Zhu, *Adv. Mater.*, 2017, **29**, 1606574.

235 H. Huang, X. Lia, L. Zhong, B. Qiua, Y. Yang, Z.-G. Zhang, Z. Zhang and Y. Li, *J. Mater. Chem. A*, 2018, **6**, 4670–4677.

236 Z. Hu, Z. Wang and F. Zhang, *J. Mater. Chem. A*, 2019, **7**, 7025–7032.

237 J. Zhang, G. Xu, F. Tao, G. Zeng, M. Zhang, Y. Yang, Y. Li and Y. Li, *Adv. Mater.*, 2019, **31**, 1807159.

238 C. Xu, K. Jin, Z. Xiao, Z. Zhao, X. Ma, X. Wang, J. Li, W. Xu, S. Zhang and L. Ding, *Adv. Funct. Mater.*, 2021, **31**, 2107934.

239 Z. Hu, J. Wang, X. Ma, J. Gao, C. Xu, X. Wang, X. Zhang, Z. Wang and F. Zhang, *J. Mater. Chem. A*, 2021, **9**, 6797.

240 Z. Hu, Z. Wang, Q. An and F. Zhang, *Sci. Bull.*, 2020, **65**, 131.

241 P. Cheng, H. C. Wang, Y. Zhu, R. Zheng, T. Li, C. H. Chen, T. Huang, Y. Zhao, R. Wang and D. Meng, *Adv. Mater.*, 2020, **32**, 2003891.

242 W. Zeng, C. Xie, W. Wang, S. Li, X. Jiang, S. Xiong, L. Sun, F. Qin, H. Han and Y. Zhou, *Sol. RRL*, 2020, **4**, 1900480.

243 P. Cheng, Y. Liu, S.-Y. Chang, T. Li, P. Sun, R. Wang, H.-W. Cheng, T. Huang, . Meng, S. Nuryyeva, C. Zhu, K.-H. Wei, B. Sun, X. Zhan and Y. Yang, *Joule*, 2019, **3**, 432–442.

244 B. Guo, W. Li, G. Luo, X. Guo, H. Yao, M. Zhang, J. Hou, Y. Li and W.-Y. Wong, *ACS Energy Lett.*, 2018, **3**, 2566–2572.

245 J. Gilot, M. M. Wienk and R. A. J. Janssen, *Adv. Mater.*, 2010, **22**, E67–E71.

246 P. Cheng, J. Wang, X. Zhan and Y. Yang, *Adv. Energy Mater.*, 2020, **10**, 2000746.

3294 | *J. Mater. Chem. A*, 2022, **10**, 3255–3295

This journal is © The Royal Society of Chemistry 2022

247 W. Huang, S.-Y. Chang, P. Cheng, D. Meng, B. Zhu, S. Nuryyeva, C. Zhu, L. Huo, Z. Wang, M. Wang and Y. Yang, *Nano Lett.*, 2018, **18**, 7977–7984.

248 Y. Qin, Y. Chen, Y. Cui, S. Zhang, H. Yao, J. Huang, W. Li, Z. Zheng and J. Hou, *Adv. Mater.*, 2017, **29**, 1606340.

249 L. Meng, Y.-Q.-Q. Yi, X. Wan, Y. Zhang, X. Ke, B. Kan, Y. Wang, R. Xia, H.-L. Yip, C. Li and Y. Chen, *Adv. Mater.*, 2019, **31**, 1804723.

250 Y. Firdaus, Q. He, Y. Lin, F. Nugroho, V. M. L. Corre, E. Yengel, A. H. Balawi, A. Seitkhan, F. Laquai, C. Langhammer, F. Liu, M. Heeney and T. D. Anthopoulos, *J. Mater. Chem. A*, 2020, **8**, 1164–1175.

251 G. Liu, J. Jia, K. Zhang, X. Jia, Q. Yin, W. Zhong, L. Li, F. Huang and Y. Cao, *Adv. Energy Mater.*, 2019, **9**, 1803657.

252 S. Qin, Z. Jia, L. Meng, C. Zhu, W. Lai, J. Zhang, W. Huang, C. Sun, B. Qiu and Y. Li, *Adv. Funct. Mater.*, 2021, **31**, 2102361.

253 J. Wang, Z. Zheng, Y. Zu, Y. Wang, X. Liu, S. Zhang, M. Zhang and J. Hou, *Adv. Mater.*, 2021, **33**, 2102787.

254 P. Cheng, H. C. Wang, R. Zheng, Y. Zhu, S. Dai, Z. Li, C. H. Chen, Y. Zhao, R. Wang and D. Meng, *Adv. Mater.*, 2020, **32**, 2002315.

255 H. Liu, Y. Li, S. Xu, Y. Zhou and Z. Li, *Adv. Funct. Mater.*, 2021, **31**, 2106735.

256 T. Xia, C. Li, H. Ryu, J. Guo, J. Min, H. Woo and Y. Sun, *Chem. - Eur. J.*, 2020, **26**, 12411–12417.

257 Q. Tu, C. Tang and Q. Zheng, *J. Mater. Chem. A*, 2019, **7**, 3307–3316.

258 W. Li, M. Chen, J. Cai, E. L. K. Spooner, H. Zhang, R. S. Gurney, D. Liu, Z. Xiao, D. G. Lidzey, L. Ding and T. Wang, *Joule*, 2019, **3**, 819–833.

259 Q. Guo, X. Zhu, X. Dong, Q. Zhu, J. Fang, X. Guo, W. Ma, M. Zhang and Y. Li, *J. Mater. Chem. A*, 2019, **7**, 24366–24373.

260 J. Cai, H. Wang, X. Zhang, W. Lia, D. Lia, Y. Mao, B. Dua, M. Chen, Y. Zhuang, D. Liu, H.-L. Qin, Y. Zhao, J. A. Smithe, R. C. Kilbridee, A. J. Parnelle, R. A. L. Jonese, D. G. Lidzeye and T. Wang, *J. Mater. Chem. A*, 2020, **8**, 4230–4238.

261 E. He, Z. Zheng, I. Lu, F. Guo, S. Gao, X. Pang, G. Mola, L. Zhao and Y. Zhang, *J. Mater. Chem. A*, 2020, **8**, 11381–11390.

262 X. Li, K. Weng, H. Ryu, J. Guo, X. Zhang, T. Xia, H. Fu, D. Wei, J. Min, Y. Zhang, H. Woo and Y. Sun, *Adv. Funct. Mater.*, 2020, **30**, 1906809.

263 Y. J. Kim, D. S. Chung and C. E. Park, *Nano Energy*, 2015, **15**, 343–352.

264 S. Li, W. Liu, M. Shi, J. Mai, T.-K. Lau, J. Wan, X. Lu, C.-Z. Li and H. Chen, *Energy Environ. Sci.*, 2016, **9**, 604–610.

265 Q.-Y. Li, J. Xiao, L.-M. Tang, H.-C. Wang, Z. Chen, Z. Yang, H.-L. Yip and Y.-X. Xu, *Org. Electron.*, 2017, **44**, 217–224.

266 N. Zheng, K. Mahmood, W. Zhong, F. Liu, P. Zhu, Z. Wang, B. Xie, Z. Chen, K. Zhang, L. Ying, F. Huang and Y. Cao, *Nano Energy*, 2019, **58**, 724–731.

267 X. Zhu, S. Liu, Q. Yue, W. Liu, S. Sun and S. Xu, *CCS Chem.*, 2021, 1070.

268 N. Y. Doumon, M. V. Dryzhov, F. V. Houard, V. M. Corre, A. Chatri, P. Christodoulis and L. Koster, *ACS Appl. Mater. Interfaces*, 2019, **11**, 8310–8318.

269 S. Park and H. J. Son, *J. Mater. Chem. A*, 2019, **7**, 25830–25837.

270 X. Du, T. Heumueller, W. Gruber, A. Classen, T. Unruh, N. Li and C. J. Brabec, *Joule*, 2019, **3**, 215–226.

271 H. Yin, K. Chiu, G. Li, C. Yan, H. Tang, C. Zhang, Y. Xiao, H. Zhang, W. Yu, H. Hu, X. Lu and X. Hao, *Adv. Electron. Mater.*, 2019, **5**, 1900497.

272 J. Guo, Y. Wu, R. Sun, W. Wang, J. Guo, Q. Wu, X. Tang, C. Sun, Z. Luo, K. Chang, Z. Zhang, J. Yuan, T. Li, W. Tang, E. Zhou, Z. Xiao, L. Ding, Y. Zou, X. Zhan, C. Yang, Z. Li, C. J. Brabec, Y. Li and J. Min, *J. Mater. Chem. A*, 2019, **7**, 25088–25101.

273 D. Baran, N. Gasparini, A. Wadsworth, C. Tan, N. Wehbe, X. Song, Z. Hamid, W. Zhang, M. Neophytou, T. Kirchartz, C. J. Brabec, J. R. Durrant and I. McCulloch, *Nat. Commun.*, 2018, **9**, 2059.

274 H. Liu, W. Wang and Y. Zhou, *J. Mater. Chem. A*, 2021, **9**, 1080.

275 A. S. Gertsen, M. Castro, R. R. Søndergaard and J. W. Andreasen, *Flexible Printed Electron.*, 2020, **5**, 014004.

276 R. Brandt, F. Zhang, T. Andersend, D. Angmod, M. Shic, L. Gureviche, F. C. Krebsd, J. Andreasend and D. Yua, *RSC Adv.*, 2016, **6**, 41542–41550.

277 X. Gu, Y. Zhou, K. Gu, T. Kurosawa, Y. Guo, Y. Li, H. Lin, B. C. Schroeder, H. Yan, F. M. Lopez, C. J. Tassone, C. Wang, S. C. B. Mannsfeld, H. Yan, D. Zhao, M. F. Tone and Z. Bao, *Adv. Energy Mater.*, 2017, **7**, 1602742.

278 E. Destouesse, M. Top, J. Lamminaho, H.-G. Rubahn, J. Fahlteich and M. Madsen, *Flexible Printed Electron.*, 2019, **4**, 045004.

279 Q. Wu, J. Guo, R. Sun, J. Guo, S. Jia, Y. Li, J. Wang and J. Min, *Nano Energy*, 2019, **61**, 559–566.

280 L. Ye, Y. Xiong, H. Yao, A. Gadisa, H. Zhang, S. Li, M. Ghasemi, N. Balar, A. Hunt, B. T. O'Connor, J. Hou and H. Ade, *Chem. Mater.*, 2016, **28**, 7451–7458.

281 B. Lina, L. Zhanga, H. Zhao, X. Xu, K. Zhou, S. Zhang, L. Gou, B. Fan, L. Zhang, H. Yan, X. Gu, L. Ying, F. Huang and Y. Cao, *Nano Energy*, 2019, **59**, 277–284.

282 X. Wang, L. Zhang, L. Hu, Z. Xie, H. Mao, L. Tan, Y. Zhang and Y. Chen, *Adv. Funct. Mater.*, 2021, 2102291.

283 W. Xu, X. Ma, J. H. Son, S. Y. Jeong, L. Niu, C. Xu, S. Zhang, Z. Zhou, J. Gao and H. Y. Woo, *Small*, 2021, 2104215.

284 H. Ning, Q. Jiang, P. Han, M. Lin, G. Zhang, J. Chen, H. Chen, S. Zeng, J. Gao and J. Liu, *Energy Environ. Sci.*, 2021, **14**, 5919.

285 J. Gao, W. Gao, X. Ma, Z. Hu, C. Xu, X. Wang, Q. An, C. Yang, X. Zhang and F. Zhang, *Energy Environ. Sci.*, 2020, **13**, 958.

286 Y. Wang, F. Wang, J. Gao, Y. Yan, X. Wang, X. Wang, C. Xu, X. Ma, J. Zhang and F. Zhang, *J. Mater. Chem. C*, 2021, **9**, 9892.

This journal is © The Royal Society of Chemistry 2022

J. Mater. Chem. A, 2022, **10**, 3255–3295 | **3295**